UNIVERSITÀ DEGLI STUDI DI PADOVA
Dipartimento di Biologia
Corso di Laurea Magistrale in Biotecnologie Industriali

Monolayer-Protected Au144 Nanoclusters as Drug-Delivery System Candidates

RELATORE: Prof. Flavio Maran
Dipartimento di Scienze Chimiche

CORRELATORE: Prof. Emanuele Papini
Dipartimento di Scienze Biomediche

CONTRORELATORE: Prof. Fabrizio Mancin
Dipartimento di Scienze Chimiche

LAUREANDO: Gaetano Calabrese

ANNO ACCADEMICO: 2012/2013

Dedicated to Riccardo,
Angela e Nannina.

Because with you,
Spring
is just one smile away.

Abstract

Ogni anno a 3,2 milioni di europei è diagnosticato il cancro, soprattutto della mammella, del colon-retto o del polmone. Il numero di decessi previsto per il 2013 a causa di questa malattia supera 1,3 milioni. Sebbene notevoli progressi continuino ad essere fatti nella ricerca di terapie efficaci, il cancro rimane causa di forte preoccupazione per la salute pubblica. Infatti la caratteristica principale di questa neoplasia è la crescita incontrollata di cellule anomale con il conseguente sviluppo di metastasi, che invadono i tessuti vicini e si diffondono in tutto il corpo attraverso i vasi sanguigni e linfatici. Ad oggi, il trattamento del cancro si avvale di strumenti quali la chirurgia, la radioterapia e la chemioterapia. In particolare, gli agenti chemioterapici vengono utilizzati per la cura delle forme più difficili di tumore, e tra questi si annoverano agenti alchilanti, agenti DNA-complessanti, inibitori della mitosi o ormoni. Lo scopo di questi farmaci è quello di interferire con la replicazione, la riparazione, la traduzione del DNA, nonché il processo di divisione cellulare, in modo da rallentare e fermare la diffusione del cancro. Tra i vari agenti antitumorali, complessi metallici e composti di coordinazione sono noti essere tra i più efficaci e per questo nel corso degli ultimi tre decenni i farmaci a base di platino hanno avuto un ruolo molto importante. Tuttavia, la caratteristica sulla quale si basa la discriminazione dei target di questi farmaci è la crescita accelerata delle cellule tumorali, che porta a pesanti effetti collaterali a lungo termine a carico di cellule non cancerose. Per tanto, nonostante i numerosi anni di ricerca mirata, le prospettive a lungo termine per i pazienti portatori di forme aggressive di cancro rimane scoraggiante. Cresce dunque la necessità di nuovi studi avanzati per la progettazione di farmaci antitumorali che risolvano i difetti delle terapie convenzionali. La nuova promessa è rappresentata da nanosistemi per *drug-delivery*, sistemi che sono in grado di modificare le caratteristiche farmacologiche e terapeutiche degli agenti trasportati al fine di superare alcune di queste limitazioni. I vantaggi attesi dall'uso di questi *nanocarriers* vedono il miglioramento dell'efficacia della droga, una migliore solubilità, l'aumento dell'emivita del farmaco nel circolo sistemico e, soprattutto,

l'accumulo maggiore di farmaco entro i tessuti malati per l'effetto di *enhanced permeabillity and retention*, nonché il rilascio costante del farmaco e la sua eliminazione; il tutto eliminando o riducendo l'insorgenza di effetti collaterali nel lungo termine. L'oggetto della tesi è il possibile uso come *drug-delivery system* (DDS) di cluster d'oro protetti da monostrato, $Au_{144}SR_{60}$ (con SR=legante tiolato), aventi un diametro di core di solo 1.6 nm. La scelta è ricaduta su questo *monolayer protected cluster* (MPC) per tutta una serie di motivi legati comunque alla sua dimensione molto ridotta. Tra l'altro, sembra che al calare della dimensione del cluster aumenti la capacità di penetrazione in cellule tumorali. Abbiamo introdotto due tipi di tiolo aventi catene a base di trietilene glicole in modo da migliorare la biocompatibilità e da avere buona solubilità in acqua. Uno di questi tioli porta un gruppo carbossilico, che permette la di legare l'agente antitumorale, cisplatino. Questa coniugazione, stabile in condizioni fisiologiche, si perde a pH acidi, per tanto, produrre coniugati MPC-cisplatino internalizzati attraverso l'endocitosi, promuoverebbe l'uscita del composto attivo. Diffondendo fuori dagli endosomi può raggiungere il nucleo e lì formare addotti citotossici cisplatino-DNA. In questa tesi viene riportata la sintesi e la caratterizzazione dei vari cluster di Au_{144}, effettuata mediante spettroscopia ^{1}H-NMR, spettroscopia UV-visibile, spettroscopia IR e spettroscopia fotoelettronica a raggi X. Gli MPC sintetizzati sono quindi stati studiati dal punto di vista dell'attività citotossica *in vitro* nei confronti di cellule di adenocarcinoma, HeLa, la loro associazione in dipendenza del tempo, concentrazione e temperatura, nonché la loro localizzazione intracellulare, utilizzando un legante fluorescente all'interno del monostrato. I risultati positivi forniti da questi esperimenti hanno permesso di capire che i cluster di Au_{144} sono validi candidati come DDS nel trattamento del cancro.

Index

1 Introduction

Every year 3.2 million Europeans are diagnosed with cancer, mostly breast, colorectal and lung cancers [1]. The predicted number of cancer deaths in Europe for 2013 is over 1.3 million [2]. Although important advances continue to be made in investigation and treatment, cancer remains a great problem. The main characteristic of this malignancy is the uncontrolled growth of abnormal cells [3]. These are prone to invade the close tissues and spread toward the whole body through the blood and lymph systems giving metastases [4].

Currently, cancer treatment involves combinations of surgery, radiation, and chemotherapy. Successful results are obtained for localized therapies, such as surgery and radiotherapy, only when malignant cells are confined to a specific area. Therefore, the use of chemotherapic agents becomes essential for the fight of the whole-body-spread metastases that come with the local growth of tumors [5]. Metastases, indeed, represent the primary cause of death from cancer.

Anticancer agents used for chemotherapies are antimetabolites, alkylating agents, DNA-complexing agents, mitosis inhibitors or hormones, all systemic anti-proliferative drugs able to discriminate dividing cells and to kill them. They interfere with the process DNA replication, repair, translation and cell division, thus slowing and stopping the cancer from spreading [5].

Among anticancer drugs, metal complexes and coordination compounds are known to be the most effective, affecting directly cell division and gene expression. Over the last three decades, platinum-based drugs, particularly in cis-platin, played the major role in various cancer treatment [6]. However, all chemotherapeutic drugs rely on enhanced growth rate of cancer cells as the discriminating parameter, which leads to side effects in the long-term fatal damage of proliferating non-cancerous cells, and revealing the inefficacy of cure in solid tumors where the major part of cancerous cells do not rapidly divide [5]. Despite several years of focused research, the long-term outlook for patients carrying aggressive forms of cancer remains discouraging. Therefore, we need

new advanced studies aimed to design anticancer agents with reduced toxicity and improved therapeutic indices to face the drawbacks of conventional therapies and their intrinsic toxicity [7].

The new promise is represented by nanosystems with the ability to change the pharmacological and therapeutic features of transported anticancer drugs in order to overcome some of these limitations. Research efforts have resulted in innovative nanodevices and nanostructures for use in applications such as diagnostics, biosensing, therapeutics, and drug delivery. In particular, gold nanoparticles have been identified as promising candidates for delivery payloads such as drugs, proteins, peptides, and nucleic acids [8] [9] [10] with the expected advantages of drug efficacy enhancement, including improved solubility, increased half-life in systemic circulation, enhanced drug accumulation within diseased tissues, constant and stable drug release, finely regulated clearance, with the perspective of also lowering the insurgence of long-term side effects.

1.1 Nanosciences

Nanosciences study objects and systems having at least one dimension in the range of roughly 1 to 100 nm. Such systems are larger than molecules, but smaller than biological systems. In recent years, nanosciences and associated nanotechnologies have attracted an increasing interest beacuse it has been understood that nanomaterials could have changed our way of interacting with and improving life. Since the ancient times, humans have been using nanomaterials without knowing it. In fact, an example is the use of colloidal gold as pigment in colored glass-works and silver in the art of photography [11]. What distinguishes the modern researcher in this field is the consciousness in the application of the knowledge acquired through observation and understanding the nature of materials and their properties, which can be modulated and adapted to (very often) meet the desired requirement.

Therefore, an increasing need of facing new demanding challenges is becoming more and more important, and this requires new technologies and systems capable of providing new architectures at the nanoscale. In fact, decreasing the size of a nanostructured material changes substantially its

properties. From this point of view, nature represents an incomparable inspirational source for building nanomachines [12]. Cells represent a great example of finely regulated systems of machines that are dimensionally and structurally organized in a hierarchical form: they are capable to cooperate with each other, while interacting with the external environment, modify the surrounding environment, (re-)generate, move and reproduce themselves. All this with a high efficiency that so far cannot be obtained with artificial systems [13].

Nanomaterials, such as metal or semiconductor nanoparticles (NP), exhibit similar dimensions to biomolecules, e.g., proteins or DNA. This feature, along with the different methods available for the preparation of NP of controlled shape and size, opens an exciting route for providing building blocks for nanoscale assemblies, structures, and devices [14]. Furthermore, enzymes, antigens and antibodies, and biomolecular receptors have dimensions in the range of 2–20 nm, i.e., similar to those of most NPs. Thus the two classes of materials are structurally compatible. The conjugation of NPs with biomolecules is an attractive area of research in nanobiotechnology [15] and could provide suitable grounds for emerging biomedical applications, such as targeted entry into cells, novel biosensors for diagnostics, and drug-delivery system for cancer treatment [16] .

1.2 Monolayer-protected clusters

As opposed to their macroscopic equivalent, structures in a nanometric scale have a large number of surface atoms. Being on a surface makes these atoms experience a totally different chemical surrounding compared to the atoms in the bulk, which results in displaying different reactivity, energy, structure and electronic states. For example, reducing gold to the nanometer length scale is associated with the observation of an intense surface plasmon absorption in the visible region of the spectrum, which makes gold take a different color. The properties of a nanostructured material are strongly influenced by the atoms present on the surface, the real interface with the environment. Naked surfaces of metals or metal oxides have the ability to adsorb organic molecules through a process lowering the free energy at the interface

between metal and environment. Furthermore, adsorbed molecules that are changing the properties at the interface also play a role in the stability of these nanostructures, which otherwise would remain very reactive [17].

Self-assembled monolayer (SAM) formation with organic molecules on 2D or 3D surfaces is a particular example of the phenomenon generally known as “self-assembly”. It could be understood as a supermolecular organization of sub-components generating complex systems to minimize the total energy of the system. Chemical bonding between the sulfur and gold atoms and interactions between neighboring adsorbed molecules are the driving forces of SAM formation on gold surfaces. These interactions and bonds control the properties and stability of monolayers protecting small metal three-dimensional clusters as well as two-dimensional SAMs on metal surfaces. Alkanethiolates could be considered the typical adsorbate for SAMs, interacting mainly through intermolecular van der Waals forces. However, previous studies carried out in Prof. Maran's laboratories have shown that additional interactions, such as particularly intermolecular C=O···H-N hydrogen bonding between embedded amide groups of peptidic adsorbates, may enhance the stability of SAMs [18] [19].

High affinity of thiols for gold surfaces allows obtaining well organized organic surfaces, but also highly defined chemical functions ready to be tuned and to determine new properties. In MPCs, the monolayer is somehow similar to SAMs formed on extended 2D SAMs, but with an important difference: in a cluster of 1-2 nm diameter, about 45% of superficial atoms lay in angles, edges or vertexes and the footprint of alkanethiolates on the Au surface is higher (60%) than on a flat gold surface (33%) [18] [20]. This is because MPCs offer a three-dimensional surface and not a flat surface. It is the elevated radius of curvature of the cluster that determines a higher packing near sulfur (small footprints). On the other hand, the periphery of the MPC SAM is much less organized than that of 2D SAMs.

MPCs have the property of possessing a monolayer that can be rather easily modified. Three of the main strategies are used to modulate its composition and thus the exposed functional group.

A simple approach consists of performing the MPC synthesis with all desired thiols in solution: this is the direct synthesis. This is, e.g., the case of thiols with terminal polar functions, such as carboxylic groups [21], peptides [18]

or short ethylene glycol chains [22], also enabling water-solubility. This ability represents a fundamental feature for the perspective use of these systems in biological or biomimetic applications. This approach is used when the sought thiols are relatively cheap or easily available.

The second method exploits the intrinsic reactivity of structural parts of the cluster that make it prone to exchange protecting thiols with exogenous ones in solution. In ligand-place exchange reaction, if MPCs is capped by R-SH thiols and is exposed to a solution containing different R'-SH thiols, latter will partially replace those present in the original monolayer. Indeed, the surface of a gold nanocluster is not homogeneous but contains different structural features. Those can be considered as particularly reactive binding sites: vertexes, edges and faces have different electronic densities, which implies different reactivities. Vertexes and edges show an increased tendency to exchange ligands, while faces, considered as Au(111) surfaces, have a lower tendency. An extensive research about the thermodynamics and kinetics of exchange reactions was conducted by Murray's group [23]. It was reported that the reaction proceeds with a 1:1 stoichiometry releasing a thiol from the monolayer for each new bond with the exogenous thiol. A thiol with a longer chain and a higher steric effect will have a slower exchange: the reaction starts on edges and vertexes, where the surface of the monolayer is not densely packed, and then it involves faces. The exchange ends when a point of equilibrium is achieved. To promote ligand exchange, it is thus sufficient to increase the concentration of the exogenous thiol and let the reaction proceed for a sufficiently long time (typically 2 days). This approach is preferred for thiols intolerant to reducing condition of MPC synthesis reaction, or expensive and valuable ligands.

The last method for realizing changes in the surface consists in covalent modification of the original thiols of the monolayer with a bond-forming reaction occurring at the MPC periphery. In these reactions terminal groups of ligands are coupled with molecules, such as peptides. Click chemistry reactions are generally attractive, because they can be conducted easily with simple reagents, solvents, mild conditions and high yields. Wuelfing and Murray described the formation of amide and ester bonds onto nanoparticles carrying -COOH and -OH groups [24]. Chemical reactivity of terminal groups of SAMs on flat surfaces is still different from the terminal groups of monolayers in MPCs. Foregiven S_N2 reaction, a MPC is more prone to react faster than a 2D SAM: this is because the involved groups,

such as -Br for a ω-bromoalkyl thiol, are less densely packed on a curved surface than on a flat surface.

Our understanding and control of physical and chemical properties of gold MPCs still need to be examined in depth and represent an active area of research. On the other hand, we already know enough to fabricate highly stable MPCs. Concerning the monolayer, which protects and stabilizes the gold core, it also provides a way to decorate the outer MPC shell with molecular groups enabling specific functions. This is an issue of outmost importance for the use of these nanosystems as devices and sensors [18].

1.3 Cisplatin

After the last two decades, the pharmaceutical industry is in a relative pause with its research in truly forward-looking useful molecules for therapies. After the incredible success of antibiotics, the world placed its hope in gene therapy, but it is also important not to stop looking for alternatives. The use of organometallics or metal complexes medicine could be one of these alternatives, because of the particular reactivity of these species with living cells [25]. As a matter of fact, in these 20 years most of the major classes of drugs contain different kind of metal compounds [26]. Since these compounds are in current clinical use, new areas of application, encouraged by the association of new nanotechnological systems, are rapidly emerging.

A widely used drug for tumor treatment cancer is represented by platinum(II) complexes: four new injectable Pt(II) diamine compounds (cisplatin, carboplatin, nedaplatin and oxalilplatin) were approved for clinical use and several others cis-diamine complexes are in clinical trials [27]. Many malignancies, especially testicular and ovarian carcinoma, but also small cell lung, bladder, cervical, head and neck carcinomas [28] can be treated with cisplatin (cis-diamminedichloroplatinum(II)), one of the most active chemotherapeutic agents available.

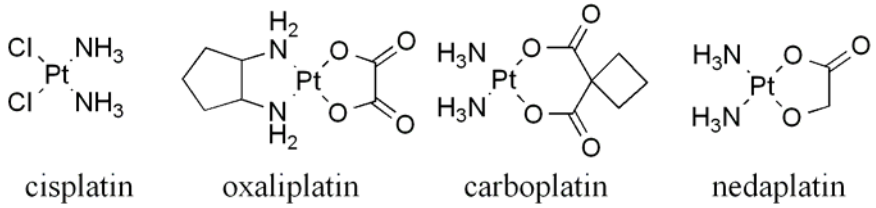

Figure 1 – *Chemical structures of some famous platinum-based anticancer agents*

Platinum(II) shows a high affinity for sulfur, and this after administrating Pt(II) complex in the human body its probability to bind biomolecules carrying sulfur-donor groups is high. In fact, sulfur is present in large amounts in peptides, proteins and enzymes, for example glutathione (GSH) and metallothioneins, and binding of platinum complexes to these components results in toxic effects. [29], [30]. Even so, a certain amount of platinum complexes is capable of binding to nitrogen-donor biomolecules, such as aminoacids or nucleic acids. DNA located in the nucleus is thought to be the primary biological target of cisplatin, while the interactions with mitochondrial DNA are less responsible for the antitumor activity of the platinum complexes [31]. The covalent bonds of platinum atom of cisplatin with purine bases occurs on the N7 position, forming 1,2- or 1,3-intrastrand crosslinks and a lower percentage of interstrand crosslinks. Binding to N7 and N1 of adenine and N3 of cytosine occurs in small amount [30].

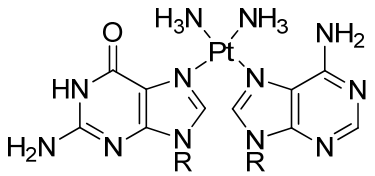

Figure 2 – *Chemical structure of interaction of cisplatin with N7 of purine bases*

Cisplatin resembles bifunctional alkylating agents. The intrastrand crosslink between two adjacent purine bases is believed to be the critical damage induced by cisplatin. Indeed, formation of cisplatin-DNA adducts interferes with DNA replication and transcription by disrupting the structure of the DNA. This alteration in the structure is recognized by the cellular DNA repairing proteins, and the increased repair of cisplatin-induced DNA damage has been associated with cisplatin treatment resistance [32]. Further studies suggested that the cytotoxicity of cisplatin is probably due to a combination of DNA damaging property with different harms including mitochondrial dysfunction, peroxidation of the cell membrane and inhibition of protein synthesis.

Despite its high effectiveness, some clinical problems derive from the use of cisplatin in anticancer therapy. Not only strong toxicity in non-cancerous tissues, but also the frequent occurrence of intrinsic and acquired resistance to the treatment [33] resulting in their poor activity against some particular tumors [34]. For example, while encouraging results can be obtained in ovarian cancer, the long-term response is disappointing due to the development of drug

resistance leading to return of the cancer and subsequent death of most of patients [35]. The mechanism behind tumor resistance to cisplatin treatment seems to be multifactorial and includes decreased drug transport, increased cellular toxic compounds exclusion, changes in DNA repair, increased tolerance of DNA adducts, and alterations in the pathway of apoptotic cell death [36]. Another important side effect of cisplatin is nephrotoxicity. Renal tubular epithelial cells become injured and it can be manifested as acute renal failure or a chronic syndrome with renal electrolyte wasting [37].

Continuous efforts are being made to reduce the toxicity of platinum anticancer complexes against normal cells, and to contrast acquired resistance to cisplatin and diminishing its nephrotoxicity [38] [39]. An example is a novel platinum(II)–terpyridine complex which interacts without covalently binding or nicking DNA and induces cell death *via* a different mechanism than cisplatin, thereby displaying selective toxicity for cancerous and fast proliferating cell lines [34]. Finally, nanoparticles have emerged as a potential tool to reduce side-effects and their use as a DDS has been extensively highlighted. The conjugation of drugs to nanoparticles has important effects on their pharmacokinetics, conjugate evolution and biodistribution, and results in a reduction of observed cisplatin-induced toxicity on healthy cells without affecting the therapeutic benefits [40].

1.4 Drug-delivery

Some small molecules have characteristics that limit their use in clinical applications, such as poor water solubility, nonspecific biodistribution and low therapeutic effects. Furthermore, the onset of drug resistance after initial treatment diminishes the in efficacy of the drug. The delivering of small molecules by nanoparticles conjugation has advantages that may overcome these limitations [41]. Indeed, a good drug delivery into a human body requires passing natural biological barriers, such as the cell membrane and the reticuloendothelial system (RES) [16]. Nonetheless, thanks to pathophysiological conditions due to anatomical changes in diseased tissues, drug-delivery with nanosystems can accomplish better site-specific and targeted delivery. In recent years, a strong effort is being put in the development of therapeutic nanoparticles anticancer

agents. Today, the use of nanoparticles in medicine also includes biosensing, bioimaging, and photothermal therapy [16].

The route of anticancer therapeutics to the tumor is a process involving three steps: the delivery to different regions of the tumor *via* blood-vessels, the diffusion through the walls of the vessels, and the path *via* interstitial space to tumor cells [42].

It has been demonstrated that up to 90% of the administrated cisplatin binds irreversibly to albumin and then reach the tumor in an inactive form without any biological effect [43]. A properly configured nanocarrier, beyond transporting the agent to the tumor, will also protect it from deactivation by plasma proteins. Encapsulation [44] and steric stabilization with polymers [45] provided excellent stability in plasma, a much longer circulation time, better efficacy, and lower toxicity than free cisplatin [40]. These unique properties have also been exploited to overcome the blood–brain barrier, delivering the agent to the brain, the most challenging target [46]. Examples are known of systems that are undetected by the immune system and display biocompatibility and biodegradability features.

The structure of tumors is highly heterogeneous. It includes clusters of tumor cells, abnormalities in the vasculature leading to highly nonuniform vascular perfusion and a dense interstitial structure with an poorly perfused center, preventing delivery of therapeutics in the core. Here the tumor presents low pH, low O_2 concentration and the most aggressive cells. These cells are able to regenerate the whole carcinoma, whether not destroyed, and, if exposed to nonlethal doses of the anticancer agent, may development drug resistance [47].

High permeability of disorganized vasculature endothelium of cancer cells with numerous gaps within the range from 100 nm to 2 μm [48] and the absence of lymphatic drainage imparts the interstitial fluid an elevated pressure [49]. This phenomenon, called *enhanced permeability and retention effect* (EPR), reduces the convective transport into the tumor mass, leaving diffusion as the primary way for transporting therapeutic drugs to the poorly perfused areas [50] [51]. EPR effect is known to be strongly size-dependent (nanostructures below 100 nm can leak out of the blood and accumulate within tumor tissues) [52], a fact that can limit the effectiveness of a given nanocarrier. Experiments in animal models suggest that the nanoparticle charge also has an influence. Generally, the physical, chemical, and biological properties of nanocarriers affect the delivery

ability. Positively charged nanoparticles improve the delivery through the route from blood vessels to cancer cells, whereas neutral or slightly negative particles between 50 and 100 nm can move more quickly within the area of large tumors, delivering drugs into deep tissues [53]. This EPR effect can be exploited for drug delivery with nanosystems because, beyond increasing accumulation of the drug within tumors, it decreases uptake by healthy tissues [54].

Nanoparticles larger than 100 nm are appropriate candidates for the EPR effect [55] but, showing limited diffusion through the interstitial space with its dense collagen matrix [56], they poorly penetrate the tumor parenchyma [47]. Decreasing the nanoparticle size may improve the rate of delivery in tumor tissue [53], indeed Sahoo *et al.* observed nanocarriers between 10 and 100 nm are easily taken up by cells [57]. Huang and co-workers reported that gold nanoparticles between 3 and 6 nm displayed unique advantages over larger nanoparticles in terms of tumor uptake and permeability [8]. The application of a targeting function to the nanoparticle could be instrumental to lead it directly to diseased tissues and cells. This will result in a selective accumulation within the malignancy, improving the therapeutic outcome of the treatment while decreasing the side effects observed in many current therapies [41].

Another important aspect to consider is the nanoparticle clearance, which also is size-dependent [55] [9]. The kidney is the organ responsible for blood filtration and for the removal of chemicals smaller than 50 KDa, corresponding to roughly 6 nm diameter, on the basis of measured coefficients for the glomerular capillary wall. Larger DDS would keep the drug within the blood [40]. When designing a nanocarrier, this constraints need to be borne in mind because they represent a lower limit for biodegradable particles and an upper limit for non-degradable systems.

The expected advantages of anticancer drug-delivery nanocarriers are: I) drug efficacy enhancement and improved solubility; II) increased half-life in systemic circulation with resistance to RES; III) enhanced drug accumulation within diseased tissues; IV) constant and stable drug release and finely regulated clearance. Greater anticancer efficacy and lower toxicity have been recognized to newly developed DDS, compared to their corresponding free agents. Some are already approved by the Food and Drug Administration for clinical use or are under clinical trial [41]. Some examples are reported in the following paragraph.

Xia *et al.* developed hollow gold nanocages with porous walls and tunable localized surface plasmon resonance properties for theranostic applications via two approaches: surface functionalization with thermally responsive polymers to control the release with near-infrared laser irradiation or high-intensity focused ultrasound, and filling the hollow interiors with a phase-change material [58]. Al-Jamal and Kostaleros reported the creation of smart theranostic liposome-based devices as templates for embedding, encapsulation, or conjugation of nanoparticles capable of gene therapy, optical imaging and drug-delivery [59]. Ambrogio *et al.* showed how molecular machinery can operate efficiently, when anchored onto a silica nanoparticle support, being able to release cargo in solution upon activation by redox, acid/base chemistry, light, or by the application of a magnetic field [60]. Considering the multiple physiological barriers that an anticancer agent must overcome to reach the tumor, Fukumura *et al.* designed a multistage nanoparticle system composed of a gelatin core with polyethyleneglycol (PEG) QDs conjugated to the surface, able to enhance their tissue penetration by changing its size, charge, shape, flexibility and surface coating to suit the transport across each barrier. [47]. Rusling and co-workers created PEG-protected carbon nanotubes with attached cisplatin and the targeting ligand Epidermal Growth Factor, successfully inhibiting the growth of head and neck tumor xenografts in mice [61]. A further offroad is the development of multifunctional nanoparticles that exploit unique optical and electrical properties [62], such as quantum dots and gold nanoparticles. These systems, beside the drug delivery function, permit to track their intracellular trafficking and localization [16], or possess magnetic resonance imaging contrast features [63].

1.5 MPCs as drug-delivery system for tumors

With reference to the subject of this thesis, it is worth stressing noticed that because of their biocompatibility, low toxicity, small size, and tunable surface functionalities colloidal gold nanoclusters represent a promise in surmounting the characteristic limitations displayed by drug delivery [64]. The first clinical trial of gold a nanoparticle as a therapeutic nanocarrier is CYT-6091. It is made of Human tumor necrosis factor alpha bound to the surface of a PEG-protected 27

nm gold nanoparticle. Successfully, in the phase I clinical trial, the results showed accumulation of gold nanoparticles in the diseased tissue [65]. In recent years, the controlled synthesis of gold nanoparticles of different sizes for biomedical uses led to make important steps forward. This is also true for the smaller MPCs. The gold–thiolate monolayer provides a way to decorate the MPC shell with molecular groups capable of accomplishing specific goals [18] [66].

Possible approaches for MPC delivery optimization are to decrease the size or surface modification. It was observed that large gold nanoparticles are rapidly opsonized by plasma proteins and eliminated by the RES in mammalian cells [67]. To bypass RES, thiolated poly-ethylene glycol could coat the surface resulting in RES clearance to liver of approximately 150-fold delay improvement compared with non-PEGylated coatings in a mice model [68]. By decreasing the zeta potential of gold nanoparticles, PEG coating is also useful to prevent aggregation in the blood but, unfortunately liver and spleen accumulation cannot be decreased. Indeed, 5 nm PEGylated gold MPCs show long time circulation in blood, and high accumulation in the liver. Thus, it is still necessary to explore the renal clearance and decrease the side effects [10]. In addition, the possibility to track the MPCs would enable a better discernment of how the organism processes nanocarriers.

Although there is not an exact size range of truly effective MPCs, until a few years ago it was thought that MPCs larger than 10 nm and smaller than 100 nm were the most effective for in-tumor accumulation [16]. Recently, Kumar *et al.* tested several small gold nanoclusters with identical surface monolayer and charge, but ranging in size from 2 to 15 nm. As opposed to what was thought before, the 2 nm MPCs showed significantly high efficacy for cancer treatment [69], so it was hypothesized that gold nanoparticles smaller than 10 nm would have special advantages in terms of tumor penetration [8].

To attempt a higher cellular selectivity, internalization, and localization in the cells of solid tumors, a range of macromolecules, such as proteins, peptides or small molecules, was attached on the surface of MPCs. Their outcome was very promising, leading to good results in delivering MPCs into solid tumors. In the last year, MPCs were suggested as the perfect nanocarrier for cisplatin due to the possibility to finely control and reproduce both synthesis and conjugation to cisplatin. Other Pt derivatives, such as Pt (IV) complexes, have also been loaded on gold MPCs without losing the anticancer effect, in some cases even enhancing

it [40]. Craig *et al*. reported a revised method for producing a cisplatin-nanocluster conjugate where the MPC was decorated with a PEG linker through a cyclic disulfide anchor and attached to cisplatin via terminal carboxylate groups. It was also reported the number of platinum per nanoparticle were ranging from 700 to 70000, showing high drug loading [9]. Ojea-Jimenez *et al.* attempted nuclear localization with cationic gold MPC-bioconjugates for gene delivery applications, where oligonucleotides loaded on the surface were transported inside the cells with higher efficiency than unbound DNA [70], the same thing could be applied to cisplatin. Harkness and Cliffel studied biomimetic MPCs for immunorecognition acting as simulants for clinically interesting viruses by mimicking the specific intermolecular forces acting in antibody–antigen binding [66]. The recent work of Zhang *et al.* shows that glutathione MPCs are metabolizable by renal clearance and have not induced appreciable toxicity responses [10]. These conclusions are very important for future cancer therapy and drug delivery.

1.6 Purpose and summary of the thesis

Nowadays we have the possibility of tuning molecular systems to make them interact with biological targets in a rather precise way in order to carry out specific functions. In the context of nanoparticles for the development of systems for drug delivery, it is conceivable to think that one can prepare vehicles able to carry the therapeutic agent only where it is needed, thereby avoiding unwanted doses of drugs in healthy tissues and the risk of long-term side-effects. In the fight against cancer, there are already several biocompatible candidates, but none of these has emerged as the ultimate DDS yet. For this reason, we are still looking for better suitable candidates. Our attention focused on ultrasmall MPCs, already subject of studies by Prof. Maran's group, in which a nanoscale gold core is surrounded by a self-assembled monolayer of thiolate ligands. In particular, we focused on Au_{144} MPC, a gold cluster stabilized by 60 thiolated ligand, with a molecular weight of 36597 Da (when protected by phenylethanethiol) and a gold core of 1.6 nm. Recent findings about the MPC size-dependency in cancer treatment suggest that particularly small MPCs, could provide particuarly good candidates for drug-delivery. In this context, $Au_{144}(SR)_{60}$ has never been used.

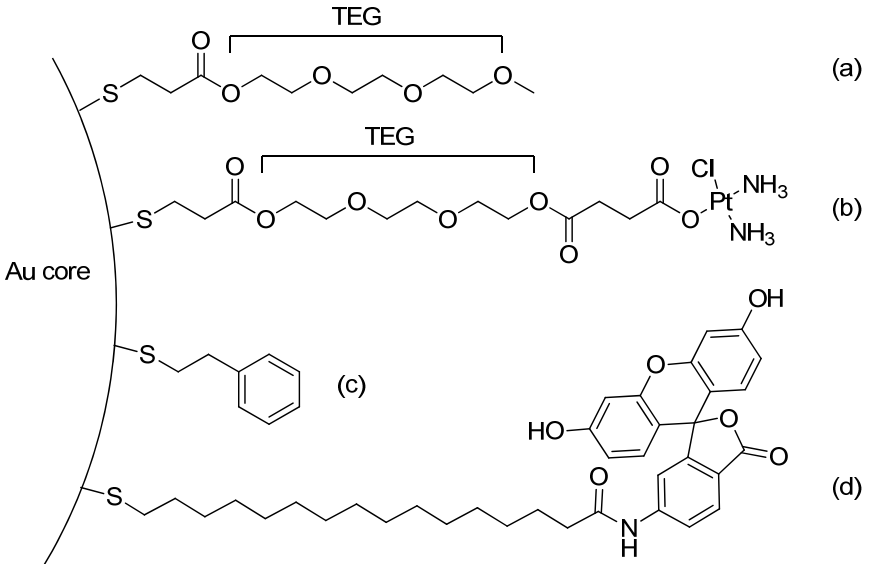

Figure 3 – *Chemical structure of TegMe (a), TegCOOH bound to cisplatin (b), phenylethanethiol (c), Fluo ligand (d).*

In this thesis, we prepared the native cluster as protected by 60 phenylethanethiolate ligands (Figure 3-c), Afterward, we took advantage of the possibility of modifying the monolayer, which opens a wide range of possibilities to refine and improve the system. As a first modification, we introduced a short thiolated triethylene glycol (TEG) (Figure 3-a) into the monolayer: this was meant to impart biocompatibility and make the MPC water-soluble. This is a key step to enable derived MPCs to disperse in human fluids for therapeutic purposes. Thus, by making what hopefully resulted to be a stealth MPC, we also expected the thiolated TEG monolayer could prevent early RES clearance, thereby increasing the lifetime of the nanocluster throughout the systemic vasculature and lowering its cytotoxic effect. This thiolated ligand was incorporated into the monolayer via a ligand-place exchange reaction, where the exogenous thiols substitute those present in the native monolayer. Donkers *et al.* studied deeply this kind of process on $Au_{144}(SC_2H_4Ph)_{60}$ and found that the number of ligands exchanged after 4 days ranges from 21 to 28 (out of 60 ligands in the monolayer), which corresponds to an exchange of 35-50% [23]. In our case, the resulting MPC would gain the ability to dissolve in an aqueous medium (thanks to the presence of TEG ligand) but without losing its solubility in organic solvents (thanks to the remaining phenylethanethiolate ligands). As consequence, both endocytic pathway and passive diffusion through cell membranes could be possibly active

as internalization routes, thereby increasing the chance of the MPC cellular uptake. The UV-vis absorption spectrum of these MPCs was checked after each functionalization step: a change in the spectrum would, in fact, suggest size modification because the size of nanoclusters and their optical properties are strongly related.

A second MPC was prepared by taking advantage of the knowledge acquired in the first synthesis. A second TEG ligand was introduced, together with the first one, in the monolayer via ligand-place exchange reaction. The two TEG ligands share the same thiolate tether, an ester moiety and a TEG portion. However, the terminal region is different: whereas TegMe (Figure 3-a) ends with methyl group, TegCOOH carries a carboxylic group, introduced by reaction with succinic anhydride: this functional group was introduced to bind eventually the anticancer agent, cisplatin (Figure 3-b).

The therapeutic active cisplatin-MPC conjugate, the third MPC, was prepared by making a bond between carboxylic acid of TegCOOH, already present in the monolayer, and cisplatin: this bond is stable under physiologic conditions, but it has been reported to cleave at low pH. Indeed, the low pH is an intrinsic characteristic of tumor cells, and also the pH within the endosomes decreases: this feature could promote the release of cisplatin after cellular internalization. The active compound could thus diffuse inside the cell and reach the nucleus [40], forming cisplatin-DNA adducts that interfere with DNA replication and transcription [32].

To summarize, since the aim of this thesis was to check whether Au_{144} MPC is a valuable candidate for drug-delivery in cancer treatments, we synthesized several MPCs, designed to be internalized and tested in cancer cells. Their chemical characterization was carried out by thermogravimetric analysis and ^{1}H-NMR, UV-visible, IR, and XPS spectroscopies. These MPCs were then tested for *in vitro* cytotoxic activity against adenocarcinoma HeLa cells. Since association as function of time, concentration and temperature studies, and intracellular localization experiments required the MPCs to be detectable by fluorescence spectroscopy, two more MPCs were prepared by introducing also a fluorescent ligand in the monolayer (Figure 3-d).

The outcome derived from this study, as detailed later, highlights the advantages of using of Au_{144} for drug delivery, and may open unprecedented routes to treat cancer.

2 Experimental

2.1. Chemicals

The following solvents, salts, and reagents were commercially available and used as received.

Solvents. Dichloromethane (VWR, ≥ 99.8% HPLC grade), Tetrahydrofuran (THF, VWR, ≥ 99.5%), Ethyl acetate (Sigma Aldrich, ≥ 99.5%), Acetonitrile (Sigma-Aldrich, ≥ 99.9%), Chloroform (Sigma-Aldrich, ≥ 99.8%), Diethyl ether (Sigma-Aldrich, ≥ 99.8%), Petroleum Ether (J.T. Baker, bp 40-65°C) n-Hexane (Carlo Erba ≥ 95.0%), Ethanol (Fluka, ≥ 99.8%), Water (Merck, HPLC grade). Low conductivity water was obtained by using deionized water, further treated with the Milli-Q purification system.

Reagents. Gold (III) chloride trihydrate (Sigma-Aldrich, ≥ 99.9%), cis-Diamineplatinum (II) dichloride (Sigma-Aldrich, ≥ 99.9%), triethylene glycol monomethyl ether (Fluka, ≥ 97.0%), triethylene glycol (Sigma-Aldrich, ≥ 99.0%), S-Trityl-3-mercaptopropionic acid (Fluorochem ≥ 99.9%,), sodium borohydride (Sigma-Aldrich, ≥ 99.0%), succinic anhydride (Sigma-Aldrich, ≥ 99.0%), 4-(dimethylamino)pyridine (DMAP, Fluka, ≥ 99.0%), trityl chloride (Sigma-Aldrich, ≥ 97.0%), 3-mercaptopropionic acid (Sigma-Aldrich, ≥ 99.0%), triethylamine (Sigma-Aldrich, ≥ 99.0%), pyridine (Fluka, ≥ 99.0%), trifluoracetic acid (Sigma-Aldrich, ≥ 99.0%), triisopropylsilane (TIIS, Sigma-Aldrich, ≥ 99.0%), tetramethyl silane (TMS, Fluka, ≥ 99.5%), 1-ethyl-3-(3-dimethylaminopropyl)carbodiimide hydrochloride (EDC·HCl, GL Biochem, ≥ 99.0%,), 1-hydroxy-7-azabenzotriazole (HOAt, GL Biochem, ≥99.0%), calcium chloride (VWR, purified granules 2-5 mm), potassium bisulfate (Fluka, ≥ 98.0%).

Some precursors for the synthesis of ligands were already available in the laboratory from previous research: Ph_3C-S-$(CH_2)_{15}$-CONH-Fluo.

Other. Silica gel (Merck, pore size 60Å, 230-400 mesh), Silica gel on TLC PET-foils (Fluka), Sephadex™ LH-20 (GE Healthcare).

2.2. Cell culture and mantainance

The experiments were performed on one *in vitro* system, established epithelial model cell line HeLa. This was used to examine the effect of the gold MPCs on malignant tumors.

The HeLa cell line is an adherent type derived from Homo sapiens. These epithelial cells were obtained from the cervix of a patient with adenocarcinoma. The complete medium for this cell line is Dulbecco's Modified Eagle Medium (DMEM) (Gibco), supplemented with 10% fetal calf serum (FCS) (EuroClone) and 1% Penicillin-Streptomycin (Pen-Strep, Gibco). Culture flasks (Becton Dickinson) were passaged three times a week.

2.3. Instruments and methods

Thin Layer Chromatography. The reaction progress was followed by thin layer chromatography (TLC) using 0.25 mm TLC PET-foils with Silica gel (Sigma Aldrich, Fluka Analytical). The visual identification was performed with UV light for compounds with aromatic and fluorescent groups, or with Iodine vapors/ $KMnO_4$ for most organic compounds.

Flash Chromatography. This chromatography was performed with Silica gel (pore size 60Å, 230-400 mesh, Sigma Aldrich, Merck) as the stationary phase.

Size-Exclusion Chromatography. Size exclusion chromatography (SEC) was performed with Sephadex™ LH-20 (GE Healthcare, granulometry 25-100 μm) as the stationary phase. For equilibration and mobile phase it was used Dichloromethane.

Fluorescence Spectroscopy. Fluorescence spectra were taken in MilliQ Water, Tetrahydrofuran and Tetrahydrofuran:Methanol 9:1 solutions with a Varian Cary®

Eclipse Fluorescence Spectrophotometer. The experiments were carried out at room temperature, acquiring both excitation and emission spectra with different wavelengths. Spectra were elaborated and plotted using SigmaPlot 9.0 software.

FT-IR Absorption Spectroscopy. Both the solid-state (KBr) and film (on KBr disk) IR absorption spectra were recorded with a Perkin-Elmer model 1720X FT-IR spectrophotometer, nitrogen-flushed, equipped with a sample-shuttle device, at 2 cm^{-1} nominal resolution, and averaging 25 scans.

UV-Vis Absorption Spectroscopy. UV-vis spectra were taken in Water, Tetrahydrofuran and CH_2Cl_2 solutions with a Thermo Scientific Evolution 60S UV-vis spectrophotometer. The MPC concentrations were chosen to provide an optical absorbance A near 400 nm of ~1.0. The experiments were carried out at room temperature, the absorption spectra were recorded from 300 to 1000 nm, and the contribution of the background was accounted for.

Nuclear Magnetic Resonance Spectroscopy. ^{1}H-NMR spectra were obtained by using a Bruker model AC 200 spectrometer or a Bruker model AM 400 spectrometer. Chloroform-d (Sigma Aldrich, ≥ 99.8%), deuterium oxide (Sigma Aldrich, 99.9 atom % D), and methanol-d_4 (Euriso-Top, 99.8%) were used as the solvents. Chemical shifts (δ) are reported as parts per million (ppm) downfield from TMS.

Thermogravimetric Analysis. Thermogravimetric analysis (TGA) was carried out with a Discovery Q5000 Thermogravimetric Analyzer (TA Instruments) working in Hi-Res Ramp mode: ramp 1.5-50 °C/min (depending on the rate of mass loss with temperature), resolution 4. TGA curves were recorded under a working N2 flux equal to 25 mL min-1 in the range of 25 to 900 °C. The measurements were carried out on carefully dried, accurately weighed 2-4 mg cluster samples and in an open platinum pan.

MTS Assay. The MTS (3-(4,5-dimethylthiazol-2-yl)-5-(3carboxymethoxyphenyl)-2-(4-sulfophenyl)--2H-tetrazolium) assay is a colorimetric assay for measuring the activity of mitochondrial enzymes that reduce the tetrazole into a formazan upon

incubation. The formazan product of MTS reduction is soluble in tissue culture medium and has an absorbance maximum at 490-500 nm. This reaction only takes place when mitochondrial reductase enzymes are active, and therefore the conversion can be directly related to the viability of cells in culture [71]. The experiment was performed by seeding 150 µl of 10,000 cells/well to designated wells of a flat-bottom 96-well plate. Treatment with MPCs samples was done on the second day followed by a 24-hour incubation at $37^{O}C$ in 5% CO_2. On the third day, treatments were removed by aspiration then replaced with DMEM-MTS (100 µl DMEM + 10 µl MTS) (Promega) solution, to be incubated for about one hour until color development. Optical densities were obtained by reading at 492 nm with Biotrak II - Plate Reader (Amersham Bioscience). All treatments were done in replicate, with negative control being the media and positive control being Cisplatin treated cells. Any cytotoxic activity resulted to a yellowish end product with a low optical density value. LD_{50} was calculated with linear regression method on Excel 2007, considering points of the curve showing linear decrease from 95% to 5% viability.

Lactate Dehydrogenase Assay. Lactate dehydrogenase (LDH) is a soluble cytosolic enzyme present in most eukaryotic cells. The increase of the LDH release into culture medium upon cell death due to damage of plasma membrane, results in increased measurable activity in culture supernatant, proportional to the number of lysed cells. A colorimetric method to measure LDH activity via a coupled reduction of tetrazolium salt into a red formazan product. The amount of the highly colored and soluble formazan can be measured at 490 nm [72].

The experiment was performed using 50 µl of supernatants removed by the MTS assay on the third day, placed in a new flat-bottom 96-well plate. It was added 50 µl of substrate solution (Promega), and incubated for about 30 minutes until color development. Optical densities were obtained by reading at 492 nm with Biotrak II - Plate Reader (Amersham Bioscience). All treatments were done in replicate, with negative control being the media and positive control being cells treated with 10 µl of lysing buffer (Promega) for 30 minutes. Any cytotoxic activity resulted to a deep pink end product with a high optical density value.

AnnexinV/Propidium Iodide Assay by Fluorescence Activated Cell Sorter (FACS). Cell death type is assessed using the stains Propidium iodide (PI) and AnnexinV-

FITC (AnnV). PI can intercalate into double-stranded DNA but can only penetrate plasmatic membranes of dying and dead cells, discriminating necrotic dead cells [73]. AnnV-FITC conjugate is highly fluorescent and provides quick and a reliable detection method for the externalized phosphatidylserine, one of the earliest indicators of apoptosis [74]. Cases labelled with both PI and AnnV-FITC, result are interpreted as late apoptosis. Quantification of cell death was done using FACS analysis, providing a method for sorting a heterogeneous mixture of biological cells into two or more containers, one cell at a time, based upon the specific light scattering and fluorescent characteristics of each cell [75].

In a flat-bottom 24-well plate, 500 µl of cells was seeded at 100,000 cells/well then incubated at 37^{O}C overnight. The following day, wells were treated with 300 µl of DMEM+10%FCS with the final treatment concentrations of MPCs. The cells were incubated for 18 hours at 37^{O}C. On the third day, cells were subjected to quantitative analysis. Using trypsin adherent cells were dislodged, resuspended in PBS then spun down at 200 g for five minutes. The supernatants were discarded then the pelleted cells were resuspended in 50 µl of Binding Buffer (Roche) in FACS tubes and then 1 µl AnnexinV-FITC (Roche), incubating it for 15 minutes at room temperature. Shortly before reading, 250 µl Binding Buffer and 15 µl of Propidium iodide (Sigma Aldrich) was added into the tubes. FACS was conducted by the FacsCanto Analyzer (Becton Dickinson) with excitation laser at 488 nm and peak emission at 617 nm. All treatments had two replications.

Measurement of Fluorescent MPCs Association to Cells by FACS. Fluorescein ligands conjugated to the MPCs emit light of approximately 520 nm. Using the 488 nm blue laser of the FacsCanto Analyzer (Becton Dickinson), MPCs association to cells was evaluated by measuring the mean fluorescence intensity (MFI) of individual cells after treatment for different hours in different concentrations up to 20 µM. All treatments were conducted in duplicate. Dead cells were excluded from the analysis by means of propidium iodide treatment.

Confocal Microscopy. In two 24-well plate, 500 µl of cells was seeded at 80,000 cells/well then incubated at 37^{O}C overnight free to grow confluent on glass coverslips The following day, wells were treated with 300 µl of DMEM+10%FCS with the final treatment concentration of 5 µm MPCs. One plate was incubated

for 3 hours at 37^{O}C and the other at 0°C. After 3x washing with PBS solution, samples were mounted onto glass slides with one drop 10 µl PBS solution and the coverglass was fixed. Analysis occurred directly under confocal microscope without any additional staining. Fluorescein ligands conjugated to the MPCs emit light of approximately 520 nm, upon 488 nm blue laser excitation. The protocols of acquisition used were provided by the instrument: FITC protocol and simple light protocol. In all cases, confocal acquisitions were performed with a TCS/SP2 Leica microscope and pictures are representative of at least three independent experiments. Images were processed and analyzed using Photoshop 7.0 software.

2.4 Synthesis and characterization

2.4.1. Thiolated ligands

*Ph_3C-S-$(CH_2)_2$-CO-TEG-CH3 (**1**).* To a solution of S-trityl-3-mercaptopropionic acid (3.01 g, 8.61 mmol) in CH_3CN anhydrous (140 ml), HOAt (1.25 g, 9.18 mmol) and EDC·HCl (1.85 g, 9.18 mmol) were added under rapid stirring at 50°C giving a clear yellow solution. It was followed by addition of a solution of Triethylene glycol monomethyl ether (4.24 g, 25.8 mmol) in CH_3CN anhydrous (10 ml) and DMAP (1.45 g, 11.8 mmol). After stirring for 24 hours at 50°C, the reaction mixture was dried under reduced pressure and purified with flash chromatography (eluent: petroleum ether/ethyl acetate, 3:2; Rf = 0.22) to give **1**, as a colorless dense liquid. Yield = 96%; ^{1}H-NMR (200MHz, $CHCl_3$-*d*) δ 2.30 (t, 2H, α-CH_2), 2.39 (t, 2H, β-CH_2), 3.40 (s, 3H, O-CH_3), 3.55-3.75 (m, 8H, O-CH_2), 3.65 (t, 2H, COOCCH_2), 4.21 (t, 2H, COOCH_2), 7.19-7.42 (m, 15H, 3Ph).

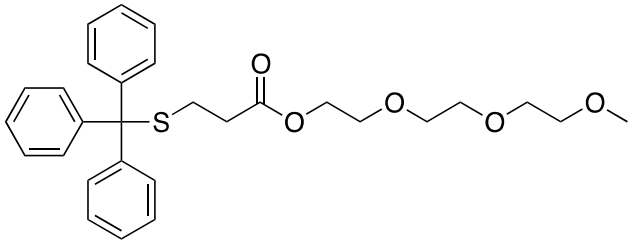

Figure 4 – *Chemical structure of Ph_3C-S-$(CH_2)_2$-CO-TEG-CH_3 (**1**).*

*Ph_3C-S-$(CH_2)_2$-CO-TEG-OH (**2**).* To a solution of S-trityl-3-mercaptopropionic acid (1.3 g, 3.73 mmol) in CH_3CN anhydrous (115 ml), HOAt (0.53 g, 3.8 mmol) and EDC·HCl (0.98 g, 5.11 mmol) were added under rapid stirring at 50°C giving a clear yellow solution. It was followed by addition of a solution of triethylene glycol (0.70 g, 4.69 mmol) in CH3CN anhydrous (3.5 ml) and DMAP (0.69 g, 5.77 mmol). After stirring for 24 hours at 50°C, the reaction mixture was dried under reduced pressure and purified with flash chromatography (eluent: petroleum ether/ethyl acetate, 3:2; Rf = 0.16) to give **2** as a colorless dense liquid. Yield = 55%; ^{1}H-NMR (200 MHz, $CHCl_3$-*d*): δ 2.30 (t, 2H, α-CH_2), 2.39 (t, 2H, β-CH_2), 3.55-3.75 (m, 8H, O-CH_2), 3.65 (t, 2H, COOCCH_2), 4.21 (t, 2H, COOCH_2), 7.19-7.42 (m, 15H, 3Ph).

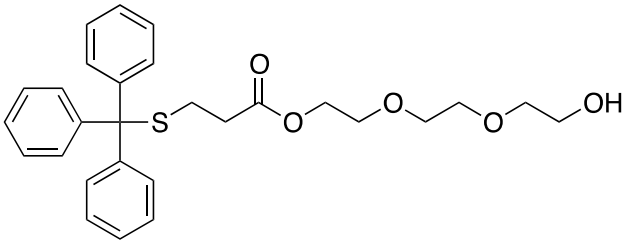

Figure 5 – *Chemical structure of Ph_3C-S-$(CH_2)_2$-CO-TEG-OH (2).*

*Ph_3C-S-$(CH_2)_2$-CO-TEG-CO-$(CH_2)_2$-COOH (**3**).* To a solution of **2** (1.02 g, 2.12 mmol) in $CHCl_3$ anhydrous (30 ml), pyridine (0.6 ml, 7.41 mmol) and succinic anhydride (0.75 g, 7.47 mmol) were added while slowly stirring. After stirring for 24 h at 65°C with reflux, the reaction mixture was dried under reduced pressure and then ethyl acetate (50 ml) was added. The crude was purified in a separation funnel by washing three times with a potassium bisulfate 10% solution (3x50 ml) and one time with deionized water (50 ml). The organic phase was collected and dried to give **3** as a colorless dense liquid. Yield = 93% (Rf **=** 0.44 in dichloromethane/ethanol 9:1); ^{1}H-NMR (200 MHz, $CHCl_3$-d): δ 2.27 (t, 2H, α-CH_2), 2.32 (t, 2H, β-CH_2), 2.65 (tt, 4H, $OCOCH_2CH_2COO$), 3.58-3.74 (m, 4H, O-CH_2), 3.64 (t, 4H, $COOCCH_2$), 4.14 (m, 4H, $COOCH_2$), 7.15-7.42 (m, 15H, 3Ph).

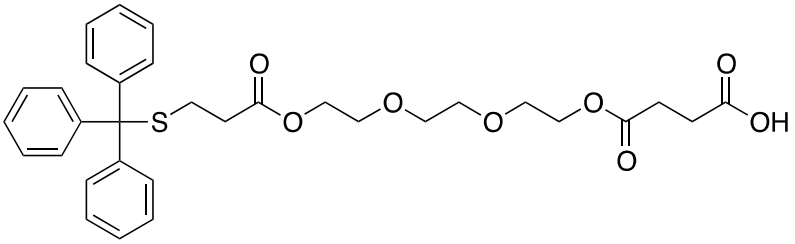

Figure 6 – *Chemical structure of Ph_3C-S-$(CH_2)_2$-CO-TEG-CO-$(CH_2)_2$-COOH (**3**).*

*HS-$(CH_2)_2$-CO-TEG-CH_3 (**4**).* Compound **1** (1.08 g, 2.18 mmol) was dissolved in 27.5 ml of a 7:2:1 mixture of CH_2Cl_2/trifluoroacetic acid/triisopropylsilane to give an intense yellow color. The solution was stirred for 15 minutes at room temperature, turning clear, and then the solvent was evaporated. The crude was dried under reduced pressure and then purified with flash chromatography (eluent: dichloromethane/ethanol 9:1; Rf **=** 0.65) to give **4** (TegMe), as a yellowish dense liquid. Yield = 96%; ^{1}H-NMR (200MHz, $CHCl_3$-*d*): δ 1.68 (t, 1H, SH), 2.69 (t, 2H, α-CH_2), 2.74 (t, 2H, β-CH_2), 3.39 (s, 3H, O-CH_3), 3.56-3.68 (m, 8H, O-CH_2), 3.65

(t, 2H, $COOCCH_2$), 4.28 (t, 2H, $COOCH_2$); IR (film on KBr): 2881, 2722, 2559, 1784, 1736, 1210, 1167, 1109 cm^{-1}.

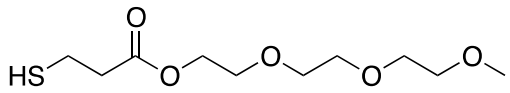

Figure 7 – *Chemical structure of HS-$(CH_2)_2$-CO-TEG-CH_3 (**4**).*

*HS-$(CH_2)_2$-CO-TEG-CO-$(CH_2)_2$-COOH (**5**).* Compound **3** (1.401 g, 2.41 mmol) was dissolved in 40 ml of a 7:2:1 mixture of CH_2Cl_2/trifluoroacetic acid/triisopropylsilane to give an intense yellow color. The solution was stirred for 15 minutes at room temperature, turning clear, and then the solvent was evaporated. The crude was dried under reduced pressure and then purified with flash chromatography (eluent: dichloromethane/ethanol 9:1; Rf **=** 0.22) to give **5** (TegCOOH) as a yellowish dense liquid. Yield = 95%; ^{1}H-NMR (200MHz, $CHCl_3$-*d*): δ 1.68 (t, 1H, SH), 2.65 (t, 2H, α-CH_2), 2.69 (t, 2H, β-CH_2), 2.67 (tt, 4H, $OCOCH_2CH_2COO$), 3.64-3.76 (m, 4H, O-CH_2), 3.66 (t, 4H, $COOCCH_2$), 4.15-4.32 (m, 4H, $COOCH_2$); IR (film on KBr): 3119 (broad), 2984, 2944, 2872, 2710, 2567, 1789, 1736, 1714, 1377, 1213, 1165 cm^{-1}.

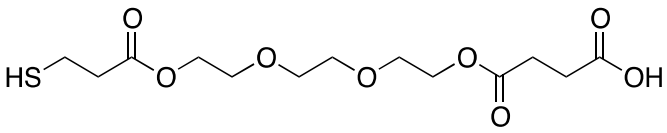

Figure 8 – *Chemical structure of HS-$(CH_2)_2$-CO-TEG-CO-$(CH_2)_2$-COOH (**5**).*

*HS-$(CH_2)_{15}$-CONH-Fluo (**6**).* Ph_3C-S-$(CH_2)_{15}$-CONH-Fluo (0.05 g, 0.06 mmol) was dissolved in 2.38 ml of a 7:2:1 mixture of CH_2Cl_2/trifluoroacetic acid/triisopropylsilane. The solution was stirred for 15 minutes at room temperature and then the solvent was evaporated. The crude product, a yellow orange solid, was washed with diethyl ether to remove the excess of trifluoroacetic acid by evaporation. The crude product was dissolved in a minimum volume of methanol (1 mL) and precipitated with petroleum ether, dropwise added. The product was filtered and dried to give **6** (Fluo Ligand) as yellow-orange solid. Yield: 94%; m.p.: 146-149°C; ^{1}H-NMR (200MHz, MeOH-d_4): δ 1.09-1.81 (m, 26H, 13CH2), 1.71 (t, 1H, SH), 2.43 (t, 2H, CH2-CO), 3.59 (m, 2H, S-CH2), 5.48 (s, 2H, OH), 6.57-7.15 (m, 6H, xanthene), 7.25 (s, 1H, NH), 7.38 (d,

1H, benzofuranone), 7.85 (d, 1H, benzofuranone), 8.12 (s, 1H, benzofuranone); IR (KBr): 3425, 2923, 2851, 2597, 1735, 1714, 1606, 1457, 1174 cm^{-1}.

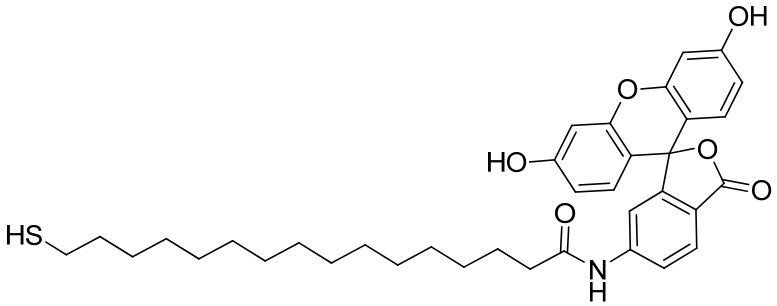

Figure 9 – *Chemical structure of HS-$(CH_2)_{15}$-CO-TEG-CONH-Fluo (**6**).*

2.4.2. Monolayer-protected gold cluster (MPC)

As it follows, we report the syntheses of Au_{144} and its MPC derivatives obtained by ligand-place exchange reactions, which are finally functionalized with cis-Pt. With respect to the latter synthetic procedure, we stress that the equivalent of the entering thiolated molecules are referred to the phenylethanethiol present in the monolayer of the Au_{144} precursor. For all the syntheses a pungent odor of phenylethanethiol released, meaning that the ligand-place exchange reaction occurred.

*Au_{144} (**7**).* For the synthesis of $Au_{144}(SC_2H_4Ph)_{60}$, we used the Brust-Schifrin two-phase approach [76] as implemented by Donkers *et al* [77]. In a 500 tri-neck rounded flask, 1.99 g (5.05 mmol) $HAuCl_4 \cdot 3H_2O$ was dissolved in 65 mL water. While stirring, 145 mL toluene and 3.20 g (5.85 mmol) of tetra-n-octylammonium bromide (TOABr) were added to the solution. After 30 minutes vigorous stirring the diphase mixture, the clear aqueous phase was removed and the remaining dark-red organic solution was cooled to 0 °C using an ice-bath. Phenylethanethiol (3.62 mL, 27 mmol) was then added to the solution, under slow stirring. The solution turned to light yellow and eventually, after 1.5 h, to opaque white. 2.4 g sodium borohydride (63.4 mmol), dissolved in 30 mL of ice-cold water, was then added to the mixture under vigorous stirring, resulting in the production of a black solution. The reaction was warmed to room temperature and stirred for next 24 hours. The crude sample was transferred to a separator funnel and washed thrice with 100 mL water. Toluene was then evaporated under reduced-pressure yielding a black product. Excess thiol was removed by adding ethanol (200 mL) to the crude product. After 2 h, the supernatant was discarded and the solid dispersed in 200 mL ethanol and left in the fridge overnight. This step was repeated thrice. Smaller nanoparticles, namely Au25, could be removed from the solid by washing with acetonitrile (10 x 10 mL). A crystalline black powder consisting of pure **7** was thus obtained, whose purity was checked by electrochemistry and UV-Vis and 1H NMR spectroscopy techniques.

*Au_{144}-TegMe (**8**).* To a solution of **7** (0.02 g, 0.55 µmol) in THF (4 ml), **4** (0.025 g, 0.1 mmol, 3 equivalent) was added under constant stirring and inert atmosphere (argon). After stirring for 24 h, the reaction mixture was dried under reduced

pressure, washed 8 times with n-hexane (10 ml), and then purified with size exclusion chromatography (with THF as the eluent) to **8** (35 mg).

*Au_{144}-[Teg(Me/COOH)] (**9**).* To a solution of **7** (0.02 g, 0.55 μmol) in THF (4 ml), **4** (0.012 g, 0.048 mmol, 1.5 equivalent) and **5** (0.017 g, 0.049 mmol, 1.5 equivalent) was added under constant stirring and inert atmosphere (argon). After stirring for 24 hours, the reaction mixture was dried under reduced pressure, washed 8 times with n-hexane (10 ml), and then purified with size exclusion chromatography (with THF as the eluent) to **9** (25 mg).

*Au_{144}-[Teg(Me/COOH)/Fluo] (**10**).* To a solution of **7** (0.02 g, 0.55 μmol) in THF (4 ml), **4** (0.011 g, 0.044 mmol, 1.35 equivalent), **5** (0.015 g, 0.044 mmol, 1.35 equivalent), and **6** (0.006 g, 0.01 mmol, 0.30 equivalent) were added under constant stirring and inert atmosphere (argon). After stirring for 24 hours, the reaction mixture was dried under reduced pressure, washed 10 times with n-hexane (10 ml), and then purified with size exclusion chromatography (with THF as the eluent) to **10** (52 mg).

Cisplatin functionalized MPCs

*Au_{144}-[Teg(Me/COOH-cis-Pt)] (**11**).* To a solution of **9** (0.03g, 0.82 μmol) in CH_2Cl_2 (3 ml), EDC·HCl (0.012 g, 0.062 mmol) in CH_2Cl_2 (2 ml) was added under rapid stirring. After 15 minutes, a yellow solution of cis-Pt (0.019 g, 0.063 mmol) in CH_2Cl_2 (2 ml) was added to the mixture. The reaction mixture was left to react for 24 h, and a red precipitate was formed, which was then separated. The crude was dried under reduced pressure, and washed 8 times with n-hexane to give **11** (34.6 mg).

*Au_{144}-[Teg(Me/COOH-cis-Pt)/Fluo]-α (**12**).* To a solution of **10** (0.03 g, 0.82 μmol) in CH_2Cl_2 (3 ml), EDC·HCl (0.012 g, 0.062 mmol) in CH_2Cl_2 (2 ml) was added under rapid stirring. After 15 minutes, a yellow solution of CisPt (0.019 g, 0.063 mmol) in CH_2Cl_2 (2 ml) was added under rapid stirring. After 15 minutes, a yellow solution of cis-Pt (0.019 g, 0.063 mmol) in CH_2Cl_2 (2 ml) was added to the mixture. The reaction mixture was left to react for 24 h, and a red precipitate was formed, which was then separated. The crude was dried under reduced pressure,

and washed 8 times with n-hexane to give **12** (49.2 mg).

*Au_{144}-[Teg(Me/COOH-cis-Pt)/Fluo]-b (**13**).* To a solution of **11** (0.005 g, 0.13 µmol) in THF (2 ml), 6 (0.0015 g, 2.34 µmol, 0.3 equivalent) was added under constant stirring and inert atmosphere (argon). After stirring for 24 hours, the reaction mixture was dried under reduced pressure, washed 10 times with n-hexane (10 ml), and then purified with size exclusion chromatography (with THF as the eluent) to give **13** (4.5 mg).

3 Results and discussion

3.1 Synthesis of water-soluble Au144

As described in the experimental section, we synthesized and employ Au_{144} as the precursor for suitably functionalized water-soluble MPCs. Au_{144} feature a 1.6 nm core consisting of 144 atoms of gold, which is surrounded and protected by 60 thiolate ligands; we used namely phenylethanethiol. It was isolated for the first time back in 1996 by Whetten and co-workers [78] and since then its physicochemical properties have been extensively studied [79] [80] [81]. Au_{144} plays an important role in the study of gold nanoclusters because it lies in between smaller (e.g. $Au_{25}L_{18}$) showing a distinct moleculelike behavior (such as well-defined HOMO-LUMO gap) and the larger Au nanoparticles exhibiting the surface plasmon resonance band. The research group of Prof. Maran is among the few ones worldwide that has the expertise in the synthesis and characterization of this kind of MPCs.

The advantages of using such small nanoclusters rely on the fact that their size is in the same range of, and therefore compatible with, that of biomolecules such as enzymes, antigens and antibodies, and biomolecular receptors. Thus the two classes of materials are structurally compatible. Nanometer size gold nanoparticles can provide a fertile ground for the emerging biomedical applications, such as targeted entry into cells and DDS for cancer treatment.

The use of Au_{144} for drug delivery is believed to provide insights into this emerging field, and the outcome derived from this study might offer unprecedented opportunities to treat cancer. They can be potentially applicable for targeted delivery and/or efficient release of drugs, thereby opening a new era toward personalized medicine.

To achieve these goals, a precise control of the MPC size and the monolayer properties is of fundamental importance. The former can be attained thanks to well-known and proven synthetic procedures, which are employed in our laboratories, and that yield $Au_{144}[S\text{-}(CH_2)_2Ph]_{60}$. The latter, instead, represents the challenging part and main target of this thesis.

3.1.1 Synthesis of ligands for MPCs

Thiolated TEG ligands. For gold nanoparticles, where thiols are the most commonly used ligands, one can replace the native ligands of an MPC, prepared according to a well-studied synthesis, with exogenous thiols. This involves reacting the original MPC with a solution of exogenous thiolated ligands, leading to what it is known as the ligand-place exchange synthesis [23].

To achieve the goal of preparing MPCs capable of interacting with biological membranes and targeting the nucleus of tumor cell, thus the MPC must exhibit solubility in the cellular environment, which implies that they must be water-soluble at the same pH condition as the target cells, the properties of the candidate ligands need to be suitably engineered. Furthermore, MPCs should carry a "label" that allows them to be easily detected by, e.g., fluorescence microscopy. Last, but not least, they should be readily functionalized with the drug that will be eventually delivered where needed.

For the synthesis of water-soluble Au_{144} MPCs we use a thiolated ligand derived from triethylene glycol (TEG). In fact, TEG provides solubility in aqueous solvents without the need of using a longer pegylated chain, and may enable the use of derived MPCs in perspective studies employing human fluids for therapeutic purposes. Furthermore, the thiolated TEG monolayer could prevent the MPCs from being subject to early reticuloendothelial system clearance, thus increasing the life of the nanocluster throughout the blood-vessels [68].

We synthesized and employed two thiolated TEG ligands, as reported in the experimental section. One bears a methyl ether terminus, whereas the second a carboxylic acid group that will undergo further functionalization with cis-Pt. The rationale is to dilute the latter in the monolayer in order to control the number of carboxylic group available to bind the anticancer drug.

Thiol function addiction. To obtain *HS-$(CH_2)_2$-CO-TEG-CH_3*, monomethyl ether TEG was reacted with S-trityl-mercaptopropionic acid, using EDC·HCl and HOAt as coupling agents. *HS-$(CH_2)_2$-CO-TEG-CO-$(CH_2)_2$-COOH* was obtained by a two-step reaction. First, an excess of triethylene glycol was reacted as described in Section 2.4.1 to give the desired thiol function only at one end of the ligand. Any side product was removed by flash chromatography. Subsequently, an ester bond between the alcoholic group of the protected thiolated TEG and succinic

anhydride was formed, providing the new carboxylic function.

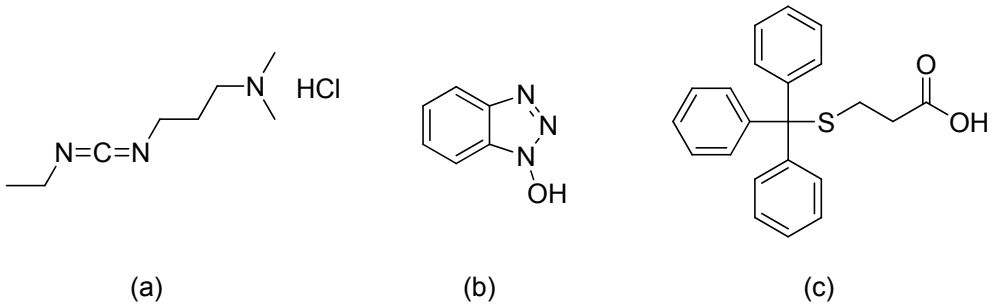

(a) (b) (c)

Figure 10 – *Representation of EDC-HCl (a), HOAt (b)and S-trityl-mercaptopropionic acid (c).*

The protection of the thiol function avoids the formation of disulfides, thus allowing safely storage of the ligands for a long time. The particular choice of triphenyl methane as the protecting group is due to some of its properties:

- ease of deprotection under mild conditions (1-5% trifluoracetic acid in dichloromethane);
- presence of an aromatic group which is detectable under UV-light during TLC analysis;
- ease of separation of the so-obtained compounds, using flash chromatography in apolar solvents.

Thiol function deprotection. For the MPCs synthesis it was necessary to remove (see Section 2.2.1) the trityl group and set the thiol free to react with gold. CH_2Cl_2, triisopropyl silane, and trifluoracetic acid were employed to obtain the desired thiolated ligand. Both products, TegMe and TegCOOH, were completely soluble in organic and aqueous solvents (dichloromethane, acetonitrile, tetrahydrofuran, dimethylformamide, dimethyl sulfoxide, water, alcohols). The characterization was carried out by NMR analysis and IR spectroscopy. Furthermore, NMR allowed to analyze the composition of the monolayer of the MPCs, providing a method to determine the amount of the different ligands forming the monolayer.

Fluorescent ligand. To visualize the MPCs in biological localization assays carried out by confocal microscopy, a fluorescent thiolated ligand was employed. The structure of ligand presents a fluorescent portion constituted by 6-amino-fluoresceine covalently bound to a hexadecanoic acid through an amide bond.

The length of the alkyl helped minimizing the undesired quench effect of the chromophore by the gold core. The thiolated fluorescent ligand was completely insoluble in any solvent, except methanol and THF. Figure 11 shows the UV-visible spectrum of the ligand, obtained in THF, showing an absorption peak at 452 nm at pH 6. It is worth noting that changing the pH from 5 to 8 resulted in a redshift of the absorption peak toward 520 nm with, a ten-fold increase of absorbance. Tsien reported that all fluorescein derivatives are strongly pH dependent, and show maximal fluorescence at pH ~7.0. The excitation maximum is usually at ca. 491 nm, whereas the emission peak, usually at 515 nm, depends (extent of protonation) on the pH which shifts toward shorter wavelengths along with a decrease of quantum efficiency [82].

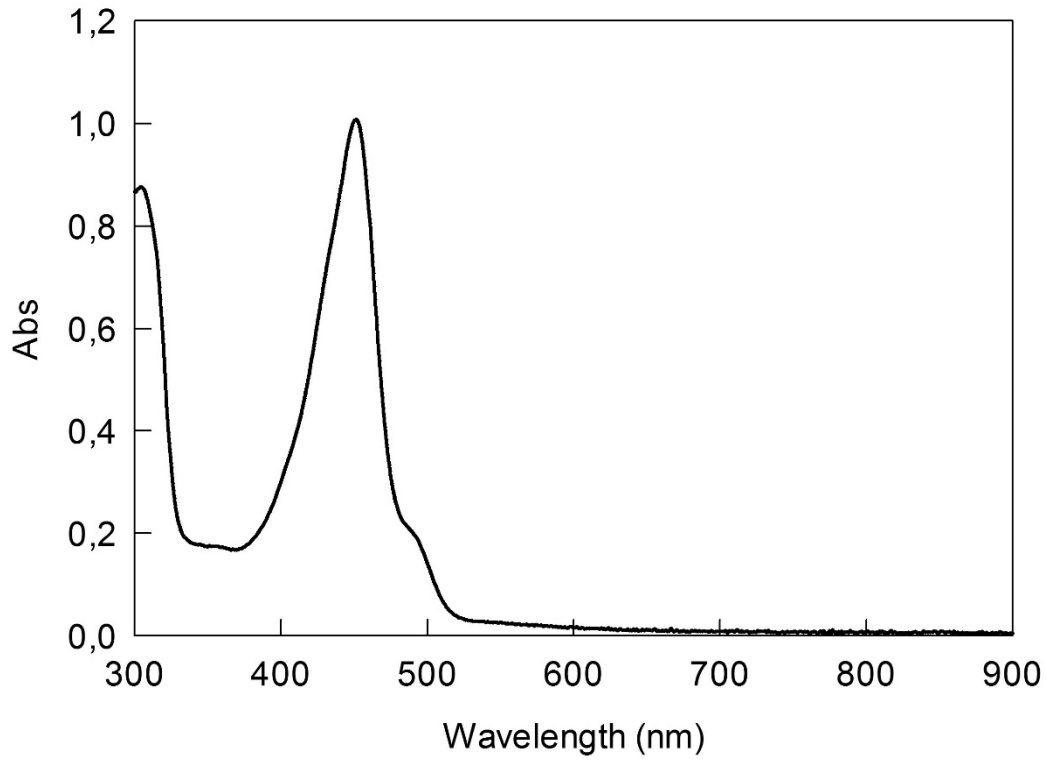

Figure 11 – *UV-Visible spectrum of Fluo ligand 1.6 mM in THF at pH 6 (—).*

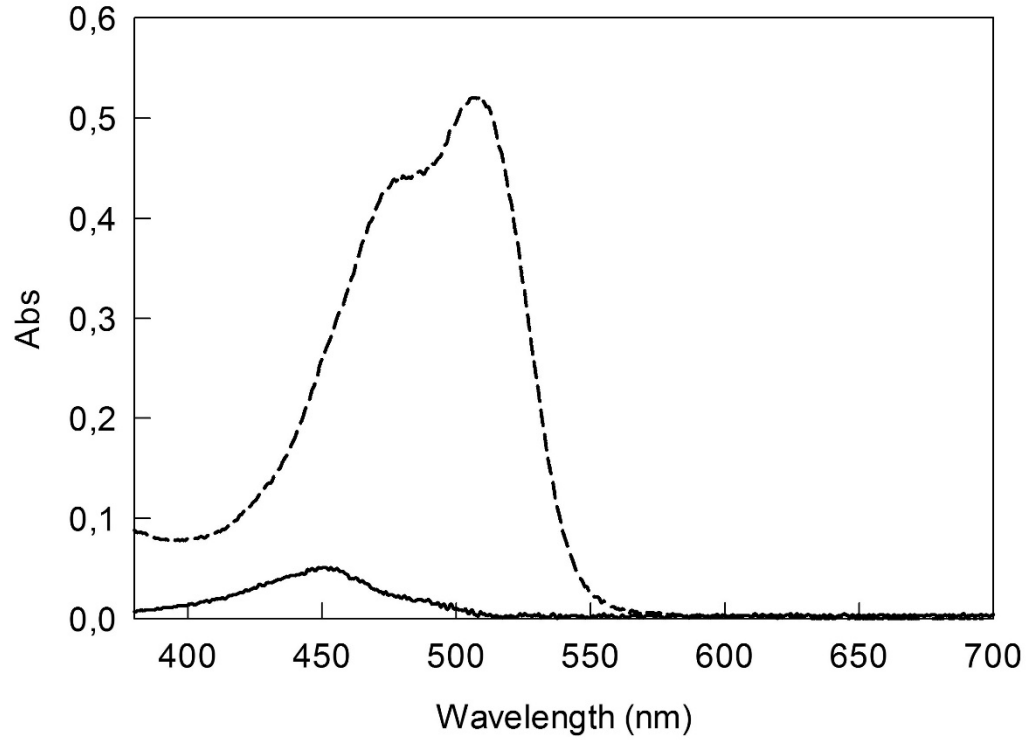

Figure 12 – *UV-Visible spectrum of Fluo ligand 14 µM in THF at pH 5 (—)and pH 8 (- - -).*

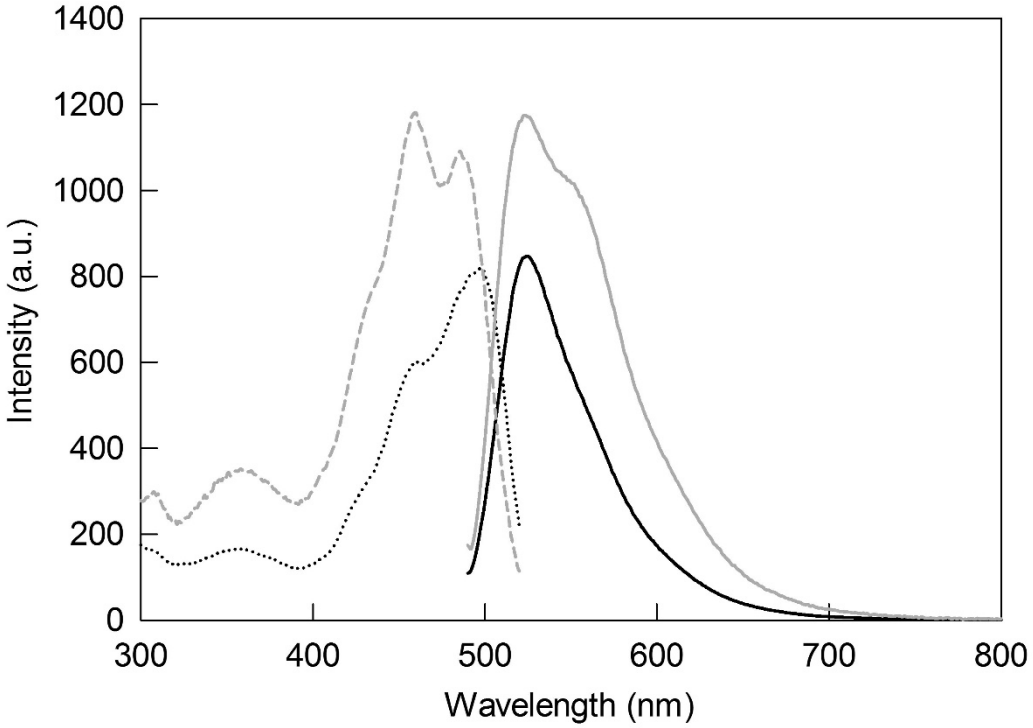

Figure 13 – *Excitation spectrum at λ_{em}=535 nm (• • •) and emission spectrum at λ_{ex}=485 nm(—) 3.5 µM and excitation spectrum at λ_{em}=535 nm (- - -) and emission spectrum at λ_{ex}=485 nm(—) 35 µM of Fluo ligand in THF/MeOH 9:1.*

From fluorescence studies on the Fluo ligand, in Figure 13 we show a clear dependence from concentration, resulting in an increase of fluorescence emission, when the concentration was increased 10 times. The maximum emission peak at 523 nm showed an increase of 40% when varying the concentration from 3.5 to 35 μM. This corresponds with findings previously reported by Tsien [82].

3.1.2 Synthesis of Au144 with HS-CH_2CH_2Ph ligand

The MPC synthesis followed a modified version of the two-phase preparation described by Brust et al. [76] and commonly used for the production of alkanethiolate coated MPCs. This procedure has been implemented by Donkers *et al.* [77]. The clusters were characterized by ^{1}H NMR spectrometry, IR and UV-vis absorption spectroscopies. As reported in Section 2.4.2, for the synthesis of $Au_{144}(SC_2H_4Ph)_{60}$, the reaction was carried using toluene as solvent in presence of TOABr. Smaller particles experience an increased driving force to aggregate to diminish surface energy, so a protective coating, or "capping" monolayer, is necessary during the synthesis to keep them in a finely dispersed state [83]. Phenylethanethiol was thus used as the protecting ligand.

Optical absorption spectra provide information on the electronic structure of MPCs. Whetten *et al*. [78] described the evolution of the absorption spectra as a function of the core size of alkanethiolate MPCs. The absorption pattern is largely independent of the monolayer. Jin *et al.* reported the UV-vis absorption spectrum of $Au_{144}(SC_2H_4Ph)_{60}$ showing an essentially featureless decay curve spanning the entire UV-vis spectrum [84], with only two barely observable shoulders at 520 nm (2.38 eV), i.e., where the surface plasmon absorption of gold is expected to emerge, and 710 nm (1.75 eV). This is not observed for nanoparticles with a diameter smaller than 2 nm due to the localization of the electrons in the molecular Au cluster orbitals.
The Au_{144} used for this thesis was characterized by UV-Vis to assess the quality of the MPC. In Figure 14 the UV-Vis spectrum shows the features of the 1.6 nm Au core.

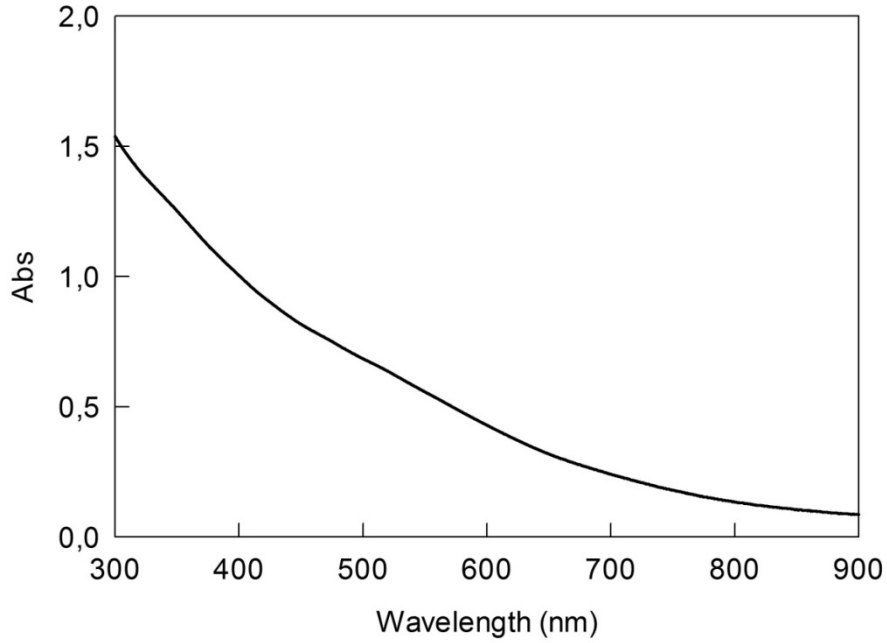

Figure 14 – *UV-Visible spectrum of Au144(S-C_2H_4-Ph)$_{60}$ 45 µM in THF (—).*

IR spectrum of the precursor Au_{144} is shown in Figure 15, and is used as a reference to compare the MPC with a mixed monolayer. The most relevant peaks visible in the spectrum of $Au_{144}(SC_2H_4Ph)_{60}$ are the tridentate sp2 C-H peaks at 3021, 3062, 3082 cm^{-1} and the C=C peak at 1600 cm^{-1} and 1495 cm^{-1}.They are attributed to phenylethanethiol, so its presence within the monolayer will be confirmed by display of these in the ligand exchanged MPCs IR spectra.

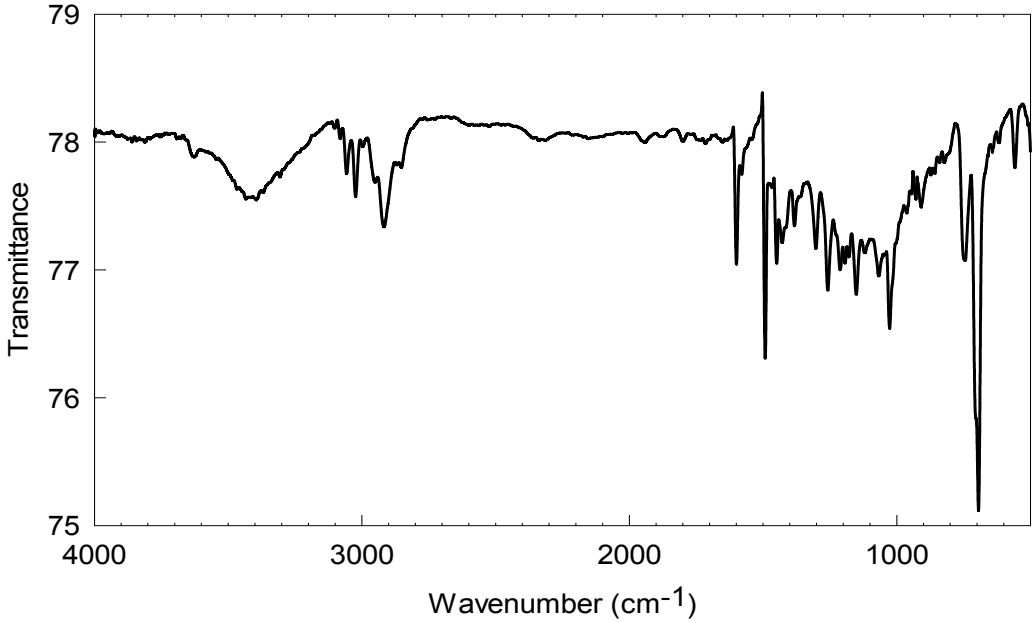

Figure 15 – *Infrared spectrum of Au144(S-C_2H_4-Ph)$_{60}$ (—).*

3.1.3 Synthesis of Au144 with TegMe Ligand via ligand exchange

To accomplish the modification of pre-synthesized $Au_{144}(SC_2H_4Ph)_{60}$, TegMe (**4**) was successfully employed. The exchange reaction is briefly depicted in Figure 16. As reported in Section 2.4.2 the exchange was carried out using a molar ratio of 3:1 for the TegMe and the phenylethanethiol already present in the monolayer. The MPCs were characterized by ^{1}H-NMR spectrometry, IR and UV-vis absorption spectroscopies, and thermogravimetric analysis (TGA).

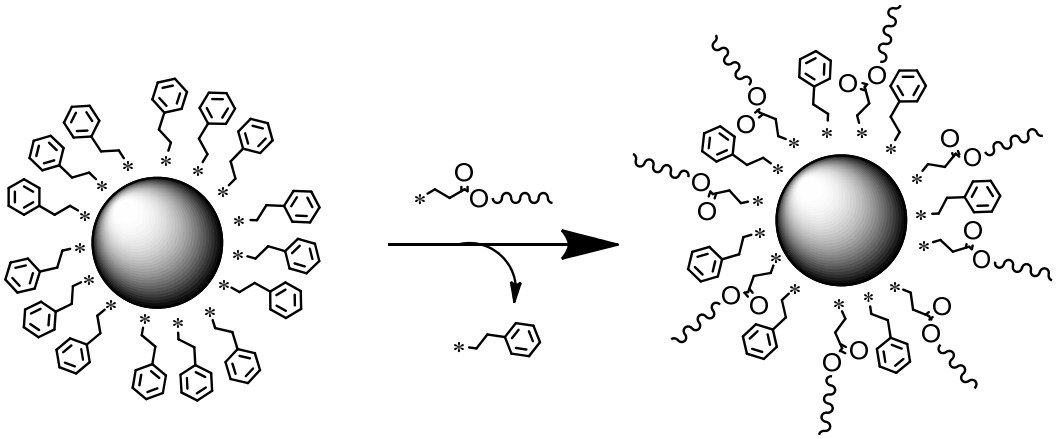

Figure 16 – *Ligand exchange reaction scheme to give Au144-TegMe (**8**)*

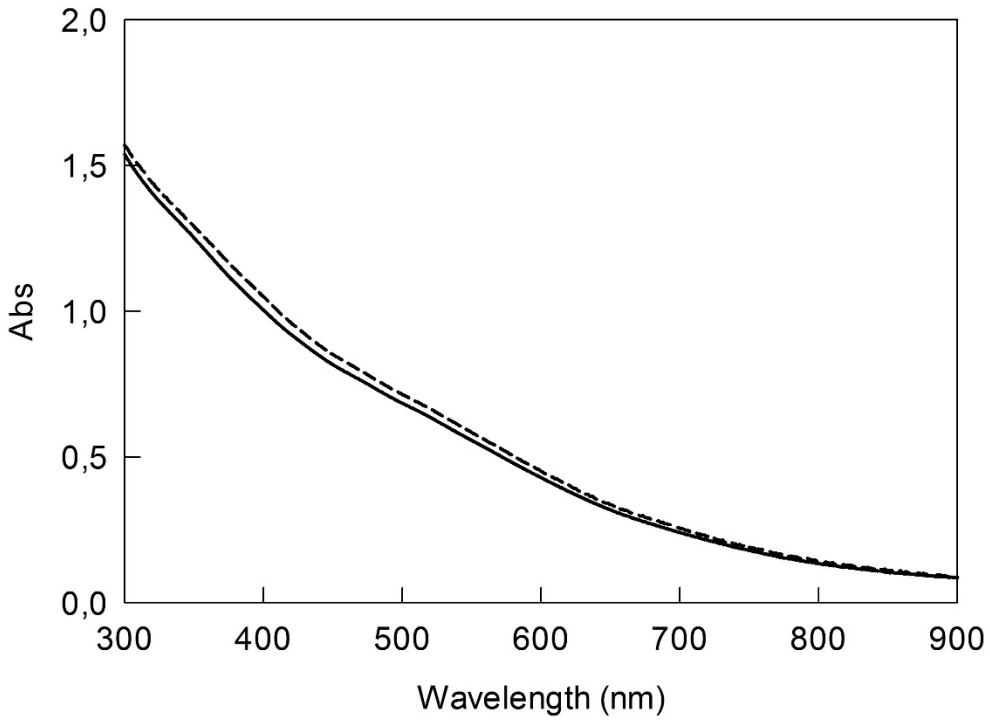

Figure 17 – *UV-Visible spectrum of Au144-TegMe (**8**) 32 µM (- - -) and Au144(S-C_2H_4-Ph)$_{60}$ 45 µM in THF (—).*

As shown in Figure 17, the UV-vis measurements confirmed that the behavior of the modified MPCs is the same as that of the starting MPC, indicating that no size modification occurred during the exchange reaction. In fact, the Au144-TegMe displays the same absorption pattern depicted in Figure 14. This is in keeping with the results of other ligand-place exchange reactions of $Au_{144}L_{60}$ [23] [81].

The resulting MPC is soluble in polar solvents, such as water, methanol, ethanol, or dimethyl sulfoxide, whereas the starting material is not. However, it still remains soluble in chloroform, dichloromethane and tetrahydrofuran. The monolayer composition and the extent of the ligand exchange was first estimated by means of ^{1}H-NMR carried out in deuterated chloroform. By considering the integrals of specific signals belonging to TegMe and phenylethanethiol (see below) it was possible to estimate the extent of exchange. The results are reported in Table 1.

Thiol	Range δ (ppm)	Integral	Protons	Ratio	Percentage	Molecules
Phenylethanethiol	6.41-7.22	4.51	5	0.90	47%	32
TegMe	4.26	2	2	1	53%	28
				1.90	100%	60

Table 1 – *Composition of thiols in the monolayer of Au144-TegMe (**8**) estimated by NMR measurements.*

For TegMe the chemical shift related to the methylene unit close to the ester bond of TEG with mercaptopropionic acid was taken as reference, while the phenyl group was considered for the phenylethanthiol. The extent of exchange was estimated to be 53%.

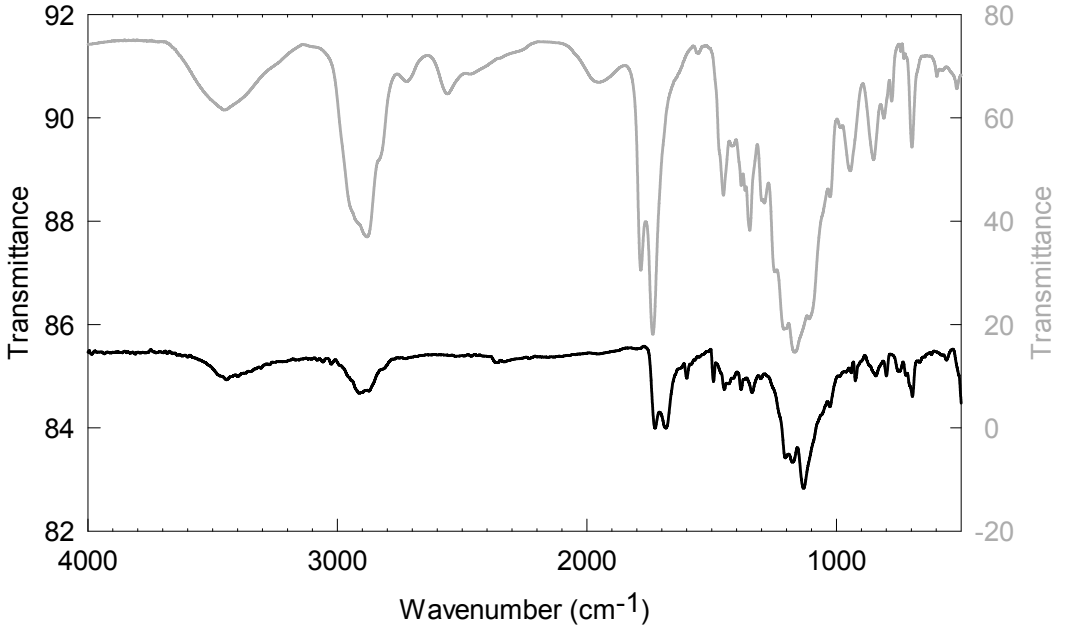

Figure 18 – *Infrared spectrum of Au144-TegMe (**8**) (—) and TegMe ligand (—).*

IR absorption spectroscopy was used as a complementary technique to confirm the presence of TegMe within the monolayer. In Figure 18, the IR spectra of Au_{144}-TegMe is shown and compared to that of TegMe ligand. As it can be observed, the spectra contain analogous features indicating that the TegMe was added to the monolayer. The phenylethanthiol's peaks are not so intense, anyway it is possible to recognize the tridentate sp2 C-H peaks at about 3060 cm^{-1} and the C=C peak at 1600 cm^{-1}.

TGA allows one to estimate the composition of the MPC. Previous thermogravimetric analysis of gold NPs protected by various types of thiolate ligand showed that the Au-S bond is broken at relatively high temperature (150 – 300°C) and the decomposition yields a metallic gold residue and volatile organic compounds, namely, the corresponding disulfides [85]. As displayed in Figure 19 for Au144-TegMe, the TGA trace displays a two stage desorption pattern which points to the presence of two ligands in the monolayer, with all due caution associated with the complexity of thermal decomposition process [86], an initial third step in which volatile solvents evaporates for T<100°C.

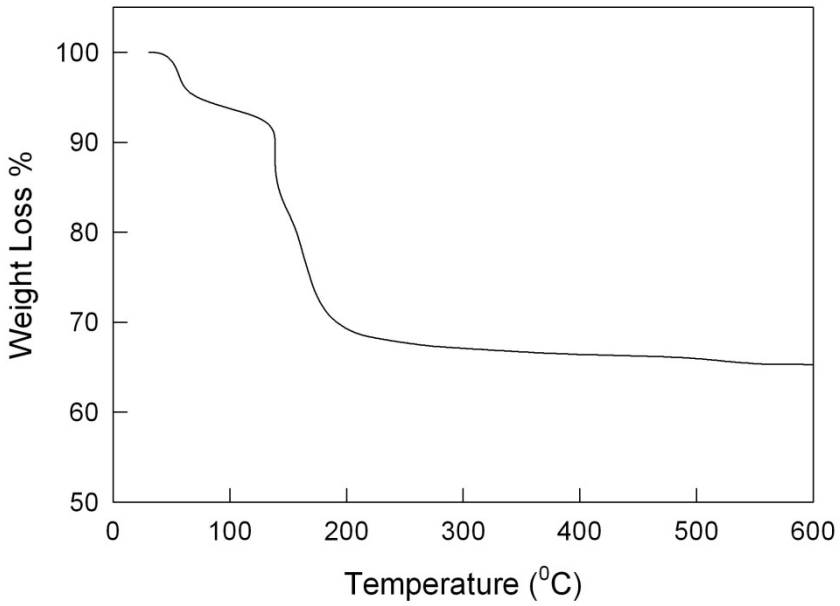

Figure 19 – *TGA analysis of Au144-TegMe (8)(—).*

The results, summarized in Table 2, highlight that the decomposition temperature (T_{dec}) of the ligands are different. TegMe decomposes at lower temperatures (T_{dec} ~ 101 – 154 °C) than that observed for phenylethanthiol (T_{dec}~ 155 – 232°C). The agreement with the ^{1}H-NMR data was generally good, confirming that an exchange of about 50% occurred.

	T°C Interval	%Weight	%Weight Loss
Residual Solvent	[0,101]	100,00%	6,00%
TegMe	[101,154]	94,00%	13,00%
Phenylethanthiol	[155,232]	81,00%	12,90%
Inorganic Residual	[233, …]	68,10%	68,10%

Table 2 – *Percentages of weight loss from TGA analysis of Au144-TegMe (**8**).*

3.1.4 Synthesis of Au144 with both TegMe and TegCOOH ligands via ligand exchange

To accomplish the modification of pre-synthesized $Au_{144}(SC_2H_4Ph)_{60}$, TegMe (**4**) and TegCOOH (**5**) in a 1:1 ratio were employed. The exchange reaction is briefly depicted in Figure 20. As reported in Section 2.4.2 the exchange was carried out using a molar ratio of 1.5:1.5:1 for the TegMe, TegCOOH and the phenylethanethiol present in the monolayer. The clusters were characterized as already described for the other MPCs.

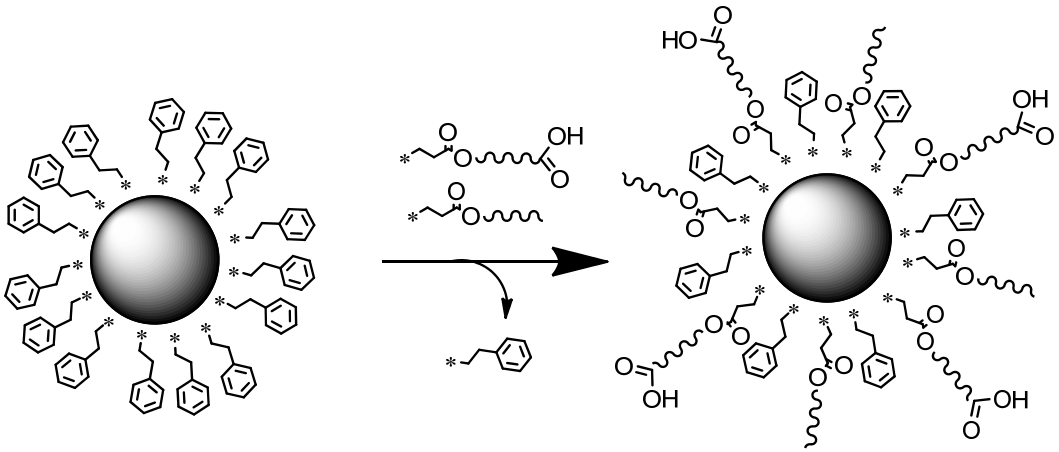

Figure 20 – *Ligand exchange reaction scheme to give Au144-[Teg(Me/COOH)] (**9**)*

As Figure 21 shows, the UV-vis results confirm that the behavior of the modified MPCs is very similar to that of the starting MPC, indicating that no size modification occurred during the exchange reaction. In fact, the Au144-[Teg(Me/COOH)] displays the same absorption pattern depicted in Figure 14.

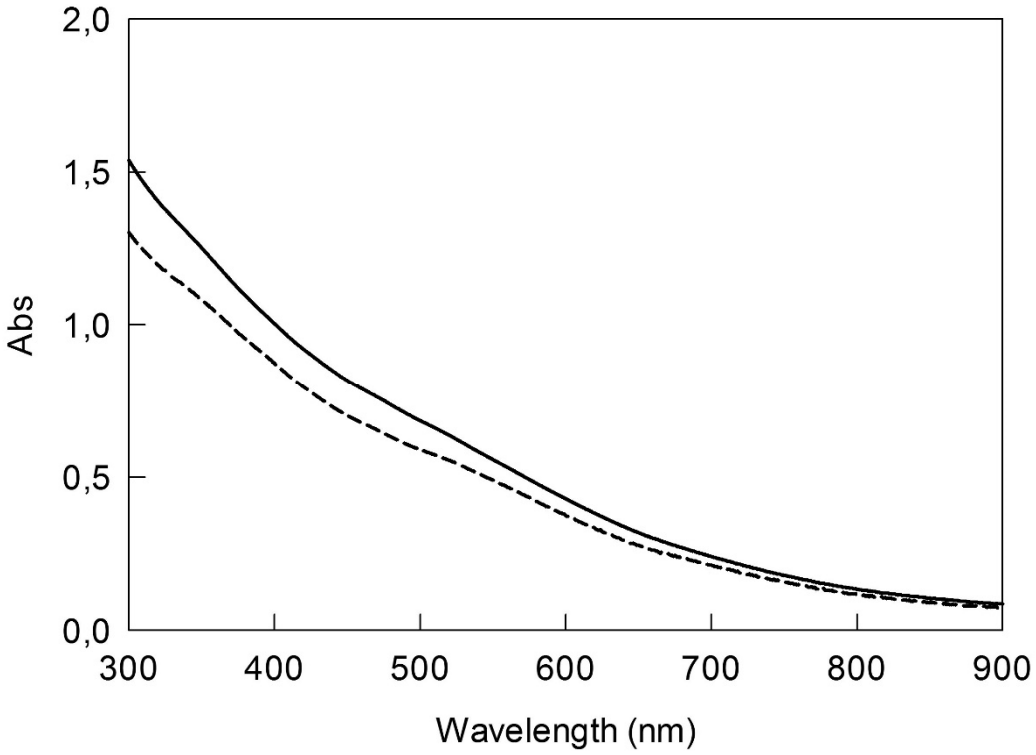

Figure 21 – *UV-Visible spectrum of Au144-[Teg(Me/COOH)] (**9**) 34 µM (- - -) and Au144(S-C_2H_4-Ph)$_{60}$ 45 µM in THF (—).*

The resulting MPC is more soluble in polar solvents, such as water, methanol, ethanol, or dimethyl sulfoxide, whereas the starting material is not. However it still remains soluble in chloroform, dichloromethane and tetrahydrofuran. The monolayer composition and the extent of the ligand exchange was estimated by ^{1}H-NMR, carried out in deuterated chloroform. By considering the integrals of specific signals belonging to TegMe, TegCOOH and phenylethanethiol, respectively, it was possible to estimate the extent of exchange. The results are reported in Table 3.

Thiol	Range δ (ppm)	Integral	Protons	Ratio	Percentage	Molecules
Phenylethanethiol	6.41-7.22	12.25	5	2.45	52%	31
TegMe	3.39	3	3	1	21%	13
TegCOOH	4.26	7.2(-2)	4	1.3	27%	16
				4.75	100%	60

Table 3 – *Composition of thiols in the monolayer of Au144-[Teg(Me/COOH)] (**9**) estimated by NMR measurements.*

As shown in Figure 22, for TegMe the chemical shift related to the terminal methyl group was taken as reference, while for phenylethanthiol the phenyl group was considered. To obtain the reference for TegCOOH, its two esteric-oxigen-bound methylenes, and one esteric-oxigen-bound methylene residue from TegMe, were taken into account with the proportion 4:2 hydrogens respectively of TegCOOH and TegMe. The total extent of exchange was estimated to be 48%, of which 21% for TegMe and 27% for TegCOOH.

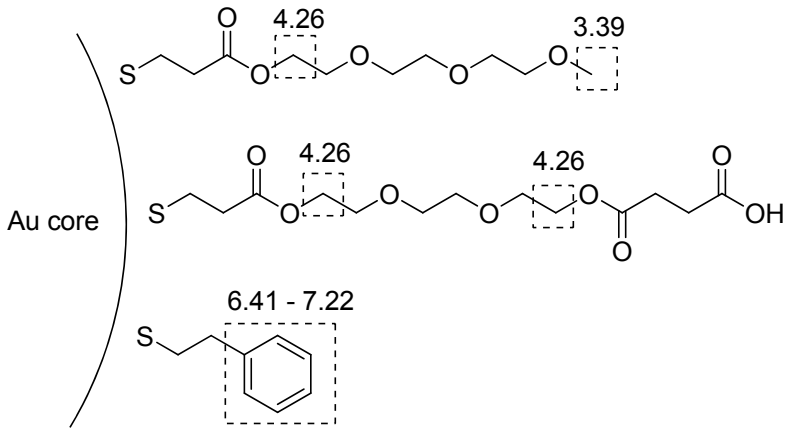

Figure 21 – *Scheme of proton chemical shifts used for integration and ligands ratio estimation.*

IR absorption spectra, shown in Figure 22, for Au144-[Teg(Me/COOH)] is compared to that of Au144-TegMe and $Au_{144}(SC_2H_4Ph)_{60}$. As it can be observed, Au144-TegMe and Au144-[Teg(Me/COOH)] are similar indicating that TegMe is included within the monolayer, but the intense carbonyl peak at 1732 cm^{-1} assessed the presence of TegCOOH in the monolayer too. The abscence of the S-H bond peak, which corresponds to the frequency of 2259 cm^{-1}, means that all ligands are present only attached to the gold core. Phenylethanthiol's peaks are not so intense, anyway it is possible to recognize easily the tridentate sp2 C-H peaks at about 3060 cm^{-1} and the C=C peak at 1600 cm^{-1}.

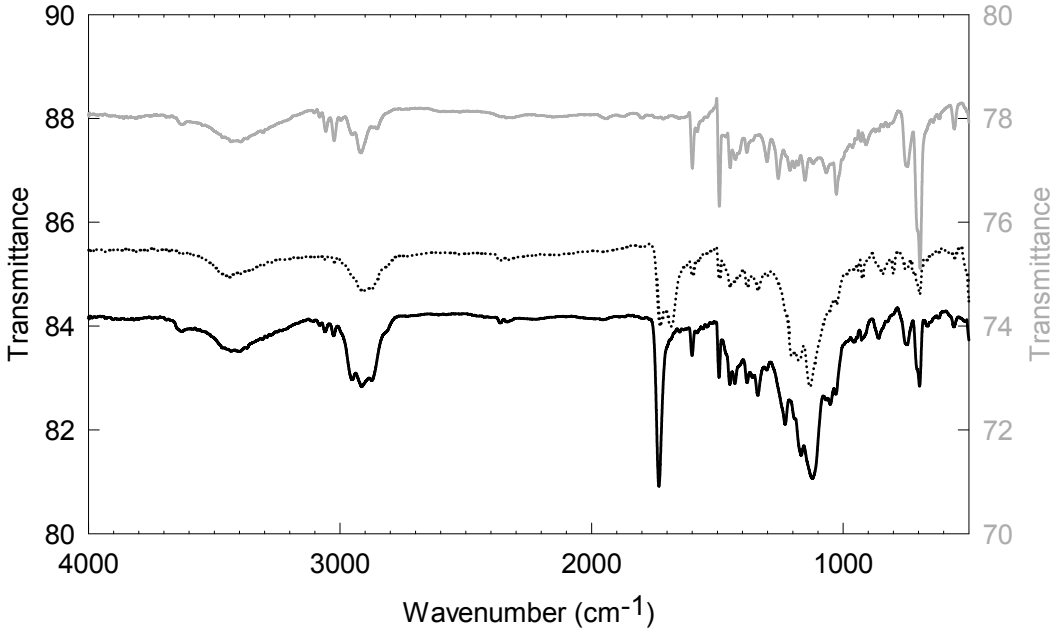

Figure 22 – *Infrared spectra of Au144-[Teg(Me/COOH)] (**9**) (—), Au144-TegMe (**8**) (• • •) and Au144(S-C_2H_4-Ph)$_{60}$ (—).*

In this case TGA, analysis did not allow estimating the composition of the MPC. The TGA traces display only one stage desorption and a prior step in which volatile solvents evaporates under 100°C. However an inorganic reside of about 64% and an organic portion of about 36% were estimated.

3.1.5 Synthesis of Au144 with both TegMe, TegCOOH and Fluo ligands via ligand exchange

To accomplish the modification of pre-synthesized $Au_{144}(SC_2H_4Ph)_{60}$ underwent ligand-place exchange reaction, briefly depicted in Figure 24, as reported in Section 2.4.2. A molar ratio of 1.35:1.35:0.3:1 for the TegMe, TegCOOH, Fluo ligand and the phenylethanethiol present in the monolayer was used. The MPCs were characterized as previous MPCs and with fluorescence spectroscopy.

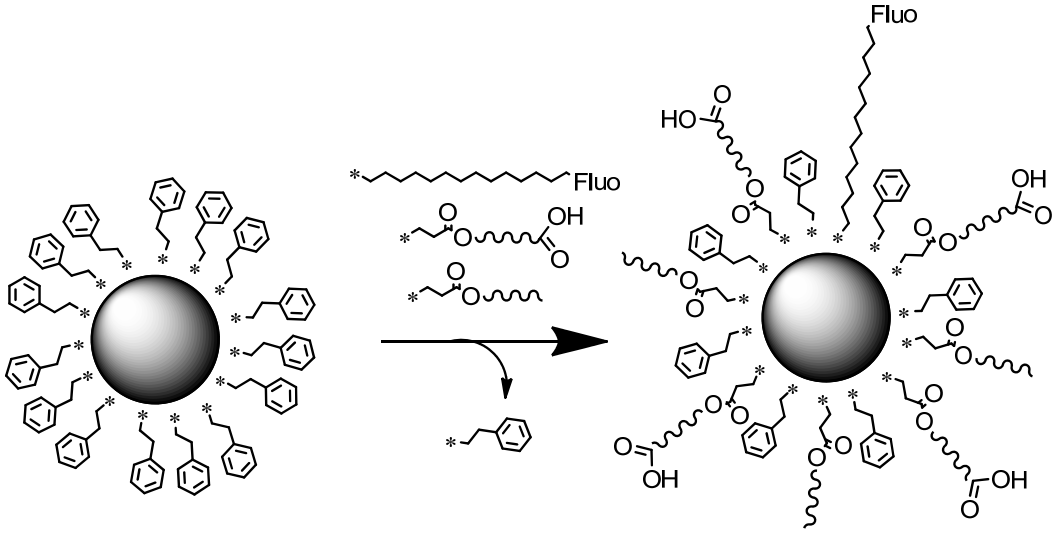

Figure 24 – *Ligand exchange reaction scheme to give Au144-[Teg(Me/COOH)/Fluo]* (***10***)

As shown in Figure 25, the UV-vis measurements confirm that the behavior of the modified MPCs is similar to that of the starting MPC, indicating that no size modification occurred during the exchange reaction. But the Au144-[Teg(Me/COOH)/Fluo] displays also the absorption pattern of the fluorescent ligand at pH 6 with its characteristic peaks at 434, 452 and 492 nm. It is worth noting to notice that in an alkaline medium the absorbance would have been higher for the pH-dependency of the Fluo ligand.

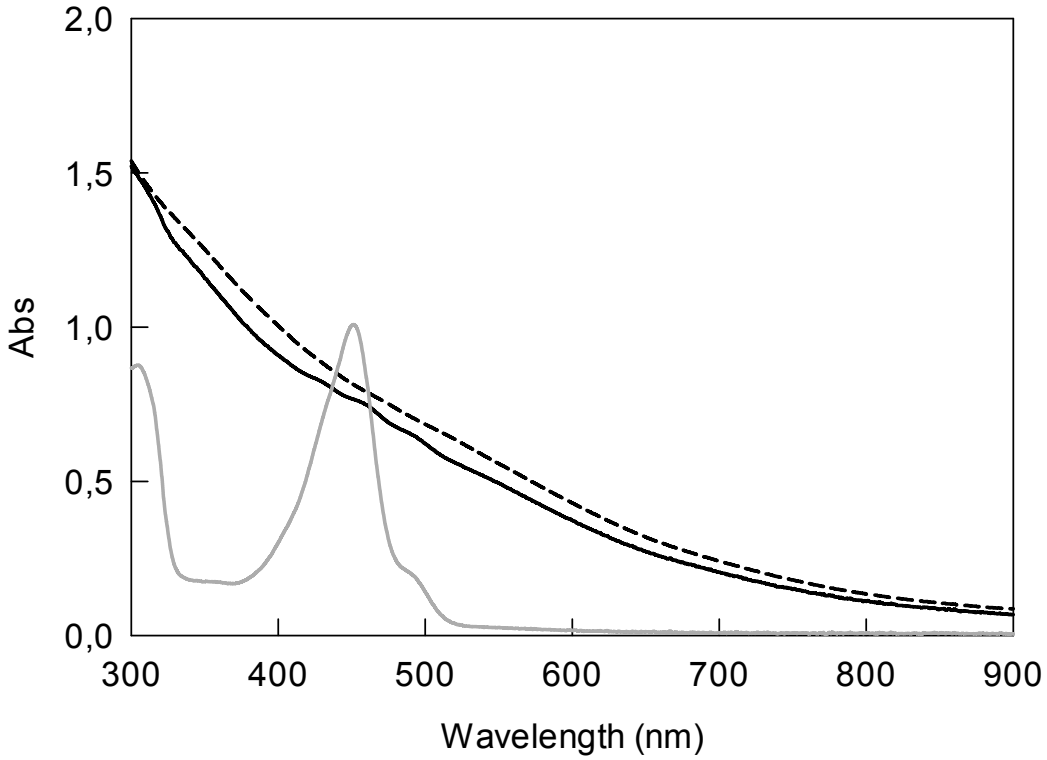

Figure 25 – *UV-Visible spectrum of Au144-[Teg(Me/COOH)/Fluo] (**10**) 10 µM (—), Au144(S-C_2H_4-Ph)$_{60}$ 45 µM (- - -) and Fluo ligand 1.6mM (—), all at pH 6 in THF.*

The solubility of this resulting MPC resembles the one of the MPCs previously described. The monolayer composition and the extent of the ligand exchange was estimated by means of ^{1}H-NMR carried out in deuterated chloroform. By considering the integrals of specific signals belonging to TegMe, TegCOOH, Fluo ligand and phenylethanethiol, respectively, it was possible to estimate the extent of exchange. The results are reported in Table 4.

Thiol	Range δ (ppm)	Integral	Protons	Ratio	Percentage	Molecules
Phenylethanethiol	6.41-7.22	18.88(-3.3)	5	3.12	49%	29
TegMe	3.39	3	3	1	16%	10
TegCOOH	4.26	8.55(-2)	4	1.63	26%	16
Fluo ligand	8.12	0.55	1	0.55	9%	5
				4.75	100%	60

Table 4 – *Composition of thiols in the monolayer of Au144-[Teg(Me/COOH)/Fluo] (**10**) estimated by NMR measurements.*

As shown in Figure 26, for TegMe the chemical shift related to the

terminal methyl group was taken as reference, while for Fluo ligand one of the benzofuranone hydrogens was considered. For phenylethanthiol the phenyl group was considered with six other benzofuranone hydrogens of Fluo ligand in the proportion 5:6. To obtain the reference for TegCOOH, its two esteric-oxigen-bound methylenes, and one esteric-oxigen-bound methylene residue from TegMe, were taken into account with the proportion 4:2 hydrogens respectively of TegCOOH and TegMe. The extent of exchange was estimated to be 51%, presenting 16% TegMe thiols, 26% TegCOOH thiols and 9% Fluo ligand.

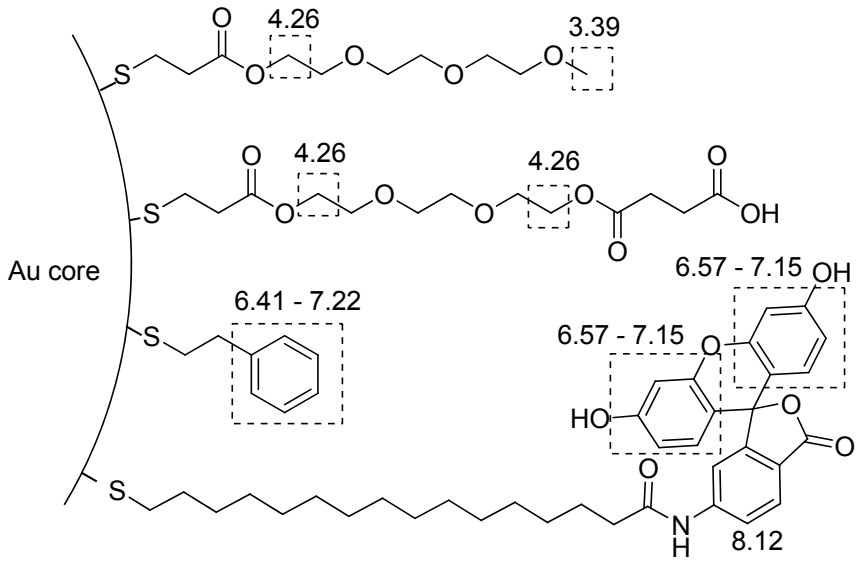

Figure 26 – *Scheme of proton chemical shifts used for integration and ligands ratio estimation.*

In Figure 27, the IR spectra of Au144-[Teg(Me/COOH)/Fluo] is reported and compared to those of Au144-[Teg(Me/COOH)] and Fluo ligand. As it can be observed, Au144-[Teg(Me/COOH)/Fluo] and Fluo ligand are very similar indicating that Fluo ligand is included within the monolayer, the spectrum also shows a broad band at 3200-3600 cm^{-1}, indicating the presence of –OH group. But the different area of the carbonyl peak at 1732 cm^{-1} attests the presence of TegCOOH in the monolayer too. The abscence of the S-H bond peak, which corresponds to the frequency of 2259 cm^{-1}, means that all ligands are present only attached to the gold core. However, the phenylethanthiol's peaks are mostly covered by the dominant presence of the Fluo ligand amide N-H at 3492 cm^{-1}, the O-H broad band at 3200-3600 cm^{-1} and the amide C=O peak at 1631 cm^{-1}.

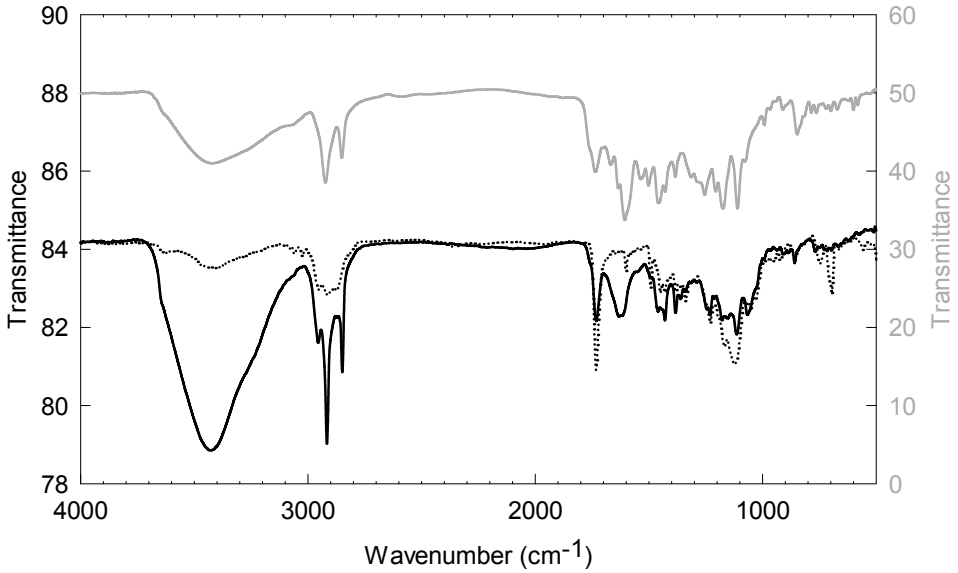

Figure 27 – *Infrared spectra of Au144-[Teg(Me/COOH)/Fluo] (**10**) (—), Au144-[Teg(Me/COOH)] (**9**) (• • •) and Fluo ligand (—).*

Au144-[Teg(Me/COOH)/Fluo] shows emission at 535 nm upon excitation at 485nm (Figure 28). The emission is dependent on the concentration of the emitter. However, the dependence is nonlinear. In fact, by comparing the outcome for 3.4 and 34 µM, one should expect a 10 fold increase in the emission intensity. A 60% decrease in fluorescence efficiency can be mainly attributed to quenching by the gold core.

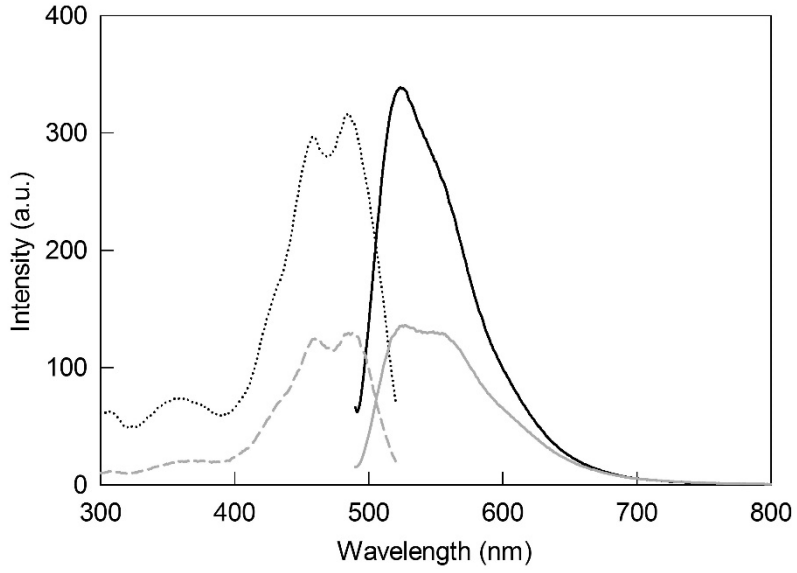

Figure 28 – *Excitation spectrum at λ_{em}=535 nm (• • •) and emission spectrum at λ_{ex}=485 nm(—) 3.4 µM and excitation spectrum at λ_{em}=535 nm (- - -) and emission spectrum at λ_{ex}=485 nm(—) 34 µM of Au144-[Teg(Me/COOH)/Fluo] (**10**) in THF/MeOH 9:1, at pH 6.*

Also in this case TGA analysis did not allow estimating the composition of the MPC. The TGA traces display only one stage desorption and a prior step in which volatile solvents evaporates under 100°C. The inorganic compound, which left a shiny gold residue on the pan was estimate to be 57%, while the organic residue was 43%

3.2 Functionalization of Au144 with cisplatin

Recently Puntes and co-workers reported the adsorption of cisplatin to gold colloids occurs via ionic interactions. In this case an uncontrolled fast release of the agent was observed when the conjugates were dispersed in ionic media [40]. The nanosystem we synthesized aimed to bind cis-Pt via complexation with the carboxylate groups present in the monolayer (previously inserted via ligand exchange) to give TegCOO-PtCl(NH_2)$_2$ species. The bond between carboxylic acid and Pt is known to be stable under physiologic conditions, but appears to break at acidic pH, resulting in the release of the active drug [40].

Au144-[Teg(Me/COOH-cis-Pt)]. To obtain the active anticancer MPC from Au144-[Teg(Me/COOH)], cisplatin was successfully employed for the complexation. A cartoon of the reaction is shown in Figure 29. As reported in Section 2.4.2 the reaction was carried using an excess of cisplatin as the monolayer of the MPC was completely exchanged by TegCOOH. The clusters were characterized as previously reported and with X-ray photoelectron spectroscopy (XPS).

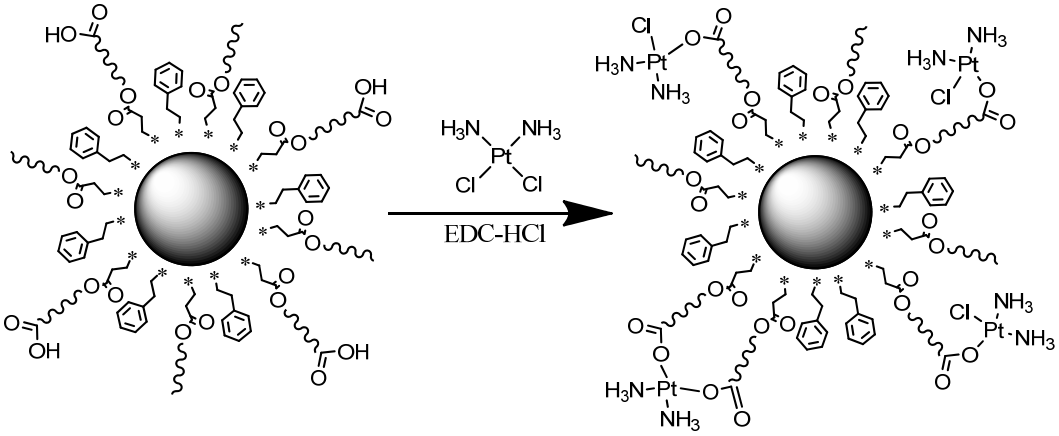

Figure 29 – *Ligand exchange reaction scheme to give Au144-[Teg(Me/COOH-cis-Pt)] (11)*

As Figure 30 shows, the UV-vis measurements confirm that the behavior of the modified MPCs is the same as that of the starting MPC, indicating that no apparent size modification occurred during the exchange reaction. In fact, the Au144-TegMe displays an almost featureless decay curve with the small shoulders at 450 nm, 520 nm and 710 nm. The former is also present in the spectrum of Figure 33.

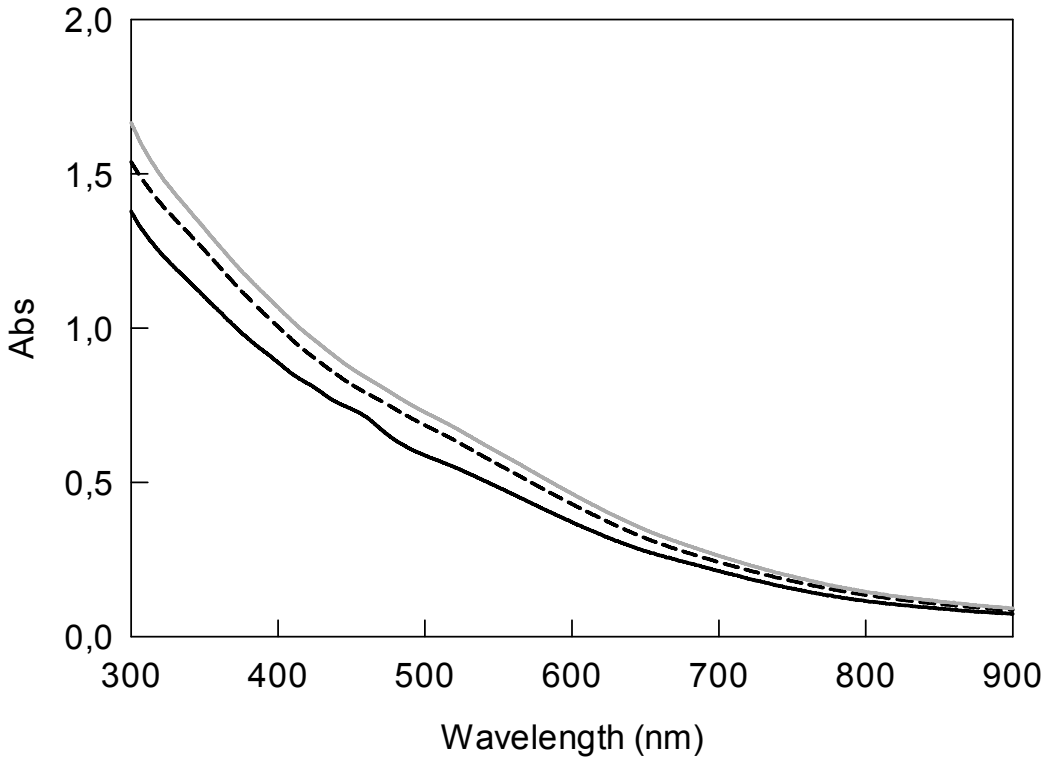

Figure 30 – *UV-Visible spectra of Au144-[Teg(Me/COOH-cis-Pt)] (**11**) 32 µM (—), Au144-[Teg(Me/COOH)] (**9**) 28 µM (—) and Au144(S-C_2H_4-Ph)$_{60}$ 45 µM in THF(- - -).*

This MPC shows essentially the same solubility displayed before reaction with cisplatin, but with slightly better solubility in water. The monolayer composition and the extent of the ligand exchange was estimated by ^{1}H-NMR carried out in deuterated acetonitrile. By considering the integrals of specific signals belonging to TegMe, TegCOOH and phenylethanethiol, respectively, it was possible to estimate the extent of exchange. The results allowed to estimate the composition of the monolayer to be 21 and 27 % for TegMe and TegCOOH respectively. The amount of phenylethanethiol exchanged was therefore 48% (about 30 ligands). The outcome suggests that the max maximum number of cis-Pt that can be bound is 16 (number of COOH ligands).

In Figure 31 the IR spectra of Au144-[Teg(Me/COOH-cis-Pt)] is compared to that of Au144-[Teg(Me/COOH)] and $Au_{144}(SC_2H_4Ph)_{60}$. Phenylethanthiol's peaks are not so intense. Anyway it is possible to recognize the three sp2 C-H peaks at about 3060 cm^{-1} and the C=C peak at 1600 cm^{-1}. By comparing Au144-

[Teg(Me/COOH)] and Au144-[Teg(Me/COOH-cis-Pt)], it can be noticed that the C=O band at 1728 cm^{-1} shows a decrease in intensity and a slightly redshift (from 1732 to 1728 cm^{-1}). Furthermore, new peaks are visible at 3302, 2951-2914, 1660, 1557 and 1400 cm^{-1}, these peaks are also present in the FT-IR spectrum of cis-Diamineplatinum (II) dichloride provided by the supplier and are similar to those reported by Wysokinski and Michalska in their vibrational analysis of cisplatin [87]. These findings suggest the presence of cisplatin attached to the carbonyl of TegCOOH.

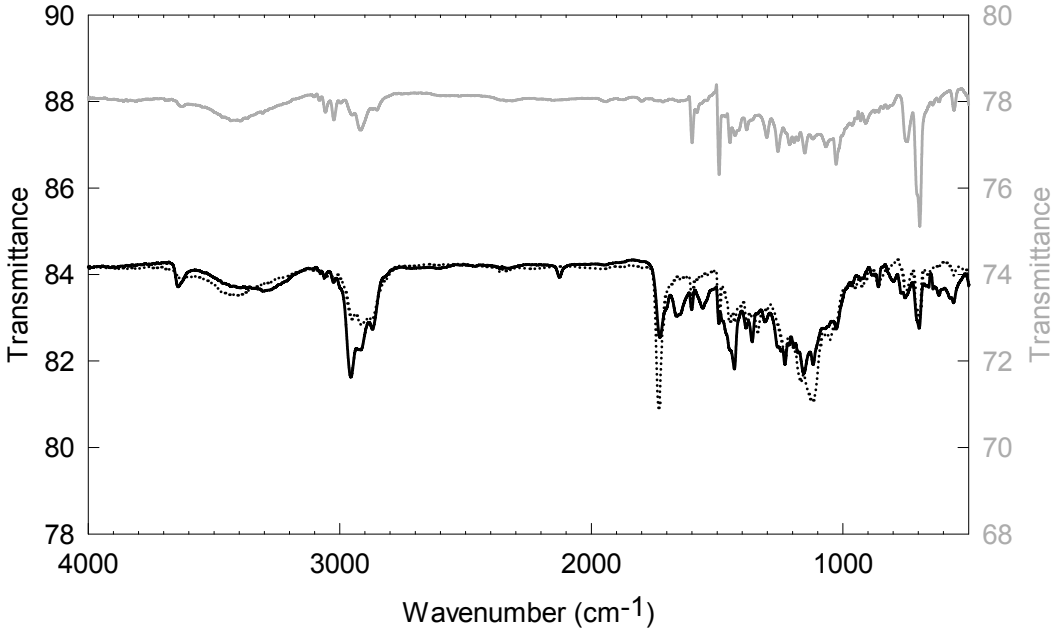

Figure 31 – *Infrared spectrum of Au144-[Teg(Me/COOH-cis-Pt)] (**11**) (—), Au144-[Teg(Me/COOH)] (**9**) (• • •) and* $Au_{144}(SC_2H_4Ph)_{60}$ *(—).*

The amount of cisplatin was also estimated by XPS analysis. The results reported in Table 5 show that Au:Pt ratio is 2.5, suggesting that there are 57 cisplatins per MPC. Furthermore, an important aspect to point out is that the estimated error for this experiment is ±5%, and the percentages of Au, S, N and Pt are smaller.

Atom	Percentage (%)	N°Atoms $_{obs}$	N°Atoms $_{exp}$
C	78.4	5645	586
O	15	1080	193
Au	*2*	*144*	*144*
S	1.9	136	60
N	1.9	136	32
Pt	0.8	57.6	16

Table 5 – *Composition of Au144-[Teg(Me/COOH-cis-Pt)] (**10**) in terms of atoms estimated by XPS measurements.*

The outcome suggests that cisplatin could have reached and affected the core composition by replacing some Au atoms. Since NMR suggested a maximum number of 16 available site for cisplatin binding, for final conclusions in the biologic section it is reasonable to use a ratio of 16 cisplatins per MPC.

Au144-[Teg(Me/COOH-cis-Pt)/Fluo] (a). To obtain the active anticancer MPC from Au144-[Teg(Me/COOH)/Fluo], cisplatin was employed for the complexation as shown in the cartoon of Figure 32. The reaction was carried using an excess of cisplatin as the monolayer of the MPC was completely exchanged by TegCOOH. The clusters were characterized as previously reported and with X-ray photoelectron spectroscopy (XPS). The clusters were characterized by ^{1}H-NMR spectrometry, IR and UV-vis absorption spectroscopies and X-ray photoelectron spectroscopy (XPS).

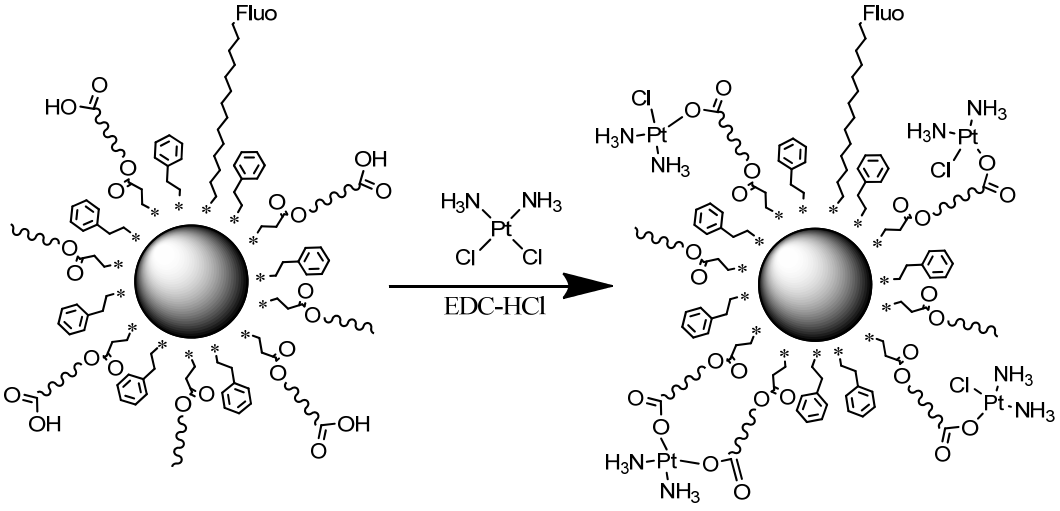

Figure 32 – *Ligand exchange reaction scheme to give Au144-[Teg(Me/COOH-cis-Pt)] (**12**)*

As shown by Figure 33, the UV-vis measurements confirm the behavior of the modified MPCs as similar to that of the starting MPC, indicating that no apparent size modification occurred during the binding of cisplatin. Au144-[Teg(Me/COOH)/Fluo] shows also the absorption pattern of the fluorescent ligand at pH 6 with its characteristic peaks at 434, 452 and 492 nm. Another shoulder appears in the range 350-450, this is present in minor form in Figure 30.

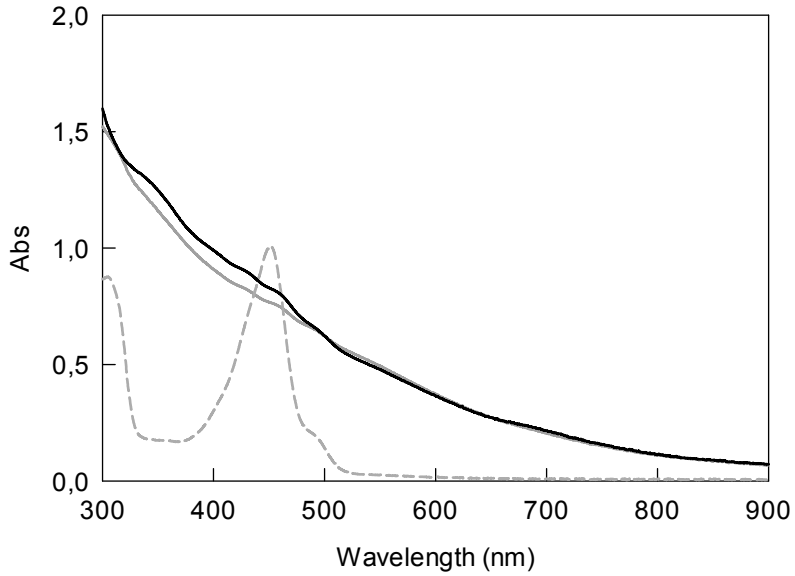

Figure 33 – *UV-Visible spectrum of Au144-[Teg(Me/COOH-cis-Pt)/Fluo] (**12**) 27 µM (—), Au144-[Teg(Me/COOH)/Fluo] (**10**) 10 µM (—), and Fluo ligand 14 µM(- - -), all at pH 6 in THF.*

The solubility is the same as before functionalization. The monolayer composition and the extent of the ligand exchange was estimated by ^{1}H-NMR carried out in deuterated chloroform. By considering the integrals of specific signals belonging to TegMe, TegCOOH, Fluo ligand and phenylethanethiol, respectively, it was possible to estimate the extent of exchange. The results are reported in Table 6.

Thiol	Range δ (ppm)	Integral	Protons	Ratio	Percentage	Molecules
Phenylethanethiol	6.41-7.22	15.33(-1.08)	5	2.85	53%	35
TegMe	3.39	3	3	1	19%	11
TegCOOH	4.26	5.22(-2)	4	1.3	25%	16
Fluo ligand	8.12	0.18	1	0.18	3%	2
				5.33	100%	60

Table 6 – *Composition of thiols in the monolayer of Au144-[Teg(Me/COOH-cis-Pt)/Fluo] (**12**) estimated by NMR measurements.*

As shown in Figure 34, for TegMe the chemical shift related to the terminal methyl group was taken as a reference, while for Fluo ligand one of the benzofuranone hydrogens was employed. For phenylethanethiol, the phenyl group was considered with six other benzofuranone hydrogens of Fluo ligand in the ratio 5:6. The methylene units in α position to the ester were used as reference for TegCOOH and TegMe with a ratio for the protons of 4:2 respectively. The total number of phenylethanethiol exchanged was 47%. The composition of the monolayer was estimated to be 19% TegMe, 25% TegCOOH and 3% Fluo ligand. The results suggest that the maximum number of cisplatins which can be bound is 15.

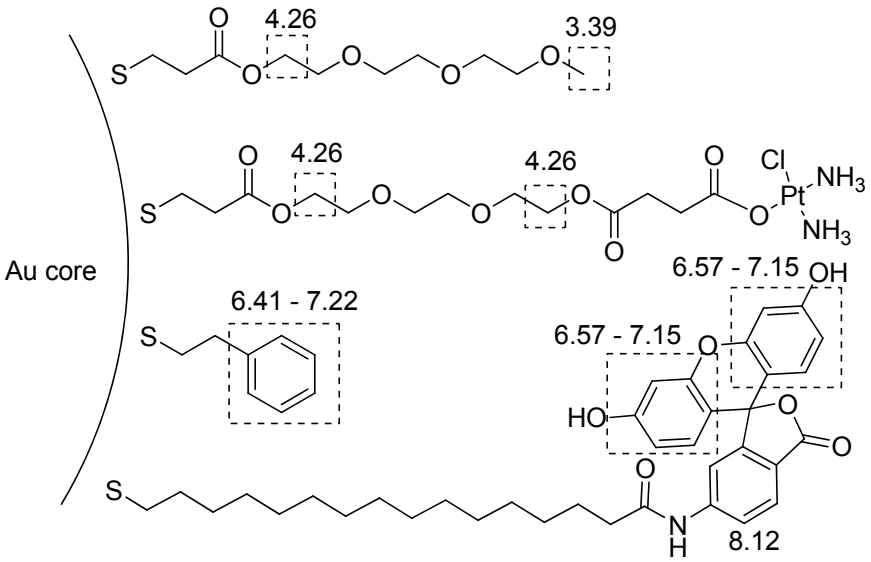

Figure 34 – *Scheme of proton chemical shifts used for integration and ligands ratio estimation.*

IR was used to verify the presence of cisplatin attached to the MPC. In Figure 35, the IR spectrum of Au144-[Teg(Me/COOH-cis-Pt)/Fluo] is compared to those of Au144-[Teg(Me/COOH)/Fluo] and Fluo ligand. Absorption peaks at 3060 cm^{-1} (three peaks, sp2 C-H) and at 1600 cm^{-1} (C=C) confirm the presence of phenylethanethiol. By comparing Au144-[Teg(Me/COOH)/Fluo] and Au144-[Teg(Me/COOH-cis-Pt)/Fluo], we observe that the C=O ester band at 1733 cm^{-1} is similar, while the amide C=O at 1631 cm^{-1} disappeared. No peak related to cis-Diamineplatinum (II) dichloride was found. These findings do not suggest the presence of cisplatin attached to the carbonyl of TegCOOH, or at least not in high concentrations.

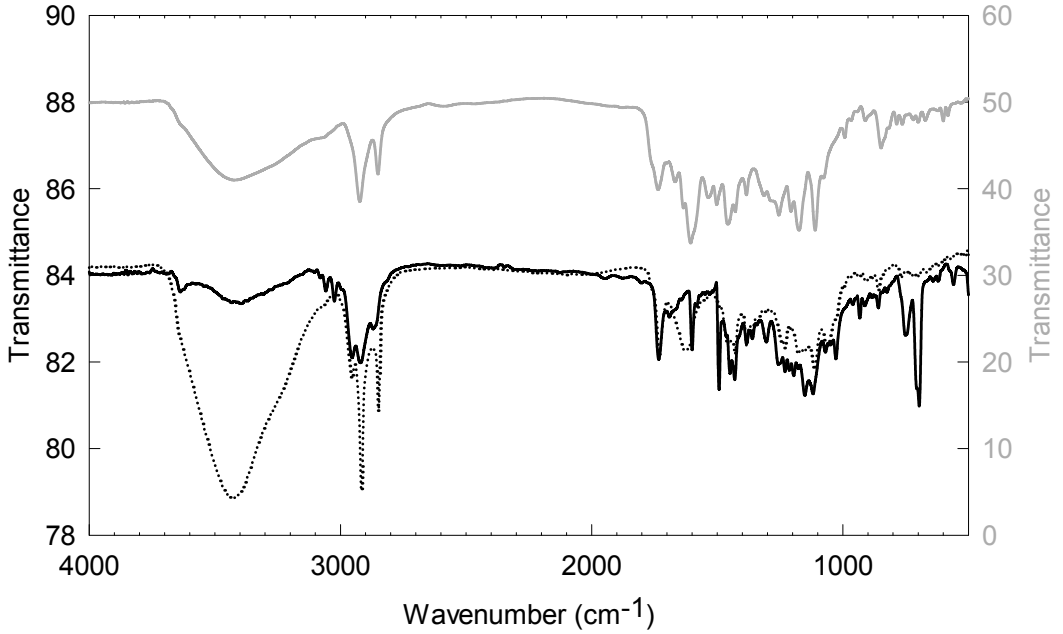

Figure 35 – *Infrared spectra of Au144-[Teg(Me/COOH-cis-Pt)/Fluo] (**12**) (—), Au144-[Teg(Me/COOH)/Fluo] (**10**) (• • •) and Fluo ligand (—).*

The amount of cisplatin was also estimated by XPS analysis. The results reported in Table 7 show that Au:Pt ratio is 2.6, suggesting that there are 55 cisplatins per MPC. Furthermore, an important aspect to point out is that the estimated error for this experiment is ±5%, and the percentages of Au, S, N and Pt are smaller.

Atom	**Percentage (%)**	**N°Atoms $_{obs}$**	**N°Atoms $_{exp}$**
C	76.8	2717	633
O	15.6	552	187
Au	*2.6*	*144*	*144*
S	1.3	72	60
N	2.1	116	30
Pt	1	55	15

Table 7 – *Composition of Au144-[Teg(Me/COOH-cis-Pt)/Fluo] (**12**) in terms of atoms estimated by XPS measurements.*

Considering qualitatively that IR did not confirm the presence of cisplatin in high concentration and XPS showed the presence of a large amount of cisplatin

associated to the MPC, the outcome suggests that cisplatin could have reached and affected the core composition by replacing some Au atoms. Anyway, in this particular case also the ester group in the benzofuranone of Fluo ligand could be involved in the formation of bonds with cisplatin, so fluorescence measurement were performed.

Au144-[Teg(Me/COOH-cis-Pt)/Fluo] shows fluorescence (Figure 36) with a maximum at 535 nm upon excitation at 485 nm. The intensity of the emission is however low. By comparing two solutions, 3.4 and 34 µM concentration respectively, we noticed that the emission dependence in the concentration is nonlinear. In fact, one should expect a 10-fold increase in the emission intensity. A 80% decrease in fluorescence efficiency can be both attributed to quenching by the gold core and something occurred during the reaction with cisplatin.

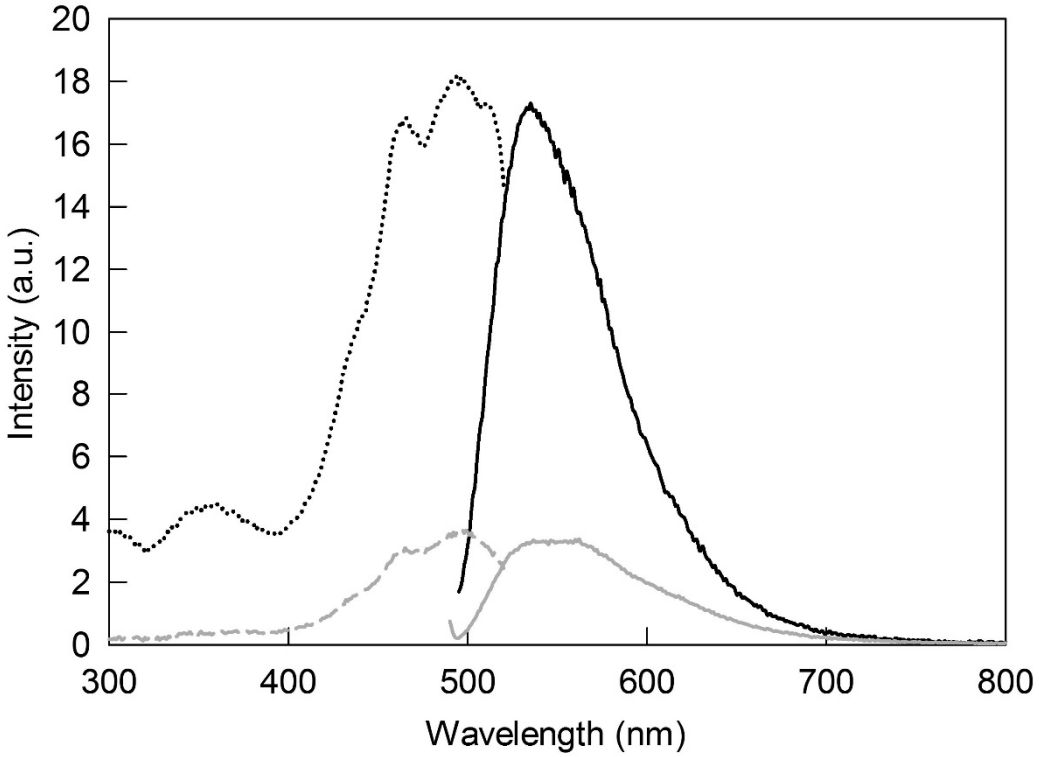

Figure 36 – *Excitation spectrum at λ_{em}=535 nm (• • •) and emission spectrum at λ_{ex}=485 nm(—) 3.4 µM and excitation spectrum at λ_{em}=535 nm (- - -) and emission spectrum at λ_{ex}=485 nm(—) 34 µM of Au144-[Teg(Me/COOH-cis-Pt)/Fluo] (**12**) in THF/MeOH 9:1, at pH 6.*

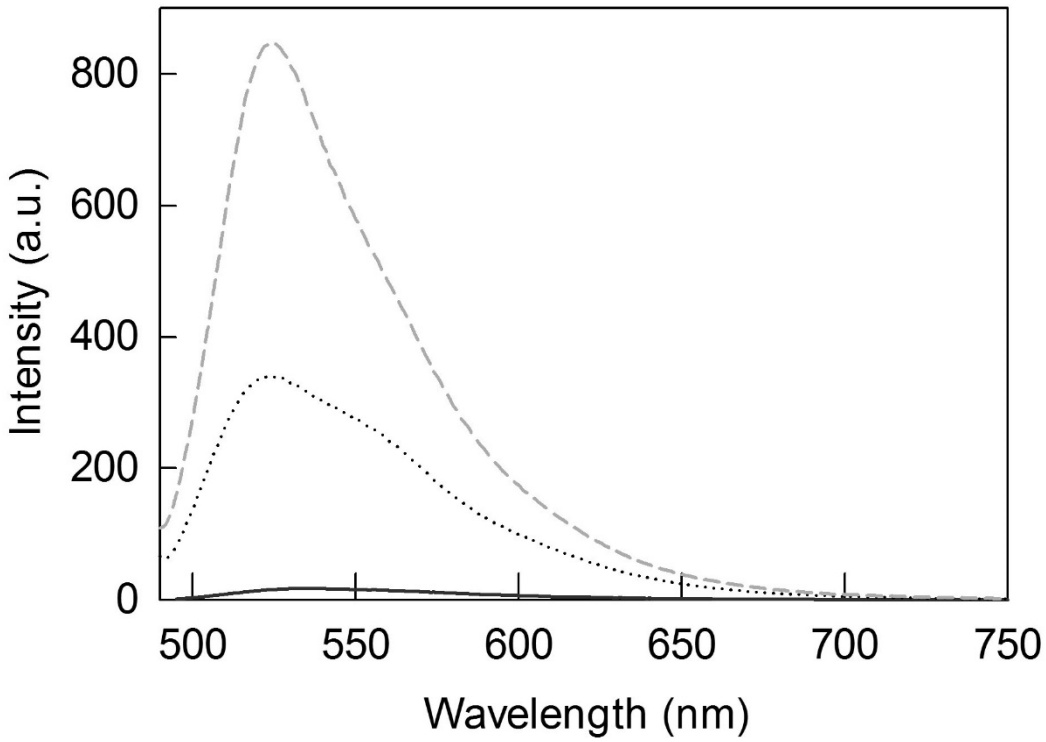

Figure 37 – *Fluorescence and emission spectra at λ_{ex}=485 nm spectra of Au144-[Teg(Me/COOH-cis-Pt)/Fluo] (**12**) 3.4 µM (—) Au144-[Teg(Me/COOH)/Fluo] (**10**) 3.4 µM (• • •) and Fluo ligand 3.5 µM (- - -) at pH 6.*

Figure 37 shows a comparison for the fluorescence emission of Au144-[Teg(Me/COOH)/Fluo], Au144-[Teg(Me/COOH-cis-Pt)/Fluo] and the Fluo ligand at the same concentration. The ratio of the fluorescence intensities for Au144-[Teg(Me/COOH)/Fluo] and Au144-[Teg(Me/COOH-cis-Pt)/Fluo] is 20. Au144-[Teg(Me/COOH)/Fluo] is 20 times more efficient than Au144-[Teg(Me/COOH-cis-Pt)/Fluo]. This is an important result that has to be taken into account to explain the outcomes of biological assays.

Au144-[Teg(Me/COOH-cis-Pt)/Fluo] (b). Finally, to assess whether the condition in which cisplatin was bound to the MPC affected also the fluorescent group, a new ligand exchange reaction with Fluo ligand was carried out on Au144-[Teg(Me/COOH-cis-Pt)] (11). In fact, depending on the pH condition fluorescein can be present in an open ring isomer providing a carboxylic group. The latter can thus be involved in coordinating cisPt. As reported in Section 2.4.2 the exchange was carried out using a molar ratio of 0.3:1 for the Fluo ligand and the thiols

present in the monolayer. The clusters were characterized with UV-vis absorption spectroscopy.

As shown in Figure 38, the UV-vis measurements confirm that the behavior of the modified MPCs is similar to that of the starting MPC, indicating that no apparent size modification occurred during the exchange reaction. Au144-[Teg(Me/COOH-cis-Pt)/Fluo]-b **12** shows also the absorption pattern of the fluorescent ligand at pH 6 with its characteristic peaks at 434, 452 and 492 nm. By comparing the UV-vis absorption spectra of Au144-[Teg(Me/COOH-cis-Pt)/Fluo]-b with the Au144-[Teg(Me/COOH-cis-Pt)/Fluo]-a described before, we observe that adding the Fluo ligand upon functionalization with cisPt leads to better results.

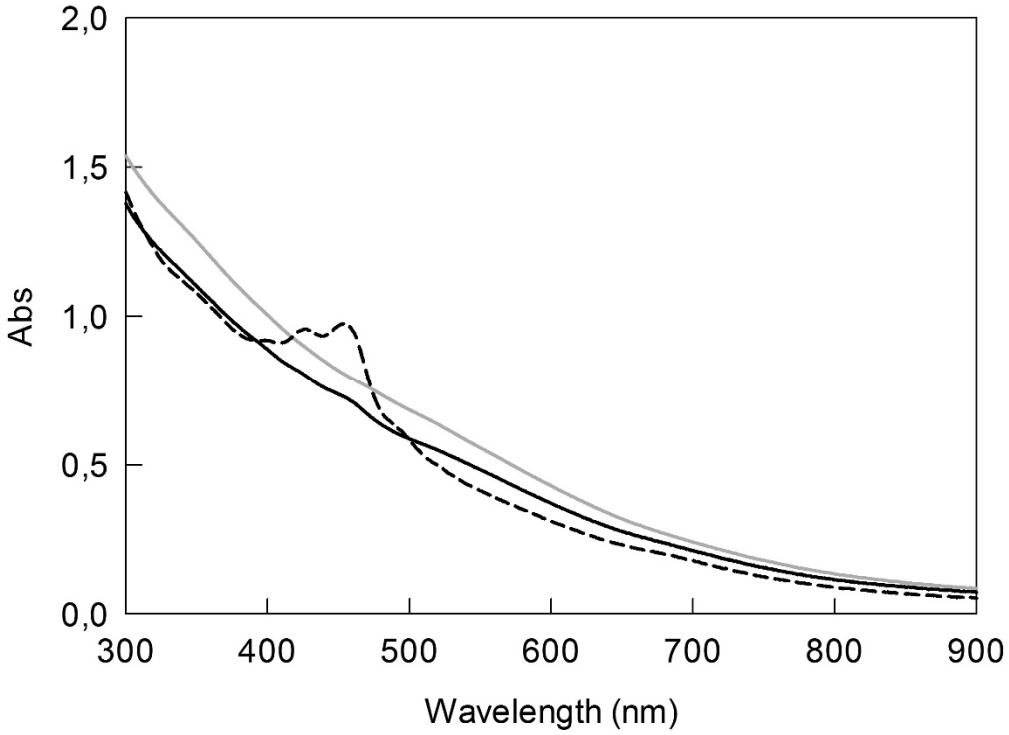

Figure 38 – *UV-Visible spectrum of Au144-[Teg(Me/COOH-cis-Pt)/Fluo]-b (**13**) 27 µM (- - -), Au144-[Teg(Me/COOH)/Fluo] (**10**) 10 µM (—), Au144(S-C_2H_4-Ph)$_{60}$ 45 µM (—).*

These findings suggest that the fluorescent ligand may experience a quenching phenomenon, due to the presence of cisplatin coordinated through its carboxylate along with that of the Au core: this can partially explain the increased number of Pt atoms measured by XPS.

The following biological section focuses on the study of the cytotoxic activity of the Au144-TegMe, Au144-[Teg(Me/COOH)] and Au144-[Teg(Me/COOH-cis-Pt)]. While association and localization studies are carried out with Au144-[Teg(Me/COOH)/Fluo] and Au144-[Teg(Me/COOH-cis-Pt)/Fluo].

All MPCs were stored at -20°C in THF, and the samples for biologic assays were previously dried at room temperature under negative pressure, dispersed in dimethyl sulfoxide (5 µl) and then water to reach a final concentration of 270 µM.

3.3 Biologic assays

3.3.1 Au144 MPCs cytotoxicity to tumor cells

The first objective of the first experiment set was to determine the effect of the monolayer-protected clusters on tumor cells. Therefore, MPCs were tested for their cytotoxic activity in epithelial cell line HeLa. Two methods were utilized in measuring cytotoxicity after 24 h of incubation, the colorimetric MTS assay and LDH assay.

In the MTS assay, the OD obtained at 492 nm is proportional to mitochondrial and ER reductase activity, and therefore to the viability of cells in culture (Figure 39 and 40).

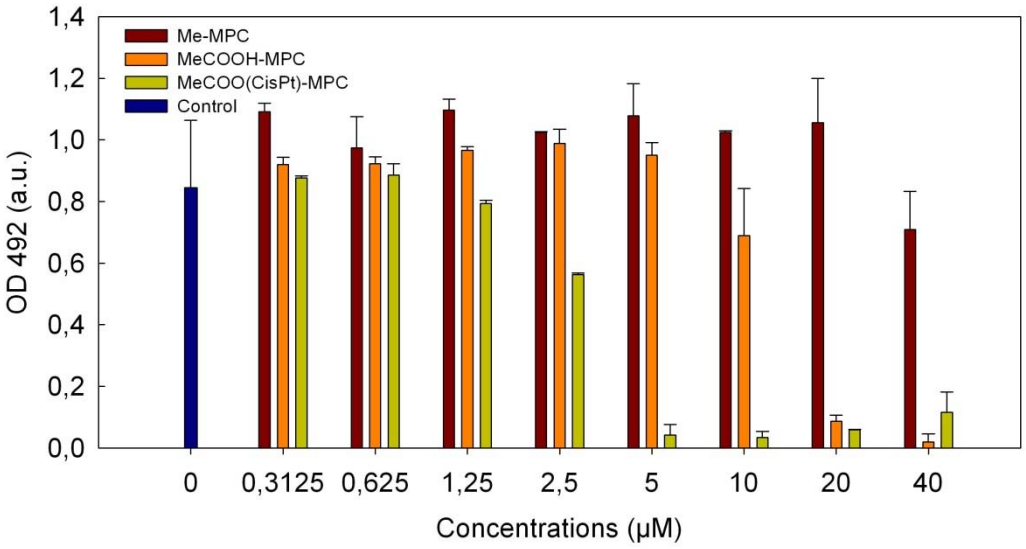

Figure 39 - The effect of different concentrations of indicated MPCs on HeLa cells was determined by measuring MTS reduction to the colored formazan product, assayed by measuring the OD_{492}. Values represent the mean + standard deviation from duplicate wells.

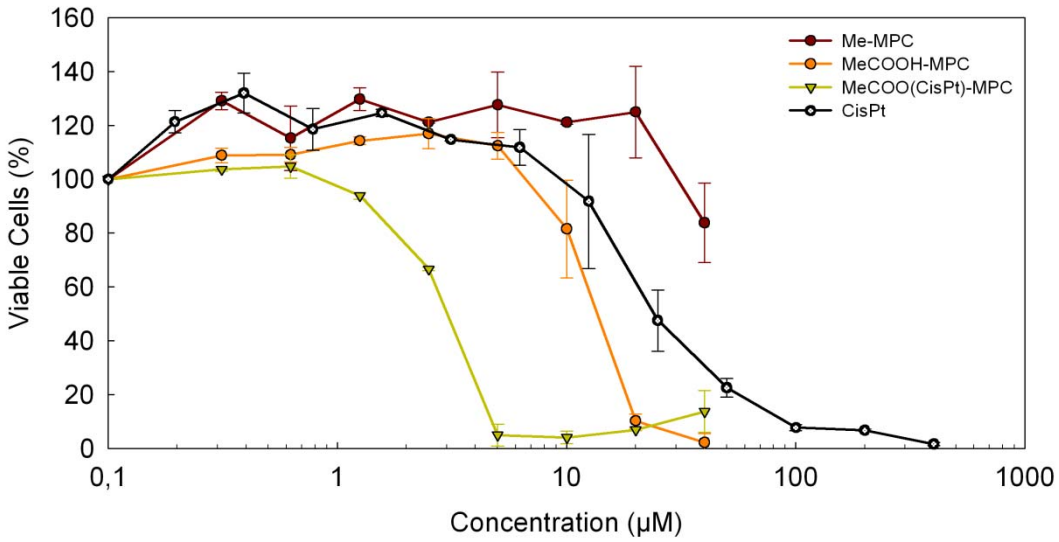

Figure 40 - The effect of different concentrations of MPCs on HeLa was determined by measuring MTS reduction to the colored formazan product, assayed by measuring the OD_{492} . The OD_{492} value of control wells of cells without treatment was set as 100%. Values represent the mean + standard deviation from duplicate wells.

Au144-TegMe had no effect on cell viability up to 20 µM with respect to the non-treated cells. MeCOOH was comparable to the negative control up to 5 µM but determined a decrease in cell viability in there range from 10µM to 40 µM (Figure 40). The presence of carboxylic terminal groups on the surface of Au144-[Teg(Me/COOH)] could be the reason for its higher toxicity compared to Au144-TegMe since they both lack the cisplatin function. Strikingly, Au144-[Teg(Me/COOH-cis-Pt)] showed a high cytotoxicity above the concentration of 1 µM, leading to an almost complete cell death over 5µM concentration, resulting significativelly more toxic than Au144-TegMes and Au144-[Teg(Me/COOH)]. Au144-[Teg(Me/COOH-cis-Pt)] and Au144-[Teg(Me/COOH)] appeared having a lower concentration for 50% cell death compared to free cisplatin (Table 8).

	LD_{50} (µM)	**R^2**
Au144-TegMe	>40	nd
Au144-[Teg(Me/COOH)]	12.96	0.9988
Au144-[Teg(Me/COOH-cis-Pt)]	2.58	0.9991
Cisplatin	21.70	0.9994

Table 8 – *The median lethal dose (LD_{50}) of some MPCs and CisPt in HeLa cells was determined by calculating with linear regression the concentration needed to kill 50% of the cell population. The R^2, coefficient of determination, is an indicator of how well the curve fits original data.*

The above described cytotoxic efficacy order were validated by LDH assay. The presence of the LDH leaked into the culture medium upon cell death by necrosis due to damage of plasma membrane, enables a coupled reduction of tetrazolium salt into a red formazan product, resulting in a change in absorbance at 492 nm.

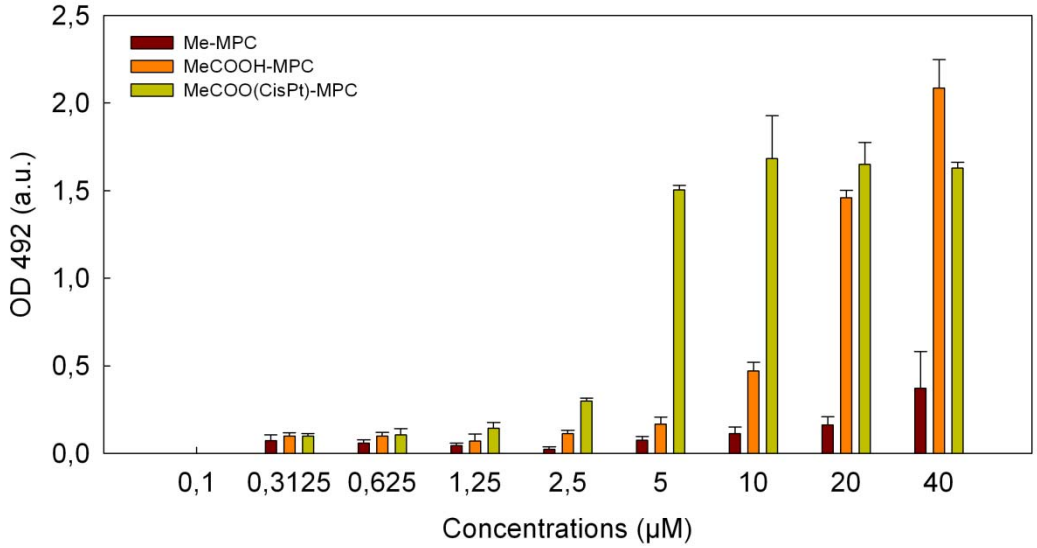

Figure 41 - *The effect of different concentrations of MPCs on HeLa cell was determined with LDH assay by measuring the* OD_{492} *. Values represent the mean + standard deviation from duplicate wells.*

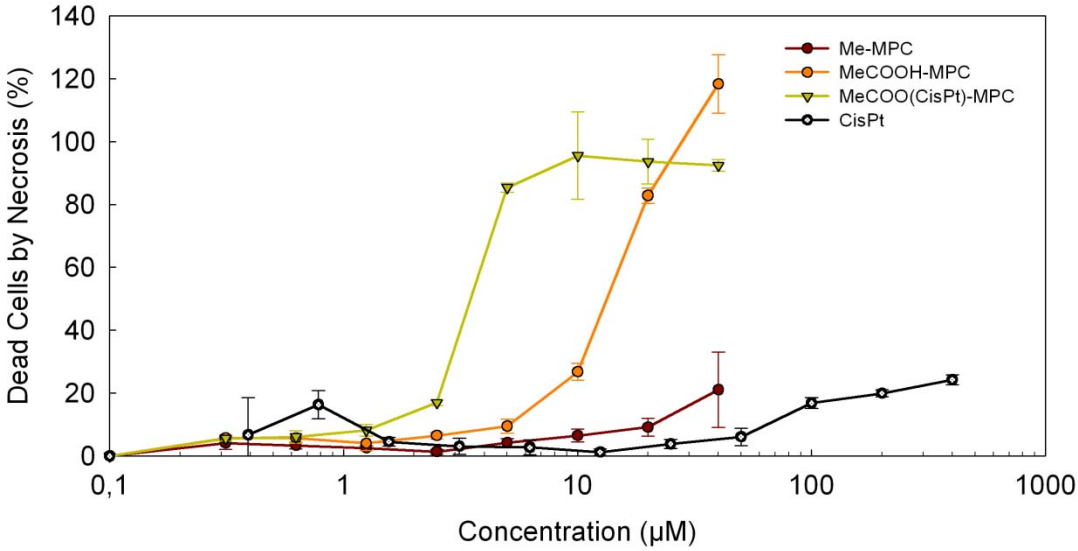

Figure 42 - *The effect of different concentrations of MPCs and CisPt on HeLa cell number was determined by measuring the total amount of LDH from the lysed population of cells. The fluorescence value of control wells of cells treated with lysis buffer is set as 100%. Values represent the mean + standard deviation from duplicate wells.*

Au144-TegMe confirmed previous results being comparable with the non-treated cells (0%) for all tested concentrations. Au144-[Teg(Me/COOH)] were comparable to the negative control up to 5 µM, showing increase in cell death in there range from 10µM to 40 µM (Figure 42). Au144-[Teg(Me/COOH-cis-Pt)] showed high toxicity from 1 µM, leading to an almost complete cell death over 5µM.

MPCs cytotoxicity was further characterised by AnnexinV-FITC/Propidium Iodide assay using FACS, to analyze the kind of death induced. PI can intercalate into double-stranded DNA but can only penetrate plasmatic membranes of necrotic dead cells [73]. AnnV-FITC conjugate detects externalized phosphatidylserine, an indicator of apoptosis [74]. Cells labeled with both PI and AnnV-FITC are interpreted as late apoptosis.

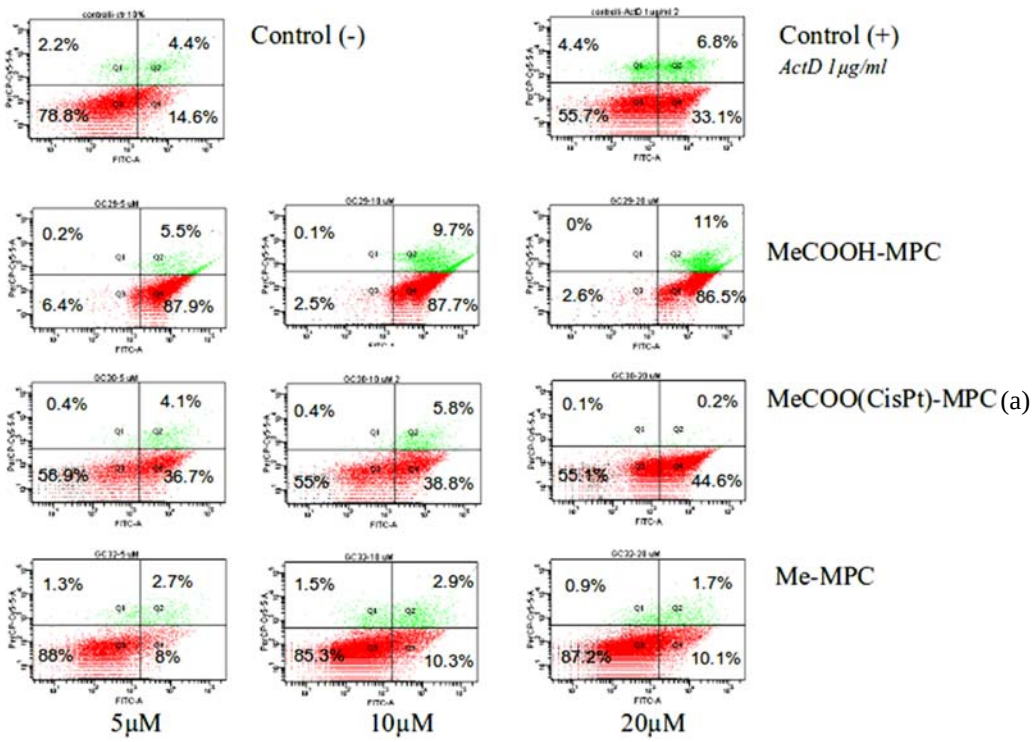

(a)

Figure 43 – *Dot plots of Hela cells treated with different MPCs at different concentrations for 18 h. Fixed number of 1000 events. Plots show AnnV-FITC single positive along the x-axis (lower right quadrant, apoptosis), single positives for PI along the y-axis (upper left quadrant, necrosis). The upper right quadrant of the plot indicates cells positive for both fluorescent markers (late apoptosis).*

Figure 43 shows the percentages for each death type after 18 h incubation with MPCs (5-20 μM). Au144-TegMes percentage of induced mortality remains below 20% and is not considerably different from the control setup. Au144-[Teg(Me/COOH)] toxicity resulted from both apoptosis and necrosis/late apoptosis. In contrast, Au144-[Teg(Me/COOH-cis-Pt)] toxicity appears to occur only *via* apoptosis. However, considering that in the 5-20 μM range LDH assay show a massive release of cytosolic content, we must conclude that the majority of cells were fully disassembled as a result of Au144-[Teg(Me/COOH-cis-Pt)] cytotoxic effect. Au144-[Teg(Me/COOH-cis-Pt)] has an LD_{50} equal to 2.58 μM. If the number of 16 cisplatins is taken into account it reaches 41.28 μM. Compared to the LD_{50} of cisplatin, 21.7 μM, it is possible to notice that efficacy of cisplatin is 1.9x Au144-[Teg(Me/COOH-cis-Pt)]. On the other hand in the case of Au144-[Teg(Me/COOH)] full cell lysis was limited at 5 μM but strong at 10 and 20 μM and permeabilised cell bodies were also detectable, in agreement with their lower toxicity compared to Au144-[Teg(Me/COOH-cis-Pt)]. In conclusion, the mechanism of cell death is heterogeneous comprising apoptotic and necrotic/late apoptotic phenotypes, with a strong tendency of full cell disruption and dispersion of cytosolic content in the medium.

These findings suggest that Au144-TegMe is not acutely cytotoxic to HeLa cells: no inherent toxicity can be attributed to these nanoclusters, *per se*, as confirmed by the 85-95% viability of cells in all the assays. Furthermore, the cytotoxicity assays employed revealed different profiles for Au144-[Teg(Me/COOH-cis-Pt)] and the other MPCs. Strong Au144-[Teg(Me/COOH-cis-Pt)] toxicity against HeLa cells was evidenced by 5-10% viability of cells already present at low concentrations leading to death by apoptotis, as result of all the assays showing statistically significant difference between the treated cells and the controls. The milder toxicity of Au144-[Teg(Me/COOH)] against HeLa cells, maybe due to the presence of exposed carboxylic groups, was proven by 5-10% viability of cells at high concentrations in all assays followed by a necrotic type and an apoptotic type cell death. Similar results were obtained for Au144-[Teg(Me/COOH)/Fluo] and Au144-[Teg(Me/COOH-cis-Pt)/Fluo]. It is important to notice that except Au144-TegMes, every MPC revealed toxicity at particle concentrations lower than free cisplatin.

3.3.2 Au144 MPCs interaction with tumor cells

Three parameters were examined to understand how Au144 monolayer-protected clusters interact with HeLa cells: concentration, time, and temperature. Obviously, the study has been conducted only with MPCs carrying the fluorescent ligand.

Concentration-dependence of MPCs association to HeLa cells

Au144-[Teg(Me/COOH)/Fluo] and Au144-[Teg(Me/COOH-cis-Pt)/Fluo] were used to treat HeLa in concentrations ranging from 5 µM to 20 µm for 24 h at 37^{O}C.

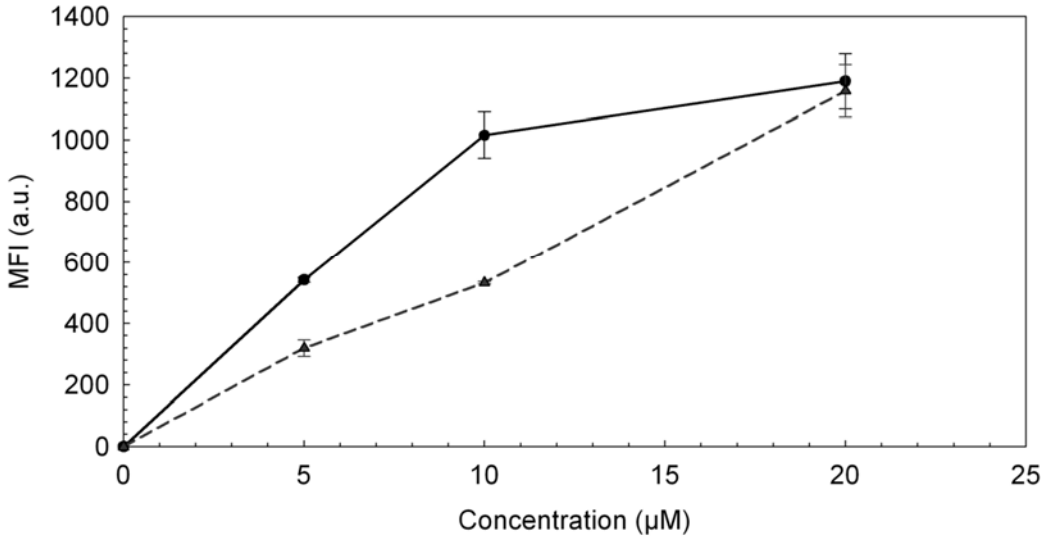

Figure 44 – *Representation of mean fluorescence intensity (MFI) representing the association to Au144-[Teg(Me/COOH)/Fluo] (**10**) 10 µM (—) and Au144-[Teg(Me/COOH-cis-Pt)/Fluo]-a (**12**) (- - -) at different concentrations of MPCs after 24 h incubation at 37°C. Fluorescence intensity of Au144-[Teg(Me/COOH-cis-Pt)/Fluo] (a) was corrected for a 20x factor in respect of Au144-[Teg(Me/COOH)/Fluo] as resulting from previous fluorescence analysis showing a different intrinsic fluorescence of the two assemblies.*

The experiment revealed a multiple fold increase in association to HeLa cells as the MPCs concentration increased proving that MPCs association to HeLa cells is concentration-dependent. The uptake amount is increased 2.2 times with Au144-[Teg(Me/COOH)/Fluo] and 3.6 times with Au144-[Teg(Me/COOH-cis-Pt)/Fluo] (a) when dosing concentration was increased from 5 µM to 20 µM. This increase was continuous at all concentration points however there was an indication of reaching a maximal cell binding point for Au144-

[Teg(Me/COOH)/Fluo] as the slope of the curve obtained slightly decreased in the last part. Figure 44 demonstrates the increase of fluorescence intensity in HeLa cells corresponding to the increase of MPCs concentration.

Time- and Temperature-dependence of MPCs association

Next, HeLa cells were incubated with 5 µM Au144-[Teg(Me/COOH)/Fluo] and Au144-[Teg(Me/COOH-cis-Pt)/Fluo] (a) at different times. Cells incubated with MPCs at 37^{O}C for different times are shown in Figure 45.

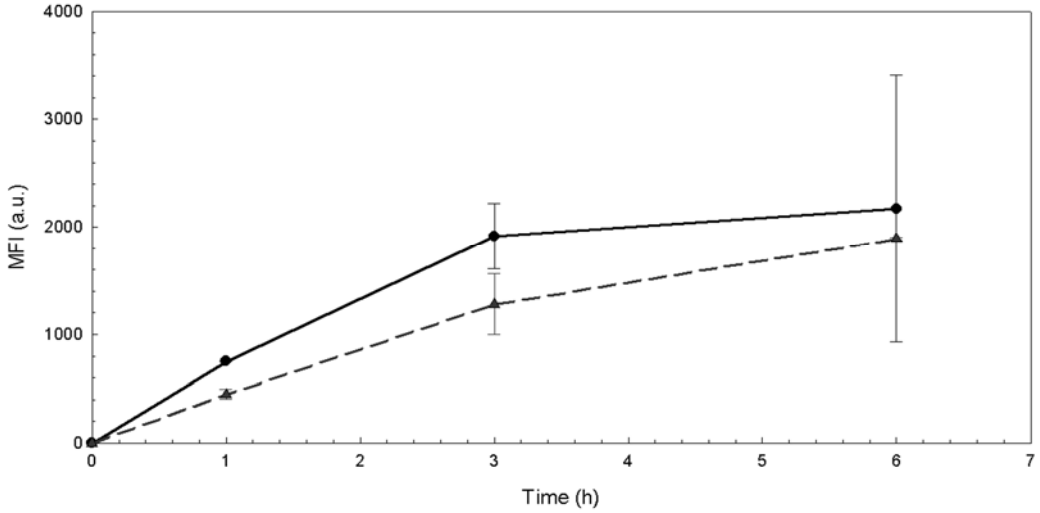

Figure 45 – *Time dependence of MPCs-association to Hela cells. HeLa were incubated with Au144-[Teg(Me/COOH)/Fluo] (10) (—) and Au144-[Teg(Me/COOH-cis-Pt)/Fluo]-a (12) (- - -) for different hours with 5µM MPCs at 37°C. MFI was then measured by FACS. Fluorescence intensity of Au144-[Teg(Me/COOH-cis-Pt)/Fluo] (a) was corrected for a 20x factor in respect of Au144-[Teg(Me/COOH)/Fluo] as above.*

Quantitative analysis of intracellular fluorescence revealed that MPCs uptake was linear until over the third hour of incubation (R^2>0.99). Between the 3 h to 6 h of incubation, cell association gradually declined as in the case of Au144-[Teg(Me/COOH-cis-Pt)/Fluo] (a) or almost steadied as seen in Au144-[Teg(Me/COOH)/Fluo] treated cells. The rate of uptake increased by 2.9-fold for Au144-[Teg(Me/COOH)/Fluo] and 4.2-fold for Au144-[Teg(Me/COOH-cis-Pt)/Fluo] (a) as time progressed from 1 h to 6h and the process is indicated to be saturable over time. As seen in the figures, the fluorescence intensity clearly increases with co-culturing time then it is presumed to reach a stable stage after 6 h. For Au144-[Teg(Me/COOH-cis-Pt)/Fluo] (a) (Figure 45), although the plateau stage indicative of saturable uptake was not distinct, the slope visibly decreased.

To further characterize the cell association of Au144-[Teg(Me/COOH)/Fluo] and Au144-[Teg(Me/COOH-cis-Pt)/Fluo] (a), cell uptake experiments were performed at varying temperatures and at different time periods.

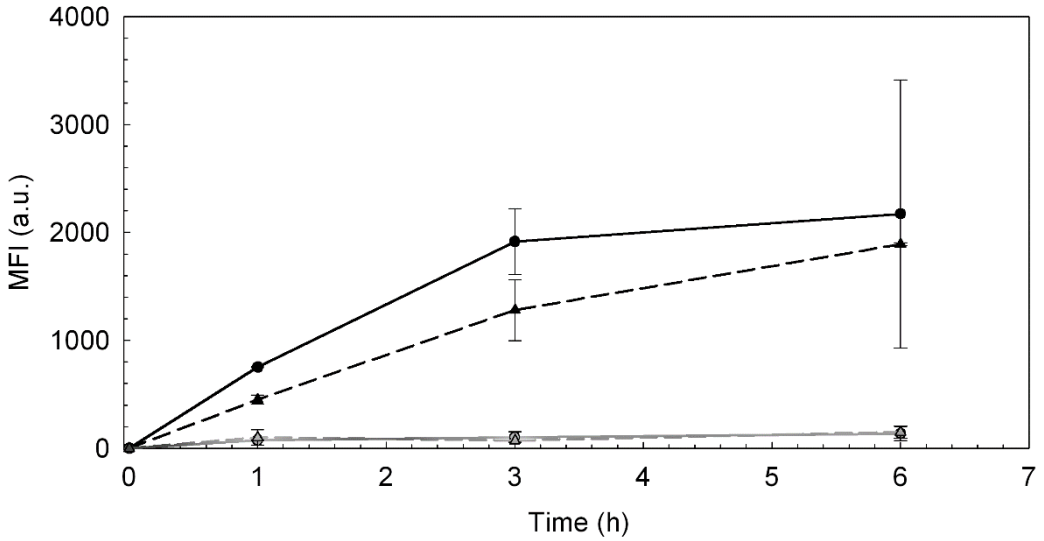

Figure 46 – *Time and temperature dependence of MPCs-association to Hela cells. Cells were incubated with Au144-[Teg(Me/COOH)/Fluo] (10) (—) and Au144-[Teg(Me/COOH-cis-Pt)/Fluo]-a (12) (- - -) at 37°C and Au144-[Teg(Me/COOH)/Fluo] (10) (—) and Au144-[Teg(Me/COOH-cis-Pt)/Fluo]-a (12) (- - -) at 0°C for the indicated times with 5μM MPCs. MFI was then measured by FACS. Fluorescence intensity of Au144-[Teg(Me/COOH-cis-Pt)/Fluo] (a) was corrected for a 20x factor in respect of FluoMeCOOH-.*

Figures 46 shows the MFI distribution of HeLa cells incubated with Au144-[Teg(Me/COOH)/Fluo] and Au144-[Teg(Me/COOH-cis-Pt)/Fluo] (a) at different temperatures for 1, 3 and 6 hours. It is evident that there was a higher accumulation of nanoparticles in cells at 37^{O}C, compared to 0^{O}C. The results suggest that Au144-[Teg(Me/COOH)/Fluo] and Au144-[Teg(Me/COOH-cis-Pt)/Fluo] (a) enter HeLa cells by an active temperature-dependent mechanism.

3.3.3 Au144 MPCs intracellular localization

To verify the findings of FACS, confocal images were obtained from HeLa cells incubated for 3h at 37°C with Au144-[Teg(Me/COOH)/Fluo] and Au144-[Teg(Me/COOH-cis-Pt)/Fluo] (a).

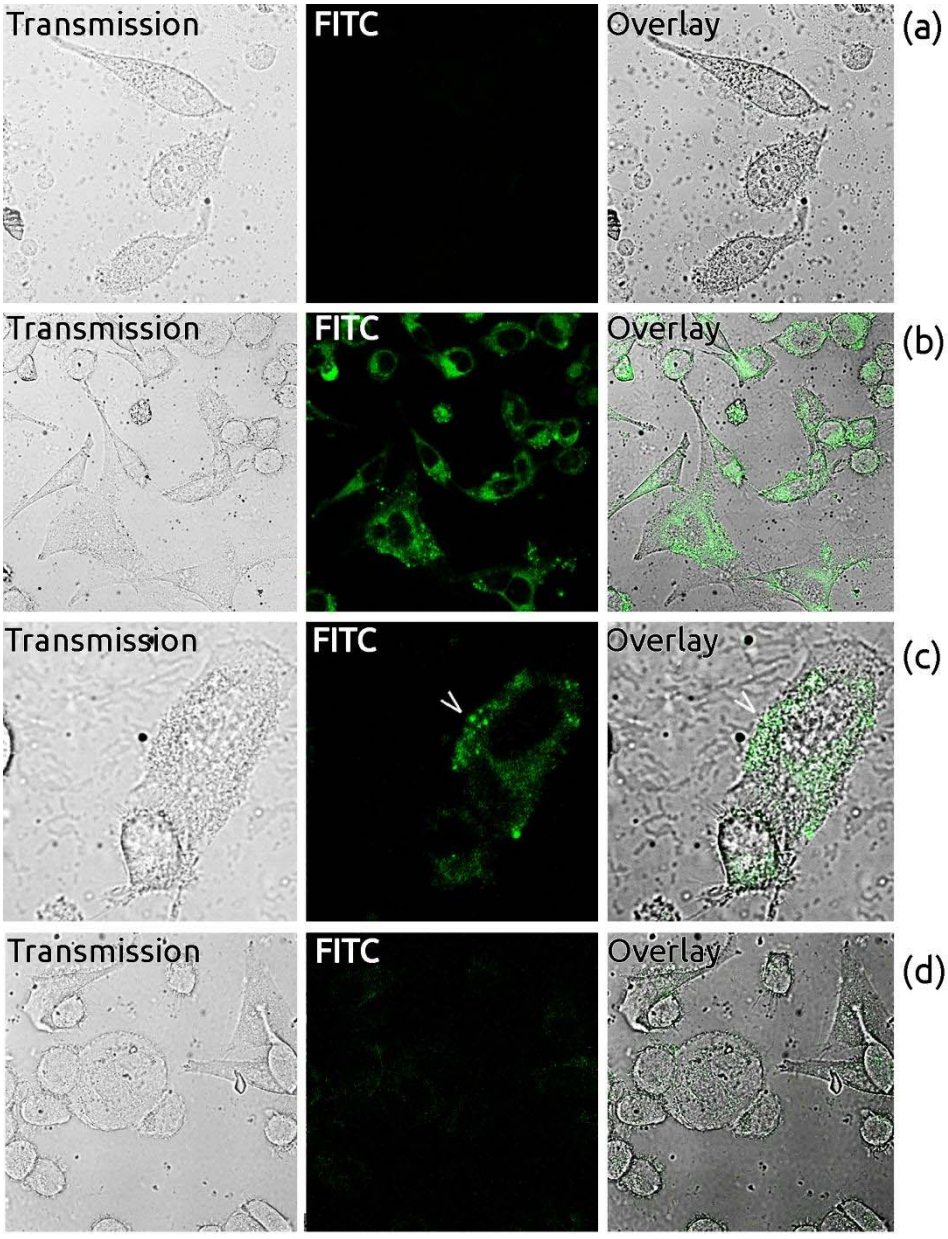

Figure 47 – *Acquisition of transmission channel, fluorescent channel (FITC) and their overlay for (a) non-treated Hela cells, (b) Hela cells treated with Au144-[Teg(Me/COOH)/Fluo], (c) Hela cells treated with FluoMeCOO-MPCs with close-up of inner circular spots, (d) Hela cells treated with Au144-[Teg(Me/COOH-cis-Pt)/Fluo].*

First it was analyzed the intrinsic fluorescence of HeLa cells with a non-treated sample. There was no appreciable fluorescence as shown in Figure 47-a. After an incubation time of 3 hours, the confocal fluorescence images (Figure 47-b) clearly show that Au144-[Teg(Me/COOH)/Fluo] are inside the cell cytoplasm. It can be seen clearly that in the cell cytoplasm there are aggregates of the green fluorescein loaded nanoparticles around the nucleus but not inside it, which strongly suggest that Au144-[Teg(Me/COOH)/Fluo] have been internalized by the cells via endosomes. Confocal microscopy showed that Au144-[Teg(Me/COOH)/Fluo] were internalized rather than adsorbed on the cell surface and were distributed in both a diffused manner in the cytoplasm and in a punctuate manner in subcellular compartments as indicated by the arrow in Figure 47-c. As expected, since the intrinsic fluorescence of Au144-[Teg(Me/COOH-cis-Pt)/Fluo] is 20 times lower compared to Au144-[Teg(Me/COOH)/Fluo], the signal of internalized nanoclusters inside HeLa cells was very weak in such case. However, it was possible to notice that also these MPCs distribute throughout the cell similarly to Au144-[Teg(Me/COOH)/Fluo] (Figure 47-d). Further study will be necessary to ascertain if the here described temperature dependent MPCs internalization in HeLa cells takes place by endocytic/pinocytic activity, by passive diffusion or by a combination of the two processes.

4 Conclusion

In this thesis we were looking for a good candidate fitting the profile of the "perfect" DDS, and our research focused on Au_{144} MPC, an ultrasmall nanocluster already subject of studies by Prof. Maran's group. Recent findings about the MPC size-dependency in cancer treatment, suggested that a particularly small MPC, such as Au_{144} could provide a good candidate for drug-delivery. By carrying out ligand-place exchange reactions on the native $Au_{144}(SR)_{60}$ MPCs (Figure 48-c), we modified the protecting monolayer with the goal of achieving specific tasks.

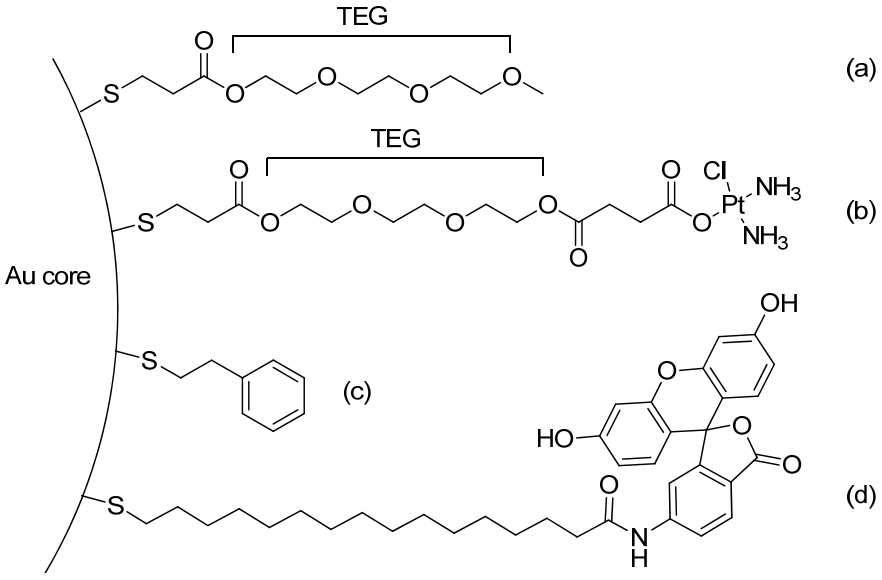

Figure 48 – *Chemical structure of TegMe (a), TegCOOH bound to cisplatin (b), phenylethanethiol (c), Fluo ligand (d).*

In the first prepared MPC, Au144-[TegMe], the TegMe ligand (Figure 48-a) was introduced in the monolayer according to a 1:1 exchange of phenylethanethiol (Figure 48-c). This MPC displayed increased water-solubility, without losing its solubility in organic solvents. Very important, in biologic assays showed no inherent toxicity as confirmed by the 85-95% viability of cells in all the

assays up to 40 μM, confirming the hypothesis of making a stealth MPC with no cytotoxic effect.

Because of the presence of the thiolated TEG ligands and the COOH groups also Au144-[Teg(Me/COOH)] gained the ability to be soluble in aqueous media. NMR studies confirmed that TegMe and TegCOOH were present in a 1:1:2 ratio with phenylethanethiol in the monolayer. The number of TegCOOH available for cisplatin coordination was thus 16 out of 60 ligands. Concerning its activity on Hela cells, it showed toxicity (with LD_{50} equal to 12.96 μM) resulting both in apoptosis and necrosis/late apoptosis, possibly because of interactions with cells via the carboxylic terminal groups.

These groups, however, were fundamental for making the bond with cisplatin, to yield Au144-[Teg(Me/COOH-cis-Pt)], the therapeutic active cisplatin-MPC conjugate. By assuming a quantitative reaction , 16 cisplatin units were present per Au144-[Teg(Me/COOH-cis-Pt)]. Strong toxicity of Au144-[Teg(Me/COOH-cis-Pt)] against HeLa cells was evidenced by 5-10% viability of cells already present at low concentrations leading to death by apoptosis (LD_{50} equal to 2.58 μM). If the number of 16 cisplatins is taken into account LD_{50} reaches 41.28 μM, higher than the LD_{50} of cisplatin, 21.7 μM. In association experiments, Au144-[Teg(Me/COOH)/Fluo] and Au144-[Teg(Me/COOH-cis-Pt)/Fluo]-a, containing the fluorescent ligand in the monolayer (Figure 48-d), showed to be time-, temperature- and concentration-dependent, while the intracellular localization experiments showed distribution in a diffused manner in the cytoplasm and in a punctuate manner in subcellular compartments. This suggests that MPCs internalization in HeLa cells occurs by both endocytic/pinocytic activity and passive diffusion, maybe due to the co-presence of both water-soluble and hydrophilic ligands in the monolayer.

To conclude, we obtained evidence of the efficacy of the cisplatin-MPC conjugate toward HeLa cells. We also demonstrated that Au_{144} MPC possesses all the characteristics needed to be considered as a good drug-delivery candidate, such as water-solubility, perfect size for exploiting enhanced permeability and retention effect; in addition, the presence of the TEG ligands is supposed to lower RES clearance and impart a long lifetime within bloodstream. Overall, this outcome provides an important step in the emerging field of gold MPCs as DDS.

5 References

[1] European Commission – Health-EU Statistic Data, **2013**.

[2] Malvezzi, M.;Bertuccio, P.; Levi, F.; La Vecchia, C.; Negri, E. *Ann. Oncol.* **2013**, *18*, 558-567.

[3] Finkel, T.; Serrano, M.; Blasco, M. A. *Nature* **2007**, *448*, 767-774.

[4] Chambers, A. F.; Groom, A. C.; MacDonald, I. C. *Nat. Rev. Canc.* **2002**, *2*, 563-572.

[5] Skeel, R. T.; Khleif, S. N. *Handbook of cancer chemotherapy,* **2011** *Lippincott Williams & Wilkins*.

[6] Kostova, I. *Recent Pat Anticancer Drug Discov.* **2006**, *1*, 1-22.

[7] Singh, A.; Settleman, J. *Oncogene* **2010**, *29*, 4741-4751.

[8] Huang, K.; Ma, H.; Liu, J.; Huo, S.; Kumar, A.; Wei, T.; Liang, X. *J. ACS nano* **2012**, *6*, 4483-4493.

[9] Craig, G. E.; Brown, S. D.; Lamprou, D. A.; Graham, D.; Wheate, N. *J. Inorg. Chem.* **2012**, *51*, 3490-3497.

[10] Zhang, X. D.; Wu, D.; Shen, X.; Liu, P. X.; Fan, F. Y.; Fan, S. *J. Biomaterials* **2012**.

[11] Brust, M.; Kiely, C*. J. Colloids Surf., A* **2002**, 202, 175-186.

[12] Min, Y.; Akbulut, M.: Kristiansen, K.; Golan, Y.; Israelachvili, J. *Nat. Mater.* **2008**, *7*, 527-538.

[13] Jovanovic-Talisman, T.: Zilman, A. *Nat. Nanotechnol.* **2011**, *6*, 397-398.

[14] Itamar, W.; Baron, R.; Willner, B. *Biosens. Bioelectron.* **2007**, *22*, 1841-1852.

[15] Parak, W. J.; Gerion, D.; Pellegrino, T.; Zanchet, D.; Micheel, C.; Williams, S. C.; Boudreau, R.; Le Gros, M. A.; Larabell, C. A.; Alivisatos, A. P. *Nanotechnology* **2003**, *14*, 15-27.

[16] Chen, C.; Mwakwari, S. C.; Oyelere, A.K. *Nanotechnol., Sci. Appl*. **2008**, *1*, 45–66.

[17] Daniel, M. C.; & Astruc, D. *Chem. Rev.* **2004**, *104*, 293.

[18] Fabris, L.; Antonello, S.; Armelao, L.; Donkers, R. L.; Polo, F.; Toniolo, C.; Maran, F. *J. Am. Chem. Soc.* **2006**, *128*, 326-336.

[19] Kaplan, J.M.; Shang, J.; Gobbo, P.; Antonello, S.; Armelao, L.; Chatare, V.; Ratner, D.M.; Andrade, R.B.; Maran, F. *Langmuir* **2013**, *29*, 8187-8192.

[20] Hostetler, M. J.; Templeton, A. C.; Murray, R. W. *Langmuir* **1999**, *15*, 3782-3789.

[21] Heinecke, C. L.; & Ackerson, C. J. *Nanoimaging* **2013**, 293-311.

[22] Larson-Smith, K.; Pozzo, D. C. *Langmuir* **2012**, *28*, 13157-13165.

[23] Donkers, R. L.; Song, Y.; Murray, R. W. *Langmuir* **2004**, *20*, 4703-4707.

[24] Wuelfing, W. P.; Gross, S. M.; Miles, D. T.; Murray, R. W. *J. Am. Chem. Soc*. **1998**, *120*, 12696-12697.

[25] Allardyce, C. S.; Dorcier, A.; Scolaro, C.; Dyson, P. *J. Appl. Organomet. Chem.* **2005**, *19* , 1-10.

[26] Sadler, P. *J. Adv. Inorg. Chem.* **1991**, *36*, 1-48.

[27] Guo, Z.; Sadler, P. *J. Adv. Inorg. Chem.* **1991**, *49*, 183-306.

[28] Rosenberg, S. A.; Yang, J. C.; Schwartzentruber, D. J.; Hwu, P.; Marincola, F. M.; Topalian, S. L.; Steinberg, S. M. *J. Clin. Oncol.* **1999**, *17*, 968-968.

[29] Lippert, B. *Cisplatin*. **1999**, *Wiley-VCH*.

[30] Reedijk, J. *Curr. Opin. Chem. Biol.* **1999**, *3*, 236-240.

[31] Fuertes, M. A.; Castilla, J.; Alonso, C.; Prez, J. M. *Curr. Med. Chem.* **2003**, *10*, 257-266.

[32] Basu, A.; Krishnamurthy, S. *J. Nucleic Acids* **2010**, 1-16.

[33] Kelland, L. *Nat. Rev. Cancer* **2007**, *7*, 573-584.

[34] Suntharalingam, K.; Duarte, A. A.; Mendoza, O.; Mann, D. J.; Vilar, R. *Metallomics* **2013**.

[35] Adams, M.; A'hern, R. P.; Calvert, A. H.; Carmichael, J.; Clark, P. I.; Coleman, R. E.; Wilkinson, P. M. Br. *J. Cancer* **1998**, *78*, 1404.

[36] Auersperg, N., Edelson, M. I., Mok, S. C., Johnson, S. W., & Hamilton, T. C. *Semin. Oncol.* **1998**, *25*, 281.

[37] Hwa Lee, R.; Mi Song, J.; Young Park, M.; Kyung Kang, S.; Keun Kim, Y.; Sup Jung, *J. Biochem. Pharmacol.* **2001**, *62*, 1013-1023.

[38] Lindauer, E.; Holler, E. *Biochem. Pharmacol*. **1996**, *52*, 7-14.

[39] Fregona, D.; Giovagnini, L.; Ronconi, L.; Marzano, C.; Trevisan, A.; Sitran, S.; Biondi, B.; Bordin, F. *J. Inorg. Biochem.* **2003**, *93*, 181–189.

[40] Comenge, J.; Sotelo, C.; Romero, F.; Gallego, O.; Barnadas, A.; Parada, T. G. C.; Puntes, V. F. *PloS one* **2012**, *7*, e47562.

[41] Chen, Z. G. *Trends Mol. Med.* **2010**, *16*, 594-602.

[42] Baish, J. W.; Stylianopoulos, T.; Lanning, R. M.; Kamoun, W. S.; Fukumura, D.; Munn, L. L.; Jain, R. K. *Proc. Natl. Acad. Sci. U. S. A.* **2011**, *105*, 1799-1803.

[43] Peleg-Shulman, T.; Najajreh, Y.; Gibson, D. *J. Inorg. Biochem.* **2002**, *91*, 306-311.

[44] Burger, K. N.; Staffhorst, R. W.; de Vijlder, H. C.; Velinova, M. J.; Bomans, P. H.; Frederik, P. M.; de Kruijff, B. *Nat. Med.* **2002**, *8*, 81-84.

[45] Cheng, L.; Jin, C.; Lv, W.; Ding, Q.; Han, X. *PloS one* **2011**, *6*, e25433.

[46] Rawat, M.; Singh, D.; Saraf, S.; Saraf, S. *Biol. Pharm. Bull.* **2006**, *29*, 1790-1798.

[47] Wong, C.; Stylianopoulos, T.; Cui, J.; Martin, J.; Chauhan, V. P.; Jiang, W.; Fukumura, D. *Proc. Natl. Acad. Sci. U. S. A.* **2011**, *108*, 2426-2431.

[48] Hobbs, S. K.; Monsky, W. L.; Yuan, F.; Roberts, W. G.; Griffith, L.; Torchilin, V. P.; Jain, R. K. *Proc. Natl. Acad. Sci. U. S. A.* **1998**, *95*, 4607-4612.

[49] Boucher, Y.; Baxter, L. T.; Jain, R. K. *Cancer Res*. **1990**, *50*, 4478-4484.

[50] Taurin, S.; Greish, K. *Tight Junctions in Cancer Metastasis* **2013**, 81-118.

[51] Matsumura, Y.; Maeda, H. *Cancer Res.* **1986**, *46*, 6387-6392.

[52] Dreher, M. R.; Liu, W.; Michelich, C. R.; Dewhirst, M. W.; Yuan, F.; Chilkoti, A. *J. Natl. Cancer Inst.* **2006**, *98*, 335-344.

[53] Saha, K.; Kim, S. T.; Yan, B.; Miranda, O. R.; Alfonso, F. S.; Shlosman, D.; Rotello, V. M. *Small* **2013**, *9*, 300-305.

[54] Brigger, I.; Dubernet, C.; Couvreur, P. *Adv. Drug Delivery Rev.* **2002**, *54*, 631-651.

[55] Perrault, S. D.; Chan, W. C. *J. Am. Chem. Soc.* **2009**, *131*, 17042-17043.

[56] McKee, T. D.; Grandi, P.; Mok, W.; Alexandrakis, G.; Insin, N.; Zimmer, J. P.; Jain, R. K. *Cancer Res.* **2006**, *66*, 2509-2513.

[57] Sahoo, S. K.; Parveen, S.; Panda, J. J. *Nanomedicine: Nanotech. Biol. Med.* **2007**, *3*, 20-31.

[58] Xia, Y.; Li, W.; Cobley, C. M.; Chen, J.; Xia, X.; Zhang, Q.; Brown, P. K. *Acc. Chem. Res.* **2011**, *44*, 914-924.

[59] Al-Jamal, W. T.; Kostarelos, K. *Acc. Chem. Res.* **2011**, *44*, 1094-1104.

[60] Ambrogio, M. W.; Thomas, C. R.; Zhao, Y. L.; Zink, J. I.; Stoddart, J. F. *Acc. Chem. Res.* **2011**, *44*, 903-913.

[61] Bhirde, A. A.; Patel, V.; Gavard, J.; Zhang, G.; Sousa, A. A.; Masedunskas, A.; Rusling, J. F. *ACS nano* **2009**, *3*, 307-316.

[62] Maysinger, D. *Org. Biomol. Chem*. **2007**, *5*, 2335-2342.

[63] Kircher, M. F.; de la Zerda, A.; Jokerst, J. V.; Zavaleta, C. L.; Kempen, P. J.; Mittra, E.; Gambhir, S. S. *Nat. Med.* **2012**, *18*, 829-834.

[64] Duncan, B.; Kim, C.; Rotello, V. M. *J. Controlled Release* **2010**, *148*, 122-127.

[65] Libutti, S. K.; Paciotti, G. F.; Byrnes, A. A.; Alexander, H. R.; Gannon, W. E.; Walker, M.; Tamarkin, L. *Clin. Cancer Res*. **2010**, *16*, 6139-6149.

[66] Harkness, K. M.; Turner, B. N.; Agrawal, A. C.; Zhang, Y.; McLean, J. A.; Cliffel, D. E. *Nanoscale* **2012**, *4*, 3843-3851.

[67] Paciotti, G. F.; Kingston, D. G.; Tamarkin, L. *Drug Dev. Res.* **2006**, *67*, 47-54.

[68] Niidome, T.; Yamagata, M.; Okamoto, Y.; Akiyama, Y.; Takahashi, H.; Kawano, T.; Niidome, Y. *J. Controlled Release* **2006**, *114*, 343-347.

[69] Kumar, A.; Zhang, X.; Liang, X. *J. Biotechnology advances* 2012.

[70] Ojea-Jiménez, I.; García-Fernández, L.; Lorenzo, J.; Puntes, V. F. *ACS Nano*, **2012**, *6*, 7692-7702.

[71] Malich, G.; Markovic, B.; Winder, C. *Toxicology* **1997**, *124*, 179-192.

[72] Amador, E.; Dorfman, L. E.; Wacker, W. E. *Clin. Chem*. **1963**, *9*, 391-399.

[73] Sawai, H.; Domae, N. *Biochem. Biophys. Res. Commun*. **2011**, *411*, 569-573.

[74] Vermes, I.; Haanen, C.; Steffens-Nakken, H.; Reutellingsperger, C. *J. Immunol. Methods* **1995**, *184*, 39-51.

[75] Loken, M. R.; Herzenberg, L. A. Ann. N. Y. Acad. Sci. **1975**, *254*, 163-171.

[76] Brust, M.;Walker, M.; Bethell, D.; Schriffin, D. J.; Whyman, R. *Chem. Commun.* **1994**, *801*.

[77] Donkers, R. L.; Lee, D.; Murray, R. W. *Langmuir* **2004**, *20*, 1945-1952.

[78] Whetten, R. L.; Khoury, J. T.; Alvarez, M. M.; Murthy, S.; Vezmar, I.; Wang, Z. L.; Landman, U. *Adv. Mater.* **1996**, *8*, 428-433.

[79] Ingram, R. S.; Hostetler, M. J.; Murray, R. W.; Schaaff, T. G.; Khoury, J. T.; Whetten, R. L.; Bigioni, T. P.; Guthrie, D. K.; First, P. N. *J. Am. Chem. Soc.* **1997**, *119*, 9279–9280.

[80] Qian, H.; Rongchao*, J. Chem. Mater.* **2011**, *23*, 2209–2217

[81] Holm, A. H.; Ceccato, M.; Donkers, R. L.; Fabris, L.; Pace, G.; Maran, F. *Langmuir* **2006**, *22*, 10584-10589.

[82] Tsien, R. Y*. Methods Cell. Biol*. **1989**, *30*, 127–156.

[83] Sardar, R.; Funston, A. M.; Mulvaney, P.; Murray, R. W. *Langmuir*, **2009**, 25, 13840–13851.

[84] Qian, H.; Jin, R. *Nano letters* **2009**, *9*, 4083-4087.

[85] Hostetler, M. J.; Wingate, J. E.; Zhong, C.-J.; Harris, J. E.; Vachet, R. W.; Clark, M. R.; Londono, J. D.; Green, S. J.; Stokes, J. J.; Wignall, G. D.; Glish, G. L.; Porter, M. D.; Evans, N. D.; Murray, R. W. *Langmuir* **1998**, *14*, 17.

[86] Wendlandt, W. W. M. Thermal Analysis, 3rd Ed.; *Wiley*: New York, **1986**.

[87] Wysokinski, R.; Michalska, D.; J. *Comput. Chem*. **2001**, *22*, 901– 912.

[88] Zhao, P.; Li, N.; Astruc, D. *Coord. Chem*. Rev. **2012**.

[89] Bianco, A.; Kostarelos, K.; Prato, M. *Expert Opin. Drug Delivery* **2008**, *5*, 331-342.

[90] Popielarski, S. R.; Hu-Lieskovan, S.; French, S. W.; Triche, T. J.; Davis, M. E. *Bioconjugate Chem*. **2005**, *16*, 1071-1080.

[91] Zhu, Y.; Chen, G.; Jin, R.; Sun, Y. *Am. J. Chem*. **2012**, *2*, 18-22.

[92] Sousa, A.; Morgan, T. M.; Brown, P. H.; Adams, A.; Jayasekara, M. P. S.; Zhang, G.; Ackerson, J. C.; Kruhlak, M. J.; Leapman, R. D. *Small* **2012**, *8*, 2277–2286.

Aknowledgments

I would like to offer my deep gratitude to Prof. Flavio Maran and Prof. Emanuele Papini, my research advisors, for their patient supervision, useful critiques and enthusiastic encouragement for this thesis project, especially in those moments I felt lost. I am glad to have had the opportunity to grow up as man of science under your expert guidance. I would like also to express my very great appreciation to Prof. Fabrizio Mancin for his willingness to give his time so generously.

I am particularly grateful for the assistance given by Dr. Federico Polo with the conception of this project and I wish to thank Dr. Regina Tavano and Dr. Sabrina Antonello, who provided me with very valuable scientific suggestions, but also genuine laughs and comforting words.

I would like to aknowledge the support provided by the persons I consider my family during the realization of this project in terms of pride, love, food, hugs, laughs, movies, walks along the river, intense working weekends, office life… and cookies! So thanks to Nonna Nannina, Angela, Silvano, Cristina and Gianni, members of my family; Paola, Laura and Sara, friends and colleagues; Maria Cristina Cognolato, colleague and supervisor at *Servizio Prevenzione e Protezione* of this University; Fabio, Stefano and Giovanna, undoubted friends; Ilaria and Giulia, friends, classmates and also labmates; Alice, Caterina and Riccardo, three wonderful persons I met one year ago and now I couldn't live without.

My special thanks are extended to the whole staff of Maran's Electrochemistry Group, in particular to Mariachiara and Jenn for their party nights, Marco and Tiziano for the shared moments in the organic lab, Adriana and Lorena for the omnipresent "background" animating our shared office.

Finally, I wish to thank all my classmates, all the professors of the industrial biotechnology course, all the members of *Servizio Prevenzione e Protezione* of *Università degli Studi di Padova*, Prof. Michela Zottini and all those people who crossed the path of my life and walked at my side, even just for a short moment, but leaving a deep sign of their passage, making me the man I am now.